ANL-7479

Argonne National Laboratory

ANALYTICAL AND EXPERIMENTAL STUDIES OF DOUBLE-PIPE COUNTER-FLOW LIQUID METAL HEAT EXCHANGERS

by

Ray Wilford Brown, Jr.

The facilities of Argonne National Laboratory are owned by the United States Government. Under the terms of a contract (W-31-109-Eng-38) between the U. S. Atomic Energy Commission, Argonne Universities Association and The University of Chicago, the University employs the staff and operates the Laboratory in accordance with policies and programs formulated, approved and reviewed by the Association.

MEMBERS OF ARGONNE UNIVERSITIES ASSOCIATION

The University of Arizona	Kansas State University	The Ohio State University
Carnegie-Mellon University	The University of Kansas	Ohio University
Case Western Reserve University	Loyola University	The Pennsylvania State University
The University of Chicago	Marquette University	Purdue University
University of Cincinnati	Michigan State University	Saint Louis University
Illinois Institute of Technology	The University of Michigan	Southern Illinois University
University of Illinois	University of Minnesota	University of Texas
Indiana University	University of Missouri	Washington University
Iowa State University	Northwestern University	Wayne State University
The University of Iowa	University of Notre Dame	The University of Wisconsin

Printed in the United States of America
Available from
Clearinghouse for Federal Scientific and Technical Information
National Bureau of Standards, U. S. Department of Commerce
Springfield, Virginia 22151
Price: Printed Copy $3.00; Microfiche $0.65

ANL-7479
Engineering and
Equipment

ARGONNE NATIONAL LABORATORY
9700 South Cass Avenue
Argonne, Illinois 60439

ANALYTICAL AND EXPERIMENTAL STUDIES OF DOUBLE-PIPE COUNTER-FLOW LIQUID METAL HEAT EXCHANGERS

by

Ray Wilford Brown, Jr.

Reactor Engineering Division

Based on a Thesis
Submitted to the Faculty of the Graduate School,
University of Notre Dame,
in Partial Fulfillment of the Requirements
for the Degree of Doctor of Philosophy

August 1968

TABLE OF CONTENTS

TABLE OF CONTENTS

LIST OF FIGURES

LIST OF FIGURES

LIST OF FIGURES

LIST OF TABLES

NOMENCLATURE

Symbol	Description
A_n	Expansion coefficient associated with nth negative eigenvalue
$B_i\{\ \}$	Bulk operator in channel i
C_n	Expansion coefficient associated with nth positive eigenvalue
c_i	Specific heat of fluid in channel i, Btu/lb-°F
D_i	Hydraulic diameter of channel i, $\frac{4 \times \text{Area}}{\text{Wetted Perimeter}}$, in.
$E_{i,n}(x_i)$	Normalized eigenfunction in stream i associated with nth positive eigenvalue
$\widetilde{E}_{i,n}(x_i)$	Normalized eigenfunction in stream i associated with nth negative eigenvalue
F, $\widetilde{F}$, G, $\widetilde{G}$	Auxiliary functions
$f_i(x_i)$	"Total" fluid conductivity relative to molecular fluid conductivity in channel i
$g_i(x_i)$	Dimensionless local velocity in channel i
$g_i^+(x_i^+)$	Dimensionless function associated with turbulent-flow approximation
H	Ratio of heat capacity to mass flowrate, c_2W_2/c_1W_1
$h_i(\ell)$	Local heat transfer coefficient in channel i, Btu/hr-ft^2-°F
I_0, I_1	Modified Bessel functions of first kind
J_0, J_1	Bessel functions of first kind
K	Relative thermal resistance of fluid, $\frac{k_1}{k_2}\frac{1-R}{R}$
K_0, K_1	Modified Bessel functions of second kind
K_w	Relative thermal resistance of wall, $\frac{k_1}{k_w}\ell n\left(\frac{r_{21}}{r_{12}}\right)$
k_i	Thermal conductivity of fluid in channel i, Btu/hr-ft-°F
k_i^+	Quantity associated with turbulent-flow approximation
k_w	Thermal conductivity of heat transfer surface, Btu/hr-ft-°F
L	Heat-exchanger length, in.
ℓ	Axial space variable, in.
N_n	Normalizing factor associated with nth positive eigenvalue
$\widetilde{N}_n$	Normalizing factor associated with nth negative eigenvalue
NTU	Number of transfer units
NTU_{FD}	Fully developed number of transfer units
$Nu_i(z)$	Local Nusselt number in channel i, h_iD_i/k_i
$Nu_i^o(z)$	Local overall Nusselt number, UD_1/k_1
Nu_{iFD}	Fully developed Nusselt number in channel i
Nu_{FD}^o	Fully developed overall Nusselt number
Nu_{AV}^o	"Length average" overall Nusselt number
Pe_i	Peclet number in channel i, Pr_iRe_i
Pr_i	Prandtl number of fluid in channel i, μ_ic_i/k_i
$P_i(x_i)$	Outlet temperature distribution of fluid in channel i
$Q_{n,k}$	Coefficient matrix element in system of equations defining expansion coefficients
$q_i(\ell)$	Local heat flux based on dimensions of channel i, Btu/hr-ft^2
R	Annular radius ratio, r_{21}/r_{22}
Re_i	Reynolds number of channel i, $u_{iAV}D_i\rho_i/\mu_i$
r_i	Radial space variable in channel i, in.
r_{12}	Radius of circular tube, in.
r_{21}	Inner radius of annular space, in.
r_{22}	Outer radius of annular space, in.
S	Symbol denoting experimental outer wall temperature function
$T_i(r_i,\ell)$	Local temperature in channel i, °F
T_{10}	Temperature of fluid entering tube side of heat exchanger, °F
T_{2L}	Temperature of fluid entering annulus side of heat exchanger, °F

Symbol	Description
$\overline{T}_i(\ell)$	Local bulk temperature in channel i, °F
TA_j	Bulk temperature measured by thermocouple j in experiment, °F
TB_j	Outer wall temperature measured by thermocouple j in experiment, °F
$U(\ell)$	Overall heat transfer coefficient, Btu/hr-ft^2-°F
$u_i(r_i)$	Local velocity in channel i, ft/hr
W_i	Weight flowrate of fluid in channel i, lb/hr
W_{H_2O}	Weight flowrate of water to cooler used in experimental apparatus, lb/hr
x_i	Dimensionless radial space variable in channel i
x_i^+	Dimensionless radial space variable used in turbulent-flow approximation
Y_0, Y_1	Bessel functions of second kind
y	Characteristic function used in presentation of theorem in Appendix A
Z	Dimensionless heat-exchanger length
z	Dimensionless axial space variable
z^+	Dimensionless axial space variable used in turbulent-flow approximation

Greek Letters

α_i	Thermal diffusivity of fluid in channel i, ft^2/hr
β_n^2	Absolute value of nth negative eigenvalue
ΔT_0	Temperature difference at fluid inlet, °F
δ_H	Heat-balance deviation in experimental test section, %
δ_c	Heat-balance deviation in experimental water cooler, %
ϵ	Heat-exchanger efficiency
ϵ_{Hi}	Eddy diffusivity of heat in channel i, ft^2/hr
ϵ_{Mi}	Eddy diffusivity of momentum in channel i, ft^2/hr
η_i	Nusselt number in channel i, normalized with respect to corresponding fully developed uniform heat-flux plug-flow value
η_0	Overall Nusselt number, normalized with respect to corresponding fully developed uniform heat-flux plug-flow value
λ_n^2	nth positive eigenvalue
$\xi_i(x_i,z)$	Dimensionless local temperature in channel i
$\overline{\xi}_i(z)$	Dimensionless local bulk temperature
σ	R/(1 - R)
$\phi(Z)$	Effectiveness coefficient
ϕ_{FD}	Fully developed effectiveness coefficient
$\psi(\lambda)$	Symbol denoting eigenvalue equation associated with positive eigenvalues
$\widetilde{\psi}(\beta)$	Symbol denoting eigenvalue equation associated with negative eigenvalues
ω^2	HKR/(1 + R)

Subscripts

AV	Denotes average value
FD	Denotes fully developed value
i	Denotes channel (1--tube, 2--annulus)
max	Denotes maximum value
min	Denotes minimum value
n, k, m	Denotes order of eigenvalue or eigenfunction
PF	Denotes plug-flow value
UHF	Denotes uniform heat-flux value
$\overline{\xi}_i(z)$	Overscore: denotes bulk temperature

ANALYTICAL AND EXPERIMENTAL STUDIES OF DOUBLE-PIPE COUNTER-FLOW LIQUID METAL HEAT EXCHANGERS

by

Ray Wilford Brown, Jr.

ABSTRACT

An analytical and experimental study of heat transfer in countercurrent, liquid metal, double-pipe heat exchangers is presented. The mathematical treatment is based on an exact solution of the basic energy equation rather than on the "traditional" practice of assuming the heat transfer coefficients of individual channels to be uniform and equal to a predetermined value. The solution presented herein is actually an extension of the classical "Graetz" problem to boundary conditions appropriate to heat exchangers. The analysis results in a solution for the fluid temperature profiles over the entire length of the heat exchanger, including the thermal-entrance regions. The mathematical analysis was used to compute heat-exchanger efficiencies and heat transfer coefficients. The analytical results indicate that the traditional method of heat-exchanger design could lead to inaccuracies when applied to liquid metal heat exchangers.

An experimental program to obtain performance curves for liquid metal heat exchangers was conducted, using a promising new technique for measuring overall heat transfer coefficients. The experimental results supported the results of the mathematical analysis, particularly for short heat exchangers, in which most of the heat transfer occurs in the thermal-entrance regions.

CHAPTER I

INTRODUCTION

Liquid metals are generally superior to nonmetallic fluids as heat transfer media because of their higher thermal conductivity, lower vapor pressure, and the fact that they remain in the liquid state over a wider temperature range. For these reasons, recent intense technological interest has developed in liquid-metal heat transfer for application to the design of liquid-metal-cooled nuclear reactors and for their use as working fluids in space power plants where small equipment size is essential.

One of the simplest of devices for the transfer of heat between two fluids is the double-pipe heat exchanger. Aside from its usefulness as a practical heat-exchange apparatus, its simple geometry makes it an ideal model for basic heat transfer investigations, both experimental and analytical. Design of such heat exchangers for practical applications is usually based on two essential assumptions. These two assumptions, which will be hereafter referred to as the "traditional method of heat exchanger design," are:

(1) The heat transfer coefficients of individual channels, tube and annulus, are relatively insensitive to the heat flux or temperature distribution along the length of the heat transfer surface.

(2) Thermal-entrance effects are negligible, and the heat transfer coefficients are uniform over the entire length of the heat exchanger.

For turbulent forced convection in nonmetallic fluids, the above assumptions lead to sufficiently accurate results for practical applications but may not always be valid when applied to liquid metals. Sleicher and Tribus[1] have illustrated the differences between turbulent forced convection with nonmetallic fluids and liquid metals by comparing their heat transfer coefficients. Figure 1.1 from a graph in Ref. 1, shows the ratio of uniform-heat-flux Nusselt numbers to uniform-wall-temperature Nusselt numbers for nonmetallic fluids and liquid metals flowing in a tube. It is evident from the graph that the heat transfer coefficients of liquid metals are strongly influenced by boundary conditions. Sleicher and Tribus also compared thermal-entry lengths for nonmetallic fluids and liquid metals flowing in a pipe with a uniform-wall-temperature boundary condition. Figure 1.2, also from a graph in Ref. 1, shows that the thermal-entry lengths required for the heat transfer coefficients of liquid metals to become fully developed can be much larger than those for nonmetallic fluids.

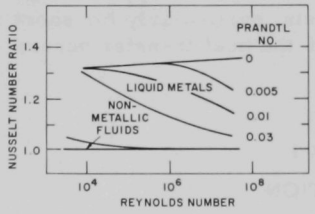

Fig. 1.1. Ratio of Nusselt Number at Uniform Heat Flux to Nusselt Number at Uniform Wall Temperature vs. Reynolds Number (from Ref. 1)

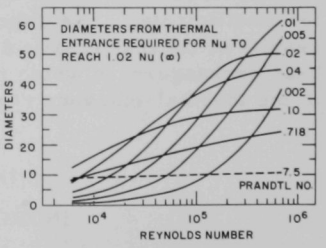

Fig. 1.2. Thermal-entry Length for a Pipe at Uniform Wall Temperature (from Ref. 1)

The results of Sleicher and Tribus indicate that the validity of the traditional method of heat-exchanger design for application to liquid metals deserves to be questioned. The present investigation, both analytical and experimental, considers liquid-metal heat transfer in countercurrent double-pipe heat exchangers. No use is made of the traditional assumptions in either analysis or experiment, the purpose being to provide an exact prediction of performance of the double-pipe heat exchanger and to investigate the range of validity, if any, of the traditional method when used for liquid metals.

CHAPTER II

LITERATURE SURVEY

A. Liquid Metal Heat Transfer in Individual Pipes and Annuli

During the past twenty-five years, most of the research in liquid metal heat transfer has been concerned with finding reliable relationships for heat transfer in pipes and annuli. These investigations considered boundary conditions of specified wall heat flux or temperature; most of the analytical work related to fully developed heat transfer paralleling the analysis of Martinelli.[2] The main object of this early research was to determine heat transfer coefficients for use in the traditional method of heat-exchanger design. Surveys of this phase of liquid metal heat transfer can be found in heat transfer texts, such as Refs. 3 and 4, and a detailed review will not be given here. Instead, attention will be focused on research on double-pipe heat exchangers whose boundary conditions cannot be initially specified except in certain limiting cases. Consistent correlations for fully developed heat transfer coefficients in pipes and annuli are of some interest, however, for comparison with the results of the present analysis and for use in calculating quantities associated with a turbulent-flow approximation. Table 2.1 gives the correlations of Buleev[5] and Dwyer[6-8] for fully developed Nusselt numbers

TABLE 2.1. Fully Developed Heat Transfer Coefficients for Liquid Metals

Author	Ref.	Heat Transfer Coefficient Predicted	Equation	
		Solutions for Turbulent Flow		
Buleev	5	Fully developed Nusselt number in a circular tube with uniform wall heat flux	$Nu = A + 4.16(Re/1000)^m Pr^{0.66}$	(2.1a)
			$A = 2.5 + 1.3 \log_{10}\left[1 + \frac{1}{Pr}\right]$	
			$m = 0.865 - 0.051 \log_{10}\left[1 + \frac{1}{Pr}\right]$	
Dwyer	6,7,8	Fully developed Nusselt number in a concentric annulus with uniform heat flux from the inner wall and an insulated outer wall	$Nu = 4.82 + \frac{0.697}{R} + 0.0222(\bar{\psi}Pe)^{\gamma}$ $\quad \bar{\psi} > 0$	(2.1b)
			$Nu = 4.98 + \frac{0.662}{R}$ $\quad \bar{\psi} < 0$	
			$\bar{\psi} = 1 - \frac{1.82}{Pr\,(\epsilon_M/\nu)^{1.4}_{MAX}}$	
			$(\epsilon_M/\nu)_{MAX} = 4.0 + 0.0029Re^{0.919}$	
			$\gamma = 0.758/R^{0.053}$	
		Solutions for Plug Flow		
Trefethen	34	Fully developed Nusselt number in a circular tube with uniform wall heat flux	$Nu = 8$	(2.1c)
Eckert and Drake	4	Fully developed Nusselt number in a circular tube with uniform wall temperature	$Nu = 5.783$	(2.1d)
Trefethen	34	Fully developed Nusselt number in a concentric annulus with uniform heat flux from the inner wall and an insulated outer wall	$Nu = \frac{8(1 - R)(1 - R^2)^2}{-R(R^4 - 4R^2 + 3 + 4 \ln R)}$	(2.1e)
Merriam	23	Fully developed Nusselt number in a concentric annulus with uniform wall temperature at the inner wall and an insulated outer wall	Annulus Ratio / Nu: 0.1 / 10.833; 0.25 / 6.966; 0.4 / 5.907; 0.5 / 5.555; 0.6 / 5.328; 0.7 / 5.174; 0.8 / 5.067; 0.9 / 4.990; 1.0 / 4.935	(2.1f)
Trefethen	34	Fully developed Nusselt number in a parallel-plate channel with one wall insulated and uniform heat flux at the other wall	$Nu = 6$	(2.1g)

in uniformly heated pipes and annuli. The results of Buleev and Dwyer are considered by the present author to be more accurate than other correlations available in the literature[9-12] because of their better agreement with experimental data. In a recent review of liquid metal heat transfer, Dwyer[8] has indicated that Eqs. (2.1a) and (2.1b) are probably the most accurate. Also included in the table are solutions for plug flow for the boundary conditions of uniform wall heat flux and uniform wall temperature. All of the Nusselt numbers in Table 2.1 are defined with respect to the equivalent hydraulic diameter of the channel.

B. Recent Theoretical Developments in Double-pipe Heat Exchangers

Recently, theoretical analyses of heat exchangers without a predetermined boundary condition for the inner wall have appeared in the literature. Bentwich and Sideman[13] analyzed a system equivalent to a cocurrent double-pipe heat exchanger in which two immiscible fluids were flowing inside a pipe with a definite interface between them. Ting[14] and Lightfoot[15] considered a heat exchanger in which the heat transfer coefficient in only one channel was specified. Stein[16] later used this model to approximate heat transfer between a liquid metal and a nonmetallic fluid. He presents an extensive review of recent theories of heat transfer in symmetrical ducts and includes a discussion of double-pipe exchangers.

The most general mathematical treatment of heat transfer in double-pipe heat exchangers is that of Stein[17] and will be presented first to introduce the reader to the mathematical treatment used in other more restricted analyses. Other analyses of double-pipe heat exchangers reviewed in this chapter are actually special cases of the general case treated by Stein. Stein's analysis considered both cocurrent and countercurrent flow, various symmetrical duct geometries, and was generalized to include laminar or turbulent flow. No simplifying assumptions regarding the heat transfer coefficients in individual channels were used. The idealizations upon which the analysis depended are listed below.

1. Physical properties were independent of temperature.
2. The fluid flow was fully developed and incompressible.
3. The flow channels were symmetrical in the sense that only two orthogonal space coordinates, one of which denoted axial distance, were required for the mathematical formulation.
4. Longitudinal heat conduction and longitudinal turbulent heat diffusion in the fluids were negligible.
5. Longitudinal heat conduction in the heat-exchanger walls was negligible.
6. The fluid inlet temperatures were uniform.
7. Frictional heating was negligible.

Stein's analysis was, in effect, an extension of the classical Graetz problem to boundary conditions appropriate to heat exchangers. In particular, a technique of separation of variables applied to energy equations written for both channels of the heat exchanger led to a solution for the temperature distribution of the form

$$\sum_n C_n E_{i,n} e^{-\lambda_n^2 z},$$

where i denotes the channel (1--tube; 2--annulus). The eigenfunctions, $E_{i,n}$, and eigenvalues, λ_n^2, were defined by a "two-region," tube and annulus, Sturm-Liouville problem. The expansion coefficients, C_n, were determined by the inlet and outlet conditions of the heat exchanger. For the cocurrent case, the temperature distribution in each channel was expressed by an infinite series of terms associated with positive eigenvalues only, and the above summation was from $n = 0$ to $+\infty$. For the countercurrent case, the temperature distributions were expressed by an infinite series of terms associated with negative as well as positive eigenvalues, and the above summation was from $n = -\infty$ to $+\infty$. Equations defining the heat-exchanger efficiency for both cocurrent and countercurrent flow were presented.

Also presented were expressions for determining fully developed or "asymptotic" heat transfer coefficients. For cocurrent flow, the fully developed Nusselt numbers were found to be proportional to the first nonzero eigenvalue. For countercurrent flow, the fully developed Nusselt numbers were proportional either to the first negative eigenvalue or to the first positive eigenvalue, depending on whether the ratio of heat capacity to mass flowrate, H, was less than or greater than unity. It was pointed out that while fully developed heat transfer only occurs near the exit end of a cocurrent heat exchanger, it may occur at either end or along the center of a countercurrent heat exchanger.

A quantity called the "effectiveness coefficient," previously introduced by Stein,[18] was suggested for use in computations for heat-exchanger design.

Calculation of eigenvalues, eigenfunctions, and expansion coefficients for the cocurrent case entailed a straightforward application of the equations defining these quantities as given by the analysis. The calculation of the eigenvalues and eigenfunctions for the countercurrent case was also straightforward, but calculation of the expansion coefficients required the solution of an infinite set of algebraic equations. This unusual aspect of the mathematical problem results from the fact that the countercurrent heat exchanger has outlet temperature distributions at each end which are unknown. As a result, when orthogonal expansions which defined the expansion coefficients were written at either end of the heat exchanger, they contained the unknown outlet temperature distributions. To overcome this difficulty, orthogonal

expansions were written for both ends of the heat exchanger. The relationships so obtained for C_n were then added and combined in such a way that an infinite set of linear algebraic equations was obtained which defined the expansion coefficients. Nunge and Gill[19,20] first used this same general method, but their procedure for combining the orthogonal expansions was different. A discussion of the actual computations necessary to find the expansion coefficients will be included in a later section.

The practical aspects of the analysis were explained with special emphasis on the importance of the effectiveness coefficient in the design of practical heat exchangers.

A limited number of computed values of the effectiveness coefficient and fully developed overall Nusselt number were presented for the cases of a laminar-flow cocurrent double-pipe heat exchanger and a plug-flow countercurrent double-pipe heat exchanger. These results indicated that the actual performance of a heat exchanger could be quite different from that predicted by specifying a uniform heat flux or uniform temperature inner wall boundary condition. It must be pointed out that the analysis presented in Ref. 17 is not valid for countercurrent flow when H = 1. For H = 1 certain terms in the solution become mathematically indeterminate and must be treated in another manner.

Stein[28] has recently extended the analysis in Ref. 17 to include the case of equal heat capacity-mass flowrates. Stein's solution considers the limit of the mathematically indeterminate terms as H approaches unity. It was shown that these mathematically indeterminate terms have a finite value and that their mathematical form can be determined. The analysis was generalized to include both laminar and turbulent flow, and various geometrical configurations. It was shown that, for H = 1, fully developed heat fluxes are always uniform, whereas local heat fluxes in the thermal-entrance region may be quite nonuniform. As the thermal resistance at the inner wall was increased, it was found that heat-flux distributions in the thermal-entrance region approach uniformity.

The author illustrates that for a small-wall thermal resistance, significant errors can result when it is assumed that the heat flux is uniform over the entire length of the heat exchanger.

1. Cocurrent Heat-exchanger Analyses

Stein[18,22] presented solutions for heat transfer in cocurrent-flow double-pipe heat exchangers. The analyses were applied to models of laminar and plug flow. To account for the effect of turbulence, an approximation (this will be referred to as the "k^+ approximation" and will be explained in detail later) was introduced which extended the accuracy of the plug-flow model for liquid metals up to Peclet numbers of 1000. Numerical results were presented for a double-pipe heat exchanger with a narrow annular space and also a parallel-plate configuration.

Merriam[23] in a combined analytical and experimental investigation of liquid metal, cocurrent flow, double-pipe heat exchangers extended the analyses of Stein[18,22] to include heat exchangers with nonnarrow annular spaces. A plug-flow model was used together with the k^+ approximation of Stein to predict local and fully developed heat transfer coefficients.

In general, the values calculated from the theory using the k^+ approximation showed agreement with the experimental data. The experimental part of this investigation will be reviewed in more detail later.

2. Analyses of Countercurrent Heat Exchangers

Nunge and Gill[19] presented a mathematical solution for heat transfer in a laminar, parallel-plate, counter-flow heat exchanger. The model used was highly idealized and consisted of two identical laminar-fluid streams in counter flow between parallel plates. A zero-thickness, zero-thermal resistance plane was postulated to separate the two streams; this allowed formulation of the problem in a single region with a continuous velocity distribution which changes sign at the interface between the fluid streams. This way of formulating the problem permitted a direct application of the theorem in Appendix A, pertaining to the existence of the negative eigenvalues. Stein[16] originally had to assert the existence of the negative eigenvalues from physical arguments. The individual eigenvalues and eigenfunctions were calculated by a numerical integration of the two-region Sturm-Liouville system. To find expressions for the expansion coefficients, the authors wrote orthogonal expansions for each end of the heat exchanger. The relations so obtained for the expansion coefficients each contained an unknown temperature distribution. To eliminate these unknowns, the two expressions were equated and, after some manipulation, an infinite set of linear algebraic equations which defined the expansion coefficients was obtained. Differences in this method for computing the expansion coefficients, the "Nunge-Gill" procedure, and the method used in Ref. 17, the "Argonne" procedure, are discussed by Stein.[25]

Solution of the infinite set of linear algebraic equations was accomplished by truncating the higher-ordered terms and solving the remaining finite set by a Gauss-Jordan reduction. The number of equations actually used by the authors in calculating the expansion coefficients could not be determined. Since only three values of positive and negative eigenvalues were reported, it seems likely that these were all that were used.

In order to check the computations, a finite-difference technique was applied to the basic energy equation to compute fluid temperature profiles, and the results were compared with temperature profiles computed from the series solution. The finite difference technique was a modification of that developed by King.[24] Agreement between the two solutions was good for the central portion of the heat exchanger, but showed discrepancies near the heat-exchanger ends, probably due to the small number of terms used in the series solution and/or inaccuracies in the expansion coefficients.

Nunge, Gill, and Stein[21] extended the previous analysis of a laminar, parallel-plate, countercurrent heat exchanger to include different fluid stream properties and a wall separating the two fluid streams. The Nunge-Gill procedure was used to compute the expansion coefficients. The paper has not been published, mainly because of difficulties associated with the method of computing the expansion coefficients. These difficulties are discussed in detail in Ref. 25.

Nunge and Gill[20] also presented a solution for a laminar, countercurrent, double-pipe heat exchanger. The method of solution used in the previous two papers was modified to fit the geometry of the double-pipe configuration.

Stein[25] has questioned the accuracy of the procedure used in the preceding three papers for calculating the expansion coefficients. Extensive calculations of heat transfer in a parallel-plate, countercurrent heat exchanger using a plug-flow model were made. The calculations revealed serious difficulties in the solution of the truncated set of linear equations using the method of the three previous papers, i.e., the Nunge-Gill procedure. These difficulties were for the most part resolved when the Argonne procedure was used for calculating the expansion coefficients. This procedure was originated by the present author as part of the research of this thesis and is described in detail in Appendix A.

It was pointed out that in order for the solution of an infinite set of equations to be meaningful, the lower-ordered solutions must converge to a definite value as more and more equations are added to the set. If a different solution is obtained for each new equation added, the system of equations does not have a unique solution. Stein suggests that the system of equations solved by Nunge and Gill in Refs. 19 and 20 may not have a unique solution or that an insufficient number of equations was used to obtain convergence. It was noted previously that the number of equations used in the calculations could not be determined nor was any mention of convergence made.

Attempts to use the Nunge-Gill procedure always resulted in ill-conditioned sets of equations, and, as a result, could not be used when more than a few equations of the set were included. The Argonne procedure always resulted in a well-conditioned set of equations. The coefficients converged uniformly as new equations were added to the set although convergence in the third to fifth decimal place was slow.

Stein presented a table comparing the optimum results of the Nunge-Gill procedure with the results of calculations made with the alternative procedure. It was noted that in all cases the Argonne procedure yielded consistently better results than the Nunge-Gill procedure. In many cases, the Nunge-Gill procedure failed completely.

Nunge[26] presented an analysis of heat transfer in laminar-flow heat exchangers. The analysis followed the work reported in Refs. 19, 20, and 21. A discussion of the convergence of the Nunge-Gill procedure as

more equations of the infinite set were used was included. Computations were performed for increasing numbers of equations up to a maximum of seven. A single example was given for which the "zeroth" order expansion coefficient converged to accuracy in the second decimal place when seven equations were used for the computation. It was not reported whether or not this was the maximum accuracy obtainable.

C. Experimental Investigations of Liquid Metal Heat Transfer in Double-pipe Heat Exchangers

Most experimental analyses of liquid metal heat transfer have been concerned with measuring heat transfer coefficients in individual pipes and annuli for a specified boundary condition. These investigations employed one of two basic types of test section, the first type being an electrically heated tube or annulus, and the second type a double-pipe heat exchanger. The assumption was usually made that the operating conditions of the heat exchanger could be controlled to achieve the desired boundary condition for the inner wall. It was generally assumed that if the ratio H of heat capacity to mass flowrate was unity, then a uniform-heat-flux boundary condition was obtained if the fluid was in counter flow, and a uniform-wall-temperature boundary condition was obtained if the fluid was flowing cocurrently.

The majority of the experimenters using double-pipe heat exchangers measured either average or fully developed overall heat transfer coefficients. An assumption about the value of the ratio of the tube-side coefficient to the annulus-side coefficient was made and then these coefficients were calculated from the overall coefficient. Theoretical relations such as those of Lyon[10] and Werner[11] were used for predicting the heat-transfer-coefficient ratio for individual channels.

Most of the experiments have been reviewed extensively by Lubarsky and Kaufman[29] and Merriam,[23] so a detailed survey will not be given here. Table 2.2 summarizes the more important heat-exchanger experiments pertinent to the present work.

As stated before, the prime objective of these experiments with heat exchangers was to measure heat transfer coefficients. The only investigation known to the present author which attempted to analyze double-pipe heat-exchanger performance more generally was that due to Merriam.[23] The experimental part of this paper will be reviewed in greater detail now.

Merriam[23] experimentally investigated the performance of a cocurrent, liquid metal, double-pipe heat exchanger by measuring efficiencies and fully developed heat transfer coefficients. A new method suggested by Stein[45] was used to measure the overall fully developed heat transfer coefficient. The method required a measurement of the outer-wall temperature distribution along the length of the heat exchanger. A plot of this outer-wall temperature vs. length on semilog paper produced a curve which was linear in the fully

TABLE 2.2. Heat Transfer Experiments with Liquid Metal Heat Exchangers

Ref.	Author	Heat-exchanger Type	Heat Transfer Fluids	Heat-exchanger Material	Heat-exchanger Length (Based on Diameter of Tube)	Approximate Inner Wall Boundary Condition	Heat Transfer Coefficient Determined	Remarks
30	Gilliland et al. (1947) (heating data)	Double-pipe, condenser	Hg in tube, steam in annulus	Nickel	44 L/D	UWT	Overall average	Possibility of thermal-contact resistance present. Data are lower than predicted by theory.
30	Gilliland et al. (1947) (cooling data)	Double-pipe, countercurrent	Hg in tube, H_2O in annulus	Nickel	160 L/D	Uncertain	Overall average	Data are lower than predicted by theory.
11	Werner et al. (1949)	Double-pipe, countercurrent	NaK in tube and annulus			UHF	Overall average	Flowrates in tube and annulus were equal for all tests. Data taken from Test Sec. 1 show scatter which can be traced to insufficient mixing of fluids before bulk-temperature measurement. Mixing baffles were installed for Test Sec. 2. Data for Test Sec. 2 show good agreement with theory.
	Test Sec. 1			Stainless steel	50 L/D			
	Test Sec. 2			Nickel	48 L/D			
31	Elser (1949)	Double-pipe, countercurrent	Hg in tube, H_2O in annulus			UHF	Fully-developed	Uncertainty about the placement of wall thermocouples, poor flow-measurement techniques, and presence of a thermal-contact resistance combine to make the data unreliable. Results were approximately 50% below the prediction of the theory.
	Test Sec. 1			Low carbon steel	120 L/D			
	Test Sec. 2			Stainless steel	123 L/D			
	Test Sec. 3			Stainless steel	146 L/D			
10,32	Lyon (1949)	Double-pipe, countercurrent	NaK in tube and annulus	Nickel		UHF	Overall average	Flowrates in each channel were equal for all tests. Data show good agreement with theory.
	Test Sec. 1				110 L/D			
	Test Sec. 2				98 L/D			
	Test Sec. 3				76 L/D			
	Test Sec. 4				160 L/D			
33	Seban (1950)	Double-pipe, countercurrent	Pb-Bi in tube and annulus			UHF	Overall average	Mass flowrates in tube and annulus were equal for all tests. Results for Test Secs. 1 and 2 showed much scatter and were approximately 50% below theory, probably due to contact resistance. Tinned test sec. results were much better and within 15% of theory.
	Test Sec. 1			Stainless steel				
	Test Sec. 2			Low carbon steel				
	Test Sec. 3			Tinned steel				
34	Trefethen (1950)	Double-pipe, countercurrent	Hg in tube and annulus			UHF	Overall average	Mass flowrates in tube and annulus were equal for all tests. Data show good agreement with theory. No difference was noted for different test sec. materials.
	Test Sec. 1			Stainless steel	55 L/D			
	Test Sec. 2			Stainless steel	53 L/D			
	Test Sec. 3			Stainless steel	67 L/D			
	Test Sec. 4			Copper	75 L/D			
	Test Sec. 5			Copper	127 L/D			
	Test Sec. 6			Copper	92 L/D			
35	Doody and Younger (1951)	Double-pipe, cocurrent and countercurrent	Hg in tube, H_2O in annulus	Steel	100 L/D	Uncertain	Average	Data are probably inaccurate due to large experimental errors. The addition of small amounts of Na to the Hg increased the heat transfer coefficients by as much as 100%.
36	Lubarsky (1951)	Double-pipe, countercurrent	Pb-Bi in tube and annulus	Stainless steel	100 L/D	UHF	Overall average	Data were slightly lower than theory. No difference was noted when magnesium was added to the lead-bismuth.
37	Bailey et al. (1952)	Double-pipe, cocurrent	Hg in tube, H_2O in annulus	Low carbon steel	41 L/D	Uncertain	Fully-developed	Data obtained were about 60% lower than that predicted by theory, due probably to the existence of a thermal-contact resistance between the Hg and the tube. The data are not considered reliable.

TABLE 2.2. (Contd.)

Ref.	Author	Heat-exchanger Type	Heat Transfer Fluids	Heat-exchanger Material	Heat-exchanger Length (Based on Diameter of Tube)	Approximate Inner Wall Boundary Condition	Heat Transfer Coefficient Determined	Remarks
38	Hall and Jenkins (1955) (sodium data)	Double-annulus, countercurrent	Sodium in both annuli	Low carbon steel	480 L/D (Based on hyd. dia. of inner annulus)	UHF	Overall average	Flowrates in tube and annulus were equal for all runs. Good agreement with theory for round tubes. No difference between heat transfer coefficients for Na and NaK was found.
38	Hall and Jenkins (1955) (NaK data)	Double-annulus, countercurrent	NaK in both annuli	Stainless steel	120 L/D (Based on hyd. dia. of inner annulus)	UHF	Overall average	Flowrates in tube and annulus were equal for all runs. Good agreement with theory for round tubes. No difference between heat transfer coefficients for Na and NaK was found.
39	Brown et al. (1957)	Double-pipe, countercurrent	Hg in tube, H_2O in annulus	Nickel	150 L/D	UHF	Local, fully developed	Velocity and temperature distributions were measured and used to calculate eddy diffusivities. Heat transfer measurements showed fair agreement with theory.
40	Baker and Sesonske (1960)	Double-pipe, countercurrent	NaK in tube and annulus	Stainless steel	88 L/D	UHF and variable heat flux	Overall average	Data show excellent agreement with theory for uniform heat flux. No difference was noted for different flowrates in each channel, due probably to the fact that the flowrate ratio did not vary significantly.
41	Andreev and Kalachev (1963)	Double-pipe		Carbon steel and stainless steel	50-60 L/D		Average	Heat transfer fluids were continuously cleaned during experiment. Data show excellent agreement with theory.
	Test Sec. 1		Heavy metal in tube to boiling water in annulus			UWT		
	Test Sec. 2		Heavy metal to heavy metal			UHF		
42	Kokorev and Ryapasov (1963)	Double-pipe, countercurrent	Mercury in tube, water in annulus	Stainless steel	65 L/D	UHF	Local, average	Nusselt numbers were calculated from a graphical integration of temperature profile data. Results show satisfactory agreement with theory.
43	Sawochka and Schleef (1964)	Double-pipe, cocurrent	Potassium in tube, sodium in annulus	Stainless steel	58 L/D	Uncertain	Local, fully developed	Heat transfer coefficients were measured by inserting thermocouples at different radial locations in the thick-walled tube. Data were lower than that predicted by theory.
23	Merriam (1965)	Double-pipe, cocurrent	Hg in tube and annulus	Nickel		Variable	Local, fully developed	Refer to detailed discussion.
	Test Sec. 1				20 L/D			
	Test Sec. 2				10 L/D			
	Test Sec. 3				8 L/D			
44	Awad (1965)	Double-pipe, condenser	NaK in tube, steam in annulus	Brass and constantan and copper	48 L/D	UWT	Local, fully developed	Local heat fluxes were calculated from radial temperature measurements in the double-cladded copper tube and used to predict local Nusselt numbers. Fully developed Nusselt numbers were calculated from detailed fluid temperature measurements at a station 44 L/D from the entrance of the tube. The data show good agreement with theory.

developed portion of the thermal field. The fully developed overall Nusselt number was proportional to the slope of this linear portion of the curve. The method also revealed over what portion of the heat exchanger the heat transfer was fully developed. Heat transfer coefficients in individual channels were measured by inserting a single thermocouple at the inner wall at a specified radial location at the exit end of the heat exchanger. By use of the heat flux calculated from the overall coefficient, the inside-wall temperatures could then be computed. Bulk-fluid measurements were made at the exit of the test section, and used with the heat flux and inside-wall temperatures to calculate the fully developed heat transfer coefficients of individual channels. Experimental values of heat-exchanger efficiency were calculated from the mercury flowrates and inlet and outlet bulk temperatures.

Inaccuracies in the data were due mainly to extraneous heat transfer through the nickel end plates of the heat exchanger. This end-conduction effect was so pronounced in the 10-L/D test section that all the data taken were discarded. The end plates of the 20-L/D test section were then modified to reduce the conduction effect. The data taken from the 20-L/D test section were considerably better than those from the 10-L/D section. The 8-L/D test section was constructed with stainless steel end plates, and the end-conduction effect virtually disappeared.

Merriam compared his experimental results with his exact analytical solution and with solutions using the traditional method. Although there was some scatter in the data, clearly defined trends could be discerned which supported the contention that the traditional method can lead to inaccuracies when applied to liquid metals.

D. Thermal-contact Resistance

Early experimental investigations of heat transfer to liquid metals yielded consistently lower results than predicted by theory. Attempts to explain this phenomena led experimenters to conclude that there existed a thermal-contact resistance between the heat-transfer surface and the liquid metal. Four separate explanations were offered to explain the existence of this contact resistance.

1. The thermal-contact resistance was due to a lack of wetting of the heat-transfer surface by the liquid metal.

2. An oxide or gas layer on the heat transfer surface increased the resistance to heat flux.

3. The presence of entrained gas in the liquid metal itself caused a reduction in the thermal conductivity of the liquid metal.

4. Local detachments of the flowing liquid metal from the heat transfer surface caused a reduction in heat transfer.

The most universally accepted explanation for the contact resistance is the first, namely, the "wetting" theory. Authors who reported a difference in heat transfer rates between a wetted and an unwetted system are Doody and Younger,[35] Untermeyer,[46] and Seban.[33] However, Trefethen[34] and Lubarsky[36] reported no difference in heat transfer between a wetted and an unwetted system. The above conflicting viewpoints may be reconciled by a consideration of the second explanation, the "surface film" theory. English and Barrett[47] believed that the use of additives to heat-transfer fluids in order to promote wetting actually caused a breakdown of oxides on the test-section walls. Also, the only essential difference between wetted and unwetted systems is that in unwetted systems a surface "dirt" film could impede heat transfer, whereas in a wetted system the heat transfer surface is being continually washed and cleaned by the flowing fluid. If care is taken to keep impurities out of a heat transfer system, then whether a system is wetted or not should have no effect on the heat transfer. Further support for this theory may be found by noting that in experiments which reported differences between wetted and unwetted systems, no precautions were taken to keep the system clean, whereas for experiments in which these precautions were taken, no difference was found.

The third explanation, the gas entrainment theory, was advanced by MacDonald and Quittenton[48] in a review of the effect of wetting in heat transfer experiments with liquid metals. They suggested that heat transfer in liquid metal systems could be impeded by the presence of gas entrained in the liquid metal itself. The authors stated that the gas would have to be in the shape of elongated or "flat" bubbles in order to have a noticeable effect on heat transfer. Calculations were presented which showed that the presence of 0.1% of gas by volume in the liquid metal could reduce heat transfer coefficients by as much as 40%.

The fourth explanation, "local detachment theory," was advanced by Stromquist[49] after he observed small transient cavities between a flowing liquid metal and a glass tube. The cavities were seen in both wetting and nonwetting systems. The conclusion was that the cavities were random detachments of the liquid metal from the tube wall. Stromquist rejected the idea that the cavities were actually pockets of gas adhering to the test-section wall.

Chelmer[50] observed local cavities similar to those of Stromquist, but concluded that they were actually bubbles of gas entrained in the system. He concluded that gas entrainment can seriously affect the performance of a liquid-metal heat transfer system due to the adverse effect on the thermal conductivity of the liquid metal.

An experimental analysis of the thermal contact resistance between stationary mercury and steel was made by Bonilla and Wang.[51] It was reported that wetting did not significantly change the contact resistance.

Mizushina et al.,[52] investigated the thermal-contact resistance between stationary mercury and nickel, copper, and chromium-plated copper surfaces. A slight thermal resistance between the nickel and chromium-plated surfaces and mercury was noted. No contact resistance was noted with copper.

The preceding investigations suggest that the prime factor governing the existence of a thermal-contact resistance is the cleanliness of the heat transfer system. Wetting alone does not seem to have an effect on heat transfer. Wetting systems, however, are to be preferred to nonwetting systems due to their self-cleaning feature. The heat transfer fluid must be isolated from gas sources in order to reduce sources of error due to gas entrainment. The local detachment theory probably is incorrect. Cavitation in a smooth channel at the moderate velocities occurring in liquid metal heat exchangers is improbable. The "local detachments" observed by Stromquist were probably gas bubbles as observed by Chelmer.

E. Special Topics in the Use of Mercury in Heat Transfer Systems

1. Wetting of Materials by Mercury

It is generally accepted that pure mercury will not wet steel surfaces, wets nickel slightly, and readily wets copper. The addition of small amounts of sodium, magnesium, or titanium to mercury will promote wetting even on steel surfaces. Most of the experiments listed in Table 2.2 used mercury with steel or nickel heat exchangers. Mercury and copper have been used in heat transfer experiments in Refs. 34, 53, and 54. In all of the experiments with mercury and copper, wetting was easily obtained.

2. Corrosion of Materials by Mercury

The Liquid Metals Handbook[55] lists mercury as mildly corrosive to ferrous metals in dynamic systems and highly corrosive to nonferrous metals in both static and dynamic systems. Experiments with mercury in contact with stainless or low carbon steel (see Refs. 37, 38, and 40) report little or no effect due to corrosion of the heat transfer surfaces by the mercury. Experiments with mercury and copper (see Refs. 34, 53, and 54) indicate that, for short-term use, mercury does not attack copper enough to cause an error in heat transfer results. Mercury amalgamates the copper surface, and, in dynamic systems, the amalgam is washed off. In long-term use, the continual amalgamation and washing of the mercury surface could cause serious eroding of the heat transfer surface.

CHAPTER III

MATHEMATICAL ANALYSIS

The analysis to be presented follows that of Stein[17]. Stein's analysis considered both cocurrent and countercurrent flow, various symmetrical-duct geometries, and was generalized to include both laminar and turbulent flow. Initially, Stein attempted to use the Nunge-Gill procedure[19] to calculate the expansion coefficients for the countercurrent case, but was unsuccessful. A more successful alternative procedure, discovered by the author, was used for computations. Application of Stein's analysis was somewhat limited since only a few numerical results for a narrow, annular-space heat exchanger were presented. The present analysis considers both narrow and nonnarrow annular-space heat exchangers in detail.

A. General Case

1. Model

The system to be analyzed is a counter-flow double-pipe heat exchanger consisting of tube and concentric annulus. The heat-exchanger fluids enter at opposite ends of the heat exchanger and flow parallel to one another, transferring heat through the separating tube wall. The model for the heat exchanger is illustrated in Fig. 3.1.

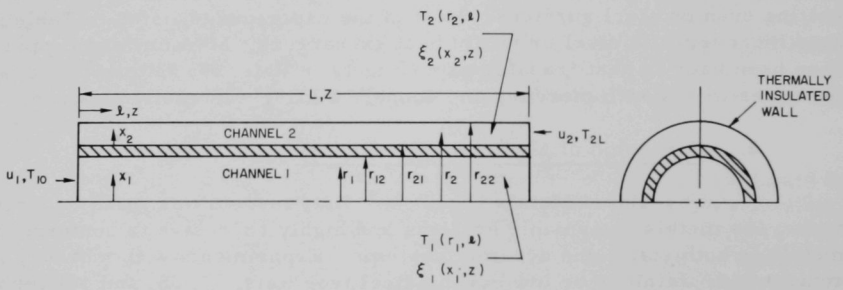

Fig. 3.1. Heat-exchanger Configuration

2. Assumptions

The assumptions upon which the analysis is based are as follows:

1) The fluids enter the heat exchanger at uniform temperature.

2) Physical properties are independent of temperature.

3) Frictional heating is negligible.

4) Axial heat conduction within the heat-exchanger walls is negligible.

5) Axial heat conduction within the heat-exchanger fluids is negligible.

6) The velocity distribution of the fluids is independent of axial position (i.e., fully developed) and is a known function of the radial coordinate.

7) The heat exchanger is in steady-state operation.

The first four assumptions are nearly always attainable in actual physical systems. The fifth assumption is nearly always valid for turbulent flow of nonmetallic fluids and is usually considered valid for turbulent flow of liquid metals when the Peclet number is larger than 100. Assumption six may be attained by including flow-development sections for the heat-exchanger fluids prior to their entering the heat exchanger. The velocity profiles may be expressed by an appropriate relation, such as the well-known parabolic distribution for laminar flow or an empirical relation for turbulent flow.

3. Governing Equations

Based on the above model and assumptions, the equation of energy conservation for the heat-exchanger fluids is

Tube:

$$\frac{1}{r_1}\frac{\partial}{\partial r_1}\left[\left(1+\frac{\epsilon_{H1}}{\alpha_1}\right) r_1 \frac{\partial T_1(r_1,\ell)}{\partial r_1}\right] = \frac{1}{\alpha_1} u_1(r_1) \frac{\partial T_1(r_1,\ell)}{\partial \ell}; \tag{3.1a}$$

Annulus:

$$\frac{1}{r_2}\frac{\partial}{\partial r_2}\left[\left(1+\frac{\epsilon_{H2}}{\alpha_2}\right) r_2 \frac{\partial T_2(r_2,\ell)}{\partial r_2}\right] = \frac{1}{\alpha_2}[-u_2(r_2)] \frac{\partial T_2(r_2,\ell)}{\partial \ell}. \tag{3.1b}$$

The above equations are valid for both laminar and turbulent flow, and have the following boundary conditions.

Entrance:

$$T_1(r_1,0) = T_{10} \quad \text{(constant)}; \tag{3.1c}$$

$$T_2(r_2,L) = T_{2L} \quad \text{(constant)}; \tag{3.1d}$$

Interior:

Tube centerline:

$$\frac{\partial T_1(0,\ell)}{\partial r_1} = 0; \tag{3.1e}$$

Continuity of heat flux across inner wall:

$$r_{12}k_1 \frac{\partial T_1(r_{12},\ell)}{\partial r_1} = r_{21}k_2 \frac{\partial T_2(r_{21},\ell)}{\partial r_2}; \tag{3.1f}$$

Simple conduction of heat across inner wall:

$$-r_{12}k_1 \frac{\partial T_1(r_{12},\ell)}{\partial r_1} = \frac{k_w}{\ell n\left(\frac{r_{21}}{r_{12}}\right)}[T_1(r_{12},\ell) - T_2(r_{21},\ell)]; \tag{3.1g}$$

Insulated outer wall:

$$\frac{\partial T_2(r_{22},\ell)}{\partial r_2} = 0. \tag{3.1h}$$

4. Dimensionless Formulation

The governing equations may be transformed into dimensionless form by introducing the following dimensionless variables:

$$x_1 = r_1/r_{12}, \quad 0 \le x_1 \le 1; \tag{3.2a}$$

$$x_2 = \frac{r_2 - r_{21}}{r_{22} - r_{21}}, \quad 0 \le x_2 \le 1; \tag{3.2b}$$

$$z = \frac{4}{Pe_1}\frac{\ell}{2r_{12}}, \quad 0 \le z \le Z; \tag{3.2c}$$

$$\xi_i(x_i,z) = \frac{T_i(r_i,\ell) - T_{10}}{T_{2L} - T_{10}}, \quad 0 \le \xi_i \le 1, \quad i = 1,2. \tag{3.2d}$$

In terms of these dimensionless variables, the governing equations become:

Tube:

$$\frac{1}{x_1}\frac{\partial}{\partial x_1}\left[f_1(x_1)\, x_1 \frac{\partial \xi_1(x_1,z)}{\partial x_1}\right] = g_1(x_1)\frac{\partial \xi_1(x_1,z)}{\partial z}; \tag{3.3a}$$

Annulus:

$$\frac{1}{x_2 + \sigma} \frac{\partial}{\partial x_2}\left[f_2(x_2)(x_2 + \sigma) \frac{\partial \xi_2(x_2,z)}{\partial x_2}\right] = -g_2(x_2)\, \omega^2 \frac{\partial \xi_2(x_2,z)}{\partial z}. \tag{3.3b}$$

The boundary conditions become:

Entrance:

$$\xi_1(x_1,0) = 0; \tag{3.3c}$$

$$\xi_1(x_2,Z) = 1; \tag{3.3d}$$

Interior:

$$\frac{\partial \xi_1(0,z)}{\partial x_1} = 0; \tag{3.3e}$$

$$K \frac{\partial \xi_1(1,z)}{\partial x_1} = \frac{\partial \xi_2(0,z)}{\partial x_2}; \tag{3.3f}$$

$$K_w \frac{\partial \xi_1(1,z)}{\partial x_1} + \xi_1(1,z) = \xi_2(0,z); \tag{3.3g}$$

$$\frac{\partial \xi_2(1,z)}{\partial x_2} = 0, \tag{3.3h}$$

where

$$f_i(x_i) = 1 + \frac{\epsilon_{Hi}}{\alpha_i}; \tag{3.4}$$

$$g_i(x_i) = \frac{u_i(x_i)}{u_{i_{AV}}}; \tag{3.5}$$

$$\omega^2 = \frac{HKR}{1 + R}; \tag{3.6}$$

$$\sigma = \frac{R}{1 - R}. \tag{3.7}$$

The solution of Eqs. (3.3a) and (3.3b) is a function of five basic dimensionless parameters: H, K, K_w, R, and Z. Also required are the

functions $f_i(x_i)$ and $g_i(x_i)$, where $g_i(x_i)$ is determined by the duct Reynolds number, and $f_i(x_i)$ is determined by both Prandtl and Reynolds numbers. The values of these parameters for a specific heat exchanger determine what will be called "the operating conditions of the heat exchanger."

In terms of physical quantities, the parameters are

$H = c_2W_2/c_1W_1$ - heat capacity-flowrate ratio;

$K = \frac{k_1}{k_2}\frac{1 - R}{R}$ - relative thermal resistance of fluid;

$K_w = \frac{k_1}{k_w} \ell n \frac{r_{21}}{r_{12}}$ - relative thermal resistance of wall;

$R = r_{21}/r_{22}$ - annular radius ratio;

$z = \frac{4}{Pe_1}\frac{\ell}{2r_{12}}$ - dimensionless axial length;

$f_i(x_i) = 1 + \frac{\epsilon_{Hi}}{\alpha_i}$ - "total" conductivity relative to molecular conductivity;

$g_i(x_i) = u_i(x_i)/u_{i_{AV}}$ - dimensionless local velocity.

5. Solution of Governing Equations

Separation of variables, applied to Eqs. 3.3a) and (3.3b), leads to a solution involving a special case of the classical Sturm-Liouville problem. In this special case an infinite number of negative as well as positive eigenvalues exist and must be included in the solution. The existence of the negative eigenvalues arises from the fact that the velocity changes sign at the inner wall of the heat exchanger. Details of the analysis are given in Appendix A. It must be pointed out that the solution given here is not directly applicable to the case for which the heat capacity-flowrate ratio, H, is unity. When H = 1, an indeterminate mathematical form appears in some of the terms of the solution and must be dealt with in another manner. Stein[28] has very recently presented a solution for the case of H = 1, in which he takes the limit of the indeterminate terms as $H \to 1$ from both above and below unity. A more detailed discussion of Ref. 28 was included in the literature survey. The case H = 1 is not considered in this thesis.

a. Temperature Distribution

The solution for the temperature distribution of the heat-exchanger fluids may be written in the form

$$\xi_1(x_1,z) = C_0 + \sum_{n=1}^{\infty}\left[A_n\tilde{E}_{1,n}(x_1)\, e^{-\beta_n^2(Z-z)} + C_nE_{1,n}(x_1)\, e^{-\lambda_n^2 z}\right]; \qquad (3.8a)$$

$$\xi_2(x_2,z) = C_0 + \sum_{n=1}^{\infty}\left[A_n\tilde{E}_{2,n}(x_2)\, e^{-\beta_n^2(Z-z)} + C_nE_{2,n}(x_2)\, e^{-\lambda_n^2 z}\right], \qquad (3.8b)$$

where

λ_n^2 - nth positive eigenvalue;

β_n^2 - absolute value of nth negative eigenvalue;

$E_{i,n}(x_i)$ - normalized eigenfunction in stream i associated with nth positive eigenvalue;

$\tilde{E}_{i,n}(x_i)$ - normalized eigenfunction in stream i associated with nth negative eigenvalue;

C_n - expansion coefficient associated with nth positive eigenvalue;

A_n - expansion coefficient associated with nth negative eigenvalue.

b. Eigenvalue Equation

The eigenvalues λ_n^2 and β_n^2 are the squares of the positive roots of the equations

$$\psi(\lambda) = 0; \qquad (3.9a)$$

$$\tilde{\psi}(\beta) = 0, \qquad (3.9b)$$

where

$$\psi(\lambda) = K_w \frac{dG(0,\lambda)}{dx_2}\frac{dF(1,\lambda)}{dx_1} + \frac{dG(0,\lambda)}{dx_2}F(1,\lambda) - K\frac{dF(1,\lambda)}{dx_1}G(0,\lambda) \qquad (3.10a)$$

and

$$\tilde{\psi}(\beta) = K_w \frac{d\tilde{G}(0,\beta)}{dx_2}\frac{d\tilde{F}(1,\beta)}{dx_1} + \frac{d\tilde{G}(0,\beta)}{dx_2}\tilde{F}(1,\beta) - K\frac{d\tilde{F}(1,\beta)}{dx_1}\tilde{G}(0,\beta) \qquad (3.10b)$$

The above functions, $\tilde{F}$, F, G, and $\tilde{G}$, are defined by Eqs. (3.13) to (3.16).

c. The Eigenfunctions

The normalized eigenfunctions $\tilde{E}_{i,n}(x_i)$ and $E_{i,n}(x_i)$ are given by the following equations:

$$E_{1,n}(x_1) = \frac{\dfrac{dG(0,\lambda_n)}{dx_2} F(x_1,\lambda_n)}{\sqrt{|N_n|}}; \tag{3.11a}$$

$$\tilde{E}_{1,n}(x_1) = \frac{\dfrac{d\tilde{G}(0,\beta_n)}{dx_2} \tilde{F}(x_1,\beta_n)}{\sqrt{|\tilde{N}_n|}}; \tag{3.11b}$$

$$E_{2,n}(x_2) = \frac{K\dfrac{dF(1,\lambda_n)}{dx_1} G(x_2,\lambda_n)}{\sqrt{|N_n|}}; \tag{3.11c}$$

$$\tilde{E}_{2,n}(x)_2 = \frac{K\dfrac{d\tilde{F}(1,\beta_n)}{dx_1} \tilde{G}(x_2,\beta_n)}{\sqrt{|\tilde{N}_n|}}; \tag{3.11d}$$

$$N_n = \left[\frac{dG(0,\lambda_n)}{dx_2}\right]^2 B_1\{[F(x_1,\lambda_n)]^2\} - HK^2\left[\frac{dF(1,\lambda_n)}{dx_1}\right]^2 B_2\{[G(x_2,\lambda_n)]^2\}; \tag{3.12a}$$

$$\tilde{N}_n = \left[\frac{d\tilde{G}(0,\beta_n)}{dx_2}\right]^2 B_1\{[\tilde{F}(x_1,\beta_n)]^2\} - HK^2\left[\frac{d\tilde{F}(1,\beta_n)}{dx_1}\right]^2 B_2\{[\tilde{G}(x_2,\beta_n)]^2\};$$

$$n = 1,2,3, \ldots, \tag{3.12b}$$

where the notation $B_i\{\ \}$, indicates a "mixing cup" or bulk average as defined by Eqs. (3.22a) and (3.22b) in Section 6.a.

The functions F, $\tilde{F}$, G, and $\tilde{G}$ are the solutions of the following initial-value problems:

$$\frac{d}{dx_1}\left[f_1(x_1)\, x_1 \frac{dF(x_1,\lambda)}{dx_1}\right] + \lambda^2 x_1 g_1(x_1)\, F(x_1,\lambda) = 0; \tag{3.13a}$$

$$\frac{dF(0,\lambda)}{dx_1} = 0; \qquad F(0,\lambda) = 1; \tag{3.13b}$$

$$\frac{d}{dx_2}\left[f_2(x_2)(x_2+\sigma)\,\frac{dG(x_2,\lambda)}{dx_2}\right] - \lambda^2\omega^2 g_2(x_2)(x_2+\sigma)\,G(x_2,\lambda) = 0; \tag{3.14a}$$

$$\frac{dG(1,\lambda)}{dx_2} = 0; \qquad G(1,\lambda) = 1; \tag{3.14b}$$

$$\frac{d}{dx_1}\left[f_1(x_1)\,x_1\,\frac{d\tilde{F}(x_1,\beta)}{dx_1}\right] - \beta^2 x_1 g_1(x_1)\,\tilde{F}(x_1,\beta) = 0; \tag{3.15a}$$

$$\frac{d\tilde{F}(0,\beta)}{dx_1} = 0; \qquad \tilde{F}(0,\beta) = 1; \tag{3.15b}$$

$$\frac{d}{dx_2}\left[f_2(x_2)(x_2+\sigma)\,\frac{d\tilde{G}(x_2,\beta)}{dx_2}\right] + \beta^2\omega^2 g_2(x_2)(x_2+\sigma)\,\tilde{G}(x_2,\beta) = 0; \tag{3.16a}$$

$$\frac{d\tilde{G}(1,\beta)}{dx_2} = 0; \qquad \tilde{G}(1,\beta) = 1. \tag{3.16b}$$

d. Expansion Coefficients

The expansion coefficients A_n and C_n are defined by the following infinite set of linear algebraic equations:

$$\sum_{k=1}^{\infty}\left[B_1\{\tilde{E}_{1,n}(x_1)\,\tilde{E}_{1,k}(x_1)\}\left(1-e^{-\beta_k^2 Z}\right)A_k - B_1\{\tilde{E}_{1,n}(x_1)\,E_{1,k}(x_1)\}\left(1-e^{-\lambda_k^2 Z}\right)C_k\right] = B_1\{\tilde{E}_{1,n}(x_1)\}; \tag{3.17a}$$

$$\sum_{k=1}^{\infty}\left[-B_1\{E_{1,n}(x_1)\,\tilde{E}_{1,k}(x_1)\}\left(1-e^{-\beta_k^2 Z}\right)A_k + B_1\{E_{1,n}(x_1)\,E_{1,k}(x_1)\}\left(1-e^{-\lambda_k^2 Z}\right)C_k\right] = -B_1\{E_{1,n}(x_1)\}, \tag{3.17b}$$

with

$$n = 1,2,3,\ldots,$$

and for the zeroth-order coefficient:

$$C_0 = \frac{1}{N_0}\left\{\sum_{k=1}^{\infty}\left[B_1\{\tilde{E}_{1,k}(x_1)\}\left(1 - e^{-\beta_k^2 Z}\right)A_k - B_1\{E_{1,k}(x_1)\}\left(1 - e^{-\lambda_k^2 Z}\right)C_k\right]\right\} - \frac{H}{N_0}, \tag{3.18}$$

where

$$N_0 = 1 - H. \tag{3.19}$$

The solution of the above system of algebraic equations is accomplished by truncating the higher-ordered terms and equations, and then solving the remaining finite set of equations. Nunge and Gill[19,20] used a similar set of equations to compute expansion coefficients for a laminar-flow heat exchanger. The difference between their procedure and the present one is in the form of the infinite set of equations. The present formulation yields a set of equations whose coefficient matrix has off-diagonal elements which approach zero as the order is increased, and diagonal elements which approach unity as the order is increased. In the coefficient matrix of the Nunge-Gill set of equations, all of the elements approach infinity as the order is increased. Because of the magnitude of the coefficients in the Nunge-Gill formulation, the set of equations is ill-conditioned for computation, since it is necessary to do computations with numbers which become unmanageably large. The present procedure, on the other hand, results in a set of equations which is well-conditioned for computations, since the computations are performed with matrix elements whose magnitudes do not vary significantly. The computational procedure used to calculate the expansion coefficients will be discussed in a later section.

6. Definitions

a. Bulk or "Mixing-cup" Averages

The bulk or mixing-cup average of quantity, indicated by the bulk average operator $B_i\{\}$, is defined as:

Tube:

$$B_1\{\} = \frac{\int_0^{r_{12}} u_1(r_1)\{\}r_1\,dr_1}{\int_0^{r_{12}} u_1(r_1)r_1\,dr_1}; \tag{3.20}$$

Annulus:

$$B_2\{\ \} = \frac{\int_{r_{21}}^{r_{22}} u_2(r_2)\{\ \} r_2\, dr_2}{\int_{r_{21}}^{r_{22}} u_2(r_2) r_2\, dr_2}. \tag{3.21}$$

Expressed in the dimensionless form, the above expressions become:

Tube:

$$B_1\{\ \} = 2\int_0^1 g_1(x_1)\{\ \} x_1\, dx_1; \tag{3.22a}$$

Annulus:

$$B_2\{\ \} = \frac{2}{1 + 2\sigma}\int_0^1 g_2(x_2)\{\ \}(x_2 + \sigma)\, dx_2. \tag{3.22b}$$

Application of the bulk average operator to a temperature distribution results in the bulk temperature, indicated by an overscore:

$$B_i\{\xi_i(x_i, z)\} = \overline{\xi}_i(z).$$

b. General Heat Balance

A heat balance applied to the heat exchanger at any point along its length yields the following bulk-temperature relationship:

$$\overline{\xi}_1(z) = H[\overline{\xi}_2(z) - \overline{\xi}_2(0)]; \tag{3.23}$$

at $z = Z$,

$$\overline{\xi}_1(Z) = H[1 - \overline{\xi}_2(0)]. \tag{3.24}$$

By expressing the bulk temperatures in terms of the series solution, Eqs. (3.8a) and (3.8b), and applying the orthogonality condition (see Appendix A), the following may be derived:

$$\overline{\xi}_1(z) - H\overline{\xi}_2(z) = (1 - H)\, C_0. \tag{3.25}$$

At the ends of the heat exchanger, the above equation becomes

$$\overline{\xi}_1(Z) = (1 - H)\, C_0 + H; \tag{3.26}$$

$$\bar{\xi}_2(0) = \frac{H - 1}{H} C_0. \tag{3.27}$$

c. Heat-exchanger Efficiency

The efficiency of a counter-flow heat exchanger is defined as the ratio of actual heat transferred to that which would be transferred if the heat exchanger were infinitely long:

$$\text{actual heat transferred} = c_1 W_1[T_{10} - \bar{T}_1(L)]$$

$$= c_2 W_2[\bar{T}_2(0) - T_{2L}];$$

$$\text{heat transferred for infinite length} = (c_i W_i)_{min}[T_{10} - T_{2L}].$$

The ratio of the preceding quantities yields

$H < 1$:

$$\epsilon = \frac{\bar{\xi}_1(Z)}{H} = 1 - \bar{\xi}_2(0). \tag{3.28a}$$

$H > 1$:

$$\epsilon = \bar{\xi}_1(Z) = H[1 - \bar{\xi}_2(0)], \tag{3.28b}$$

or, using Eqs. (3.26) and 3.27),

$H < 1$:

$$\epsilon = \frac{1 - H}{H} C_0 + 1; \tag{3.29a}$$

$H > 1$:

$$\epsilon = (1 - H) C_0 + H. \tag{3.29b}$$

As $Z \to \infty$; $\epsilon \to 1$, so, from Eqs. (3.28a), (3.28b), (3.29a), and (3.29b),

$H < 1$:

$$Z \to \infty: \bar{\xi}_1(Z) \to H; \ \bar{\xi}_2(0) \to 0; \ C_0 \to 0; \tag{3.30a}$$

H > 1:

$$Z \to \infty: \ \overline{\xi}_1(Z) \to 1; \ \overline{\xi}_2(0) \to \frac{H - 1}{H}; \ C_0 \to 1. \tag{3.30b}$$

The series expansion for the end bulk temperatures may be written:

$$\overline{\xi}_1(Z) = C_0 + \sum_{n=1}^{\infty} \left[A_n B_1\{\tilde{E}_{1,n}(x_1)\} + C_n B_1\{E_{1,n}(x_1)\} \, e^{-\lambda_n^2 Z} \right] \tag{3.31a}$$

and

$$\overline{\xi}_2(0) = C_0 + \sum_{n=1}^{\infty} \left[A_n B_2\{\tilde{E}_{2,n}(x_2)\} \, e^{-\beta_n^2 Z} + C_n B_2\{E_{2,n}(x_2)\} \right]. \tag{3.31b}$$

Letting $Z \to \infty$ and applying Eq. (3.30a) to Eq. (3.31b) and Eq. (3.30b) to Eq. (3.31a) gives

H < 1:

$$Z \to \infty: \ \sum_{n=1}^{\infty} C_n B_2\{E_{2,n}(x_2)\} \to 0; \tag{3.32a}$$

H > 1:

$$Z \to \infty: \ \sum_{n=1}^{\infty} A_n B_1\{\tilde{E}_{1,n}(x_1)\} \to 0. \tag{3.32b}$$

These equations reveal little about the individual behavior of the coefficients A_n and C_n as $Z \to \infty$. However, computations have revealed that the terms in each of the above summations are identical in sign for all values of n; therefore, since the summations approach zero as $Z \to \infty$,

H < 1:

$$C_n \to 0 \text{ as } Z \to \infty; \tag{3.32c}$$

H > 1:

$$A_n \to 0 \text{ as } Z \to \infty. \tag{3.32d}$$

d. Heat Transfer Coefficients

(1) Local Coefficients

Local heat transfer coefficients, based on wall to bulk fluid temperature differences, may be defined as follows:

Tube:

$$h_1(\ell) = \frac{q_1(\ell)}{\overline{T}_1(\ell) - T_1(r_{12},\ell)}; \tag{3.33a}$$

Annulus:

$$h_2(\ell) = \frac{q_2(\ell)}{T_2(r_{21},\ell) - \overline{T}_2(\ell)}. \tag{3.33b}$$

In dimensionless form the above equations may be expressed as Nusselt numbers:

Tube:

$$Nu_1(z) = \frac{-2\dfrac{\partial\xi_1(1,z)}{\partial x_1}}{\overline{\xi}_1(z) - \xi_1(1,z)}; \tag{3.34a}$$

Annulus:

$$Nu_2(z) = \frac{-2\dfrac{\partial\xi_2(0,z)}{\partial x_2}}{\xi_2(0,z) - \overline{\xi}_2(z)}. \tag{3.34b}$$

Energy conservation gives an alternative form of the above equations.

Tube:

$$Nu_1(z) = \frac{-\dfrac{d\overline{\xi}_1(z)}{dz}}{\overline{\xi}_1(z) - \xi_1(1,z)}; \tag{3.35a}$$

Annulus:

$$Nu_2(z) = \frac{-HK\dfrac{d\overline{\xi}_2(z)}{dz}}{\xi_2(0,z) - \overline{\xi}_2(z)}. \tag{3.35b}$$

An overall or "combined" heat transfer coefficient, based on tube properties, may also be defined:

Overall:

$$U(\ell) = \frac{q_1}{\overline{T}_1(\ell) - \overline{T}_2(\ell)} \tag{3.36}$$

In dimensionless form, the above equation becomes

$$Nu_1^o(z) = \frac{-2\dfrac{\partial \xi_1(1,z)}{\partial x_1}}{\overline{\xi}_1(z) - \overline{\xi}_2(z)}, \tag{3.37}$$

or alternatively,

$$Nu_1^o(z) = \frac{-\dfrac{d\overline{\xi}_1(z)}{dz}}{\overline{\xi}_1(z) - \overline{\xi}_2(z)}. \tag{3.38}$$

The tube, annulus, and overall Nusselt numbers are related by the familiar additive resistance relationship:

$$\frac{1}{Nu_1^o(z)} = \frac{1}{Nu_1(z)} + \frac{K_w}{2} + \frac{K}{Nu_2(z)}. \tag{3.39}$$

(2) Fully Developed Coefficients

For long heat exchangers, Eqs. (3.32c) and (3.32d) may be substituted into the series expansion for the temperature distribution of the heat exchanger fluids:

$H < 1$:

$$\xi_1(x_1,z) \approx C_0 + \sum_{n=1}^{\infty} A_n \tilde{E}_{1,n}(x_1)\, e^{-\beta_n^2(Z-z)}; \tag{3.40a}$$

$$\xi_2(x_2,z) \approx C_0 + \sum_{n=1}^{\infty} A_n \tilde{E}_{2,n}(x_2)\, e^{-\beta_n^2(Z-z)}; \tag{3.40b}$$

H > 1:

$$\xi_1(x_1,z) \approx C_0 + \sum_{n=1}^{\infty} C_n E_{1,n}(x_1)\, e^{-\lambda_n^2 z}; \tag{3.40c}$$

$$\xi_2(x_2,z) \approx C_0 + \sum_{n=1}^{\infty} C_n E_{2,n}(x_2)\, e^{-\lambda_n^2 z}. \tag{3.40d}$$

The fully developed region of heat transfer is defined as that portion of the heat exchanger where the heat transfer coefficient is independent of axial position. For this fully developed region, only the first term of the above series is needed to calculate the temperature distribution, since the higher-order exponential terms become negligible small. Depending on the operating conditions of the heat exchanger, the fully developed region may occur only in the middle or may extend to either end of the heat exchanger. For small Z, of course, a fully developed region may not exist at all.

For the fully developed region,

H < 1:

$$\xi_1(x_1,z) \approx C_0 + A_1 \tilde{E}_{1,1}(x_1)\, e^{-\beta_1^2 (Z-z)}; \tag{3.41a}$$

$$\xi_2(x_2,z) \approx C_0 + A_1 \tilde{E}_{2,1}(x_2)\, e^{-\beta_1^2 (Z-z)}; \tag{3.41b}$$

H > 1:

$$\xi_1(x_1,z) \approx C_0 + C_1 E_{1,1}(x_1)\, e^{-\lambda_1^2 z}; \tag{3.41c}$$

$$\xi_2(x_2,z) \approx C_0 + C_1 E_{2,1}(x_2)\, e^{-\lambda_1^2 z}. \tag{3.41d}$$

Using Eqs. (3.41a) to (3.41d) in Eqs. (3.35) and (3.38) yields expressions for the fully developed Nusselt numbers.

H < 1:

$$Nu_{1FD}^{\circ} = \frac{H}{1 - H}\beta_1^2; \tag{3.42a}$$

$$Nu_{1FD} = \frac{B_1\{\tilde{E}_{1,1}(x_1)\}}{\tilde{E}_{1,1}(1) - B_1\{\tilde{E}_{1,1}(x_1)\}}\beta_1^2; \tag{3.42b}$$

$$Nu_{2FD} = \frac{HKB_2\{\tilde{E}_{2,1}(x_2)\}}{B_2\{\tilde{E}_{2,1}(x_2)\} - \tilde{E}_{2,1}(0)} \beta_1^2 ; \tag{3.42c}$$

$H > 1$:

$$Nu_{1FD}^{\circ} = \frac{H}{H-1} \lambda_1^2 ; \tag{3.43a}$$

$$Nu_{1FD} = \frac{B_1\{E_{1,1}(x_1)\}}{B_1\{E_{1,1}(x_1)\} - E_{1,1}(1)} \lambda_1^2 ; \tag{3.43b}$$

$$Nu_{2FD} = \frac{HKB_2\{E_{2,1}(x_2)\}}{E_{2,1}(0) - B_2\{E_{2,1}(x_2)\}} \lambda_1^2 ; \tag{3.43c}$$

(3) Average Overall Coefficient

The "length average" overall Nusselt number is given by the relation:

$$Nu_{1AV}^{\circ}(Z) = \frac{1}{Z} \int_0^Z Nu_1^{\circ}(z)\, dz. \tag{3.44}$$

Equations (3.38) and (3.23) may be substituted into the above expression and the result integrated to give

$$Nu_{1AV}^{\circ}(Z) = \frac{H}{(1-H)\,Z} \ell n \frac{H(1 - \bar{\xi}_1(Z))}{[H - \bar{\xi}_1(Z)]}. \tag{3.45}$$

e. Effectiveness Coefficient

Equation (3.45) may be rearranged to give

$$\bar{\xi}_1(Z) = \frac{H\left[1 - e^{-\frac{H-1}{H} Nu_{1AV}^{\circ}(Z)\, Z}\right]}{H - e^{-\frac{H-1}{H} Nu_{1AV}^{\circ}(Z)\, Z}}. \tag{3.46}$$

Substitution of Eqs. (3.28a) and (3.28b) into the above yields the following relations for heat-exchanger efficiency:

H < 1:

$$\epsilon = \frac{1 - e^{-\frac{1-H}{H} Nu^{\circ}_{1AV}(Z)\, Z}}{1 - He^{-\frac{1-H}{H} Nu^{\circ}_{1AV}(Z)\, Z}}; \tag{3.47a}$$

H > 1:

$$\epsilon = \frac{H\left[1 - e^{-\frac{H-1}{H} Nu^{\circ}_{1AV}(Z)\, Z}\right]}{H - e^{-\frac{H-1}{H} Nu^{\circ}_{1AV}(Z)\, Z}}. \tag{3.47b}$$

The above expression is equivalent to that given by Kays and London.[56]

Equations (3.47a) and (3.47b) may be used to calculate heat-exchanger efficiencies if $Nu^{\circ}_{1AV}(Z)$ is known as a function of heat-exchanger length. In practical design computations, however, the assumption is often made that $Nu^{\circ}_{1AV}(Z) \approx Nu^{\circ}_{1FD}$, and Nu°_{1FD} is used in Eqs. (3.47a) and (3.47b) to calculate efficiencies. This assumption greatly simplifies the computations since Nu°_{1FD} is independent of heat-exchanger length, whereas $Nu^{\circ}_{1AV}(Z)$ is not. The assumption is subject to inaccuracies, particularly for short heat exchangers, since the fully developed coefficient does not account for the high heat fluxes occurring in the thermal-entrance regions of the heat exchanger.

A quantity called the "effectiveness coefficient," $\phi(Z)$, may be defined to account for the thermal-entrance region separately from the fully developed region:

H < 1:

$$\phi(Z) = e^{-\frac{1-H}{H}\left[Nu^{\circ}_{1AV}(Z) - Nu^{\circ}_{1FD}\right] Z}; \tag{3.48a}$$

H > 1:

$$\phi(Z) = e^{-\frac{H-1}{H}\left[Nu^{\circ}_{1AV}(Z) - Nu^{\circ}_{1FD}\right] Z}; \tag{3.48b}$$

$0 < \phi(Z) < 1.$

Substitution of the above equations into Eqs. (3.47a) and (3.47b) yields the following expressions for ϵ:

H < 1:

$$\epsilon = \frac{1 - \phi(Z)\, e^{-\frac{1-H}{H} Nu^{\circ}_{1FD} Z}}{1 - H\phi(Z)\, e^{-\frac{1-H}{H} Nu^{\circ}_{1FD} Z}}; \tag{3.49a}$$

H > 1:

$$\epsilon = \frac{H\left[1 - \phi(Z)\, e^{-\frac{H-1}{H} Nu^{\circ}_{1FD} Z}\right]}{H - \phi(Z)\, e^{-\frac{H-1}{H} Nu^{\circ}_{1FD} Z}}. \tag{3.49b}$$

The effectiveness coefficient must be calculated from known values of ϵ and Nu°_{1FD}. For sufficiently large Z, computations indicate that $\phi(Z)$ reaches an asymptotic or fully developed value ϕ_{FD}.

f. Number of Transfer Units

The quantity $Nu^{\circ}_{1AV}(Z)\, Z$ appears so often in the equations for heat-exchanger design that it has been given a name, "number of transfer units," and is designated by the symbol NTU. A discussion of the usefulness of NTU may be found in Ref. 56.

NTU is defined:

H < 1:

$$NTU = ZNu^{\circ}_{1AV}(Z)/H; \tag{3.50a}$$

H > 1:

$$NTU = ZNu^{\circ}_{1AV}. \tag{3.50b}$$

For the fully developed region, a fully developed NTU may be defined, based on Nu°_{1FD}, as follows:

H < 1:

$$NTU_{FD} = ZNu^{\circ}_{1FD}/H; \tag{3.51a}$$

H > 1:

$$NTU_{FD} = ZNu_{iFD}^{\circ} \tag{3.51b}$$

For long heat exchangers, NTU ≈ NTU_{FD}.

Short heat exchangers or heat exchangers with low heat transfer coefficients are characterized by small values of NTU, whereas long heat exchangers or heat exchangers with high heat transfer coefficients have large values of NTU. NTU therefore represents the "heat transfer size" of a heat exchanger.

B. Approximation for Turbulent Flow

The solution of Eqs. (3.13a) to (3.16a) for the functions F and G, necessary to compute the eigenfunctions, requires a knowledge of the functions $g_i(x_i)$ and $f_i(x_i)$. For turbulent flow, $g_i(x_i)$ and $f_i(x_i)$ must be computed from empirical relationships. An additional complication arises in the computation of $f_i(x_i)$, since a relationship between the eddy diffusivity of heat, ϵ_{H_i}, and that of momentum, ϵ_{M_i}, must usually be inferred from the analogy between heat and momentum transfer.

Once the functions $g_i(x_i)$ and $f_i(x_i)$ are determined, Eqs. (3.13a) to (3.16a) may be integrated numerically. For the simple case of a uniform velocity profile (plug flow), where $g_i(x_i) = f_i(x_i) = 1$, it is not necessary to resort to numerical techniques, however. A relatively simple expression in terms of known functions is obtained for F and G.

Generally speaking, heat transfer analyses made with a plug-flow model give results which are inaccurate in describing the physical phenomena for nonmetallic fluids and yield physically meaningful results for liquid metals only in the low Peclet number range (Pe < 50). This is due to the fact that, for liquid metals in the low Peclet number range, eddy conduction plays a minor role compared to molecular conduction in the transfer of heat and $f_i(x_i) = 1$. For liquid metals, steep temperature gradients are not localized near the duct wall so that the error resulting from using a uniform velocity, $g_i(x_i) = 1$, in this region is not significant. An approximation, introduced by Stein,[22] which extends the accuracy of the plug-flow model for liquid metals up to a Peclet number of 1000 will now be introduced.

1. k^+ Approximation

The following derivation follows the work presented in Refs. 16, 22, and 23.

a. Derivation

New radial variables, $x_i^+(x_i)$, will now be introduced such that

Tube:

$$\frac{1}{k_1^+}\frac{dx_1^+}{x_1^+} = \frac{1}{f_1(x_1)}\frac{dx_1}{x_1}; \tag{3.52a}$$

Annulus:

$$\frac{1}{k_2^+}\frac{dx_2^+}{(x_2^+ + \sigma)} = \frac{1}{f_2(x_2)}\frac{dx_2}{(x_2 + \sigma)}, \tag{3.52b}$$

where $x_i^+(0) = 0$ and the constants k_1^+ and k_2^+ are defined such that $x_i^+(1) = 1$.

A new dimensionless axial variable, $z^+(z)$, may also be defined:

$$z^+ = k_1^+ z. \tag{3.53}$$

Equations (3.3a) and (3.3b) in terms of the new space variables x_i^+ and z^+ are:

Tube:

$$\frac{1}{x_1^+}\frac{\partial}{\partial x_1^+}\left[x_1^+ \frac{\partial \xi_1(x_1^+, z^+)}{\partial x_1^+}\right] = g_1^+(x_1^+)\frac{\partial \xi_1(x_1^+, z^+)}{\partial z^+}; \tag{3.54a}$$

Annulus:

$$\frac{1}{(x_2^+ + \sigma)}\frac{\partial}{\partial x_2^+}\left[(x_2^+ + \sigma)\frac{\partial \xi_2(x_2^+, z^+)}{\partial x_2^+}\right] = \omega^2 \frac{k_1^+}{k_2^+} g_2^+(x_2^+)\frac{\partial \xi_2(x_2^+, z^+)}{\partial z^+}. \tag{3.54b}$$

The boundary conditions become:

Entrance:

$$\xi_1(x_1^+,0) = 0; \tag{3.54c}$$

$$\xi_2(x_2^+,Z^+) = 1. \tag{3.54d}$$

Interior:

$$\frac{\partial \xi_1(0,z^+)}{\partial x_1^+} = 0; \tag{3.54e}$$

$$K \frac{k_1^+}{k_2^+} \frac{\partial \xi_1(1,z^+)}{\partial x_1^+} = \frac{\partial \xi_2(0,z^+)}{\partial x_2^+}; \tag{3.54f}$$

$$K_w k_1^+ \frac{\partial \xi_1(1,z^+)}{\partial x_1^+} + \xi_1(1,z^+) = \xi_2(0,z^+); \tag{3.54g}$$

$$\frac{\partial \xi_2(1,z^+)}{\partial x_2^+} = 0, \tag{3.54h}$$

where

$$g_1^+(x_1^+) = g_1(x_1) \frac{x_1}{x_1^+} \frac{dx_1}{dx_1^+} \tag{3.55a}$$

and

$$g_2^+(x_2^+) = g_2(x_2) \left(\frac{x_2 + \sigma}{x_2^+ + \sigma} \right) \frac{dx_2}{dx_2^+}. \tag{3.55b}$$

For turbulent flows of liquid metals with small Peclet numbers, the above functions are approximately equal to unity over a large portion of the cross section of the heat-exchanger duct, whereas for all Peclet numbers, their average value over the cross section of the duct is unity. That $g_1^+(x_1^+)_{AV} = g_2^+(x_2^+)_{AV} = 1$ is evident from an integration of Eqs. (3.55a) and (3.55b).

As an approximation, it will be assumed that $g_1^+(x_1^+)$ and $g_2^+(x_2^+)$ are identically equal to unity for all values of the Peclet number. Equations (3.54a) and (3.54b) then reduce to the following:

Tube:

$$\frac{1}{x_1^+}\frac{\partial}{\partial x_1^+}\left[x_1^+\frac{\partial \xi_1(x_1^+,z^+)}{\partial x_1^+}\right] = \frac{\partial \xi_1(x_1^+,z^+)}{\partial z^+}; \tag{3.56a}$$

Annulus:

$$\frac{1}{x_2^+ + \sigma}\frac{\partial}{\partial x_2^+}\left[(x_2^+ + \sigma)\frac{\partial \xi_2(x_2^+,z^+)}{\partial x_2^+}\right] = -\omega^2\frac{k_1^+}{k_2^+}\frac{\partial \xi_2(x_2^+,z^+)}{\partial z^+}, \tag{3.56b}$$

with the boundary conditions remaining unchanged.

Equations (3.56a) and (3.56b) are identical in form to those which would be obtained by applying a plug-flow model, $g_i(x_i) = f_i(x_i) = 1$, to Eqs. (3.3a) to (3.3h) and making the following changes in the parameters K and K_w and in the axial length z:

$$K \rightarrow \frac{k_1^+}{k_2^+}K = \frac{k_1^+ k_1}{k_2^+ k_2}\frac{1-R}{R}; \tag{3.57}$$

$$K_w \rightarrow k_1^+ K_w = \frac{k_1^+ k_1}{k_w}\ell n\left(\frac{r_{21}}{r_{12}}\right); \tag{3.58}$$

$$z \rightarrow k_1^+ z = k_1^+\frac{4}{Pe_1}\frac{\ell}{2r_{12}}. \tag{3.59}$$

The actual effect of the k^+ approximation, then, is to replace the molecular conductivity, k_i, by what may be termed an effective conductivity, $k_i k_i^+$, in the plug-flow equations.

The solution of Eqs. (3.56a) and (3.56b) yields the turbulent temperature distribution of the heat-exchanger fluids as functions of x_i^+ and z^+. Since $x_i^+(0) = 0$ and $x_i^+(1) = 1$, the fluid wall and bulk temperatures are unchanged by the transformation:

$$\overline{\xi}_i(z) = \overline{\xi}_i(z^+); \tag{3.60}$$

$$\xi_1(1,z) = \xi_1(1,z^+); \tag{3.61}$$

$$\xi_2(0,z) = \xi_2(0,z^+). \tag{3.62}$$

The heat-exchanger efficiency in terms of x_i^+ and Z^+ is

H < 1:

$$\epsilon = \bar{\xi}_1(Z^+)/H; \tag{3.63a}$$

H > 1:

$$\epsilon = \bar{\xi}_1(Z^+). \tag{3.63b}$$

The Nusselt numbers as functions of x_i^+ and z^+ may be written in the following forms:

Tube:

$$Nu_1(z) = \frac{-\frac{d\bar{\xi}_1(z)}{dz}}{\bar{\xi}_1(z) - \xi_1(1,z)}$$

$$= \frac{-\frac{d\bar{\xi}_1(z^+)}{dz^+}\frac{dz^+}{dz}}{\bar{\xi}_1(z^+) - \xi_1(1,z^+)}$$

$$= \frac{-\frac{d\bar{\xi}_1(z^+)}{dz^+}}{\bar{\xi}_1(z^+) - \xi_1(1,z^+)} k_1^+; \tag{3.64}$$

Annulus:

$$Nu_2(z) = \frac{-HK\frac{k_1^+}{k_2^+}\frac{d\bar{\xi}_2(z^+)}{dz^+}}{\xi_2(0,z^+) - \bar{\xi}_2(z^+)} k_2^+; \tag{3.65}$$

Overall:

$$Nu_1^\circ(z) = \frac{-\frac{d\bar{\xi}_1(z^+)}{dz^+}}{\bar{\xi}_1(z^+) - \bar{\xi}_2(z^+)} k_1^+. \tag{3.66}$$

The heat-exchanger efficiency and Nusselt numbers for turbulent flow are related to the plug-flow values as follows:

Efficiency:

$$\epsilon = \epsilon_{PF}; \tag{3.67}$$

Tube:

$$Nu_1(z) = \left[k_1^+ \, Nu_1(z)\right]_{PF}; \tag{3.68}$$

Annulus:

$$Nu_2(z) = \left[k_2^+ \, Nu_2(z)\right]_{PF}; \tag{3.69}$$

Overall:

$$Nu_1^\circ(z) = k_1^+ \left[Nu_1^\circ(z)\right]_{PF}, \tag{3.70}$$

where the plug-flow values are calculated from Eqs. (3.3a) and (3.3b) with the conductivity k_i replaced by its effective value $k_i k_i^+$.

b. Computation of k_i^+

An expression for the quantity k_i^+ may be obtained by integrating Eqs. (3.52a) and (3.52b) over the cross section of the duct:

$$k_1^+ = \frac{\displaystyle\int_0^1 \frac{dx_1^+(x_1)}{x_1^+(x_1)}}{\displaystyle\int_0^1 \frac{1}{f_1(x_1)} \frac{dx_1}{x_1}}; \tag{3.71}$$

$$k_2^+ = \frac{\displaystyle\int_0^1 \frac{dx_2^+(x_2)}{x_2^+(x_2) + \sigma}}{\displaystyle\int_0^1 \frac{1}{f_2(x_2)} \frac{dx_2}{(x_2 + \sigma)}}. \tag{3.72}$$

Solution of the above equations for k_i^+ requires a knowledge of the eddy diffusivity of heat, $\epsilon_{Hi}(x_i)$, as a function of radial location. As mentioned previously, $\epsilon_{Hi}(x_i)$ is usually obtained from experimental values of the eddy diffusivity of momentum, $\epsilon_{Mi}(x_i)$, by assuming a relationship between them. The usual assumption is that their ratio has a constant value. An additional complication arises in the calculation of k_1^+ because the expression on the right of Eq. (3.71) is indeterminate at $x_1 = 0$.

In view of the difficulties encountered in calculating k_i^+ from Eqs. (3.71) and (3.72), an alternative method, based on Eqs. (3.68) and (3.69), will now be presented.

From Eqs. (3.68) and (3.69),

$$k_1^+ = \frac{Nu_1(z)}{[Nu_1(z)]_{PF}}; \tag{3.73}$$

$$k_2^+ = \frac{Nu_2(z)}{[Nu_2(z)]_{PF}}. \tag{3.74}$$

Similar relations hold for Nu_{iFD}:

$$k_1^+ = \frac{Nu_1FD}{[Nu_1FD]_{PF}}; \tag{3.75}$$

$$k_2^+ = \frac{Nu_2FD}{[Nu_2FD]_{PF}}. \tag{3.76}$$

If, for a specified heat-flux boundary condition, values of Nu_{iFD} and $[Nu_{iFD}]_{PF}$ are known, the above relations can be used to calculate k_i^+. Since explicit relations for Nu_{iFD} and $[Nu_{iFD}]_{PF}$ for the boundary conditions of uniform wall heat flux and temperature are available in the literature, k_i^+ may be calculated quite easily. The values obtained, of course, are only as accurate as the particular relation used to calculate Nu_{iFD} and reflect any assumptions inherent in that analysis such as the assumption about the relationship between ϵ_{Hi} and ϵ_{Mi}.

As mentioned in the literature survey, most of the research in liquid metal heat transfer has been concentrated on finding reliable relationships for heat transfer in individual pipes and annuli with specified boundary conditions at the wall. By far the most extensively investigated case was that of uniform wall heat flux. As a result, predictions of Nusselt number for uniform heat flux are considered to be more accurate than those for other boundary conditions and will be used for calculating k_i^+.

Figures 3.2 and 3.3 compare values of k_1^+ and k_2^+ calculated from Nusselt number relations in Ref. 5, 9, and 10 for uniform heat flux in tubes, and in Ref. 68, 11, and 12 for uniform heat flux in annuli. Although the values of k_i^+ differ by as much as 25% for some ranges, experimental investigations[32,34,40,58] have indicated that the predictions of Buleev[5] for

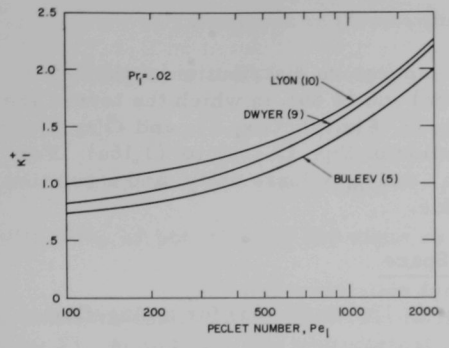

Fig. 3.2. k_1^+ vs. Peclet Number for Various Nusselt Number Relations

tubes and of Dwyer[6-8] for annuli are the most accurate. The Nusselt number relations of Refs. 5 and 6-8, as well as corresponding plug-flow values, are given in Table 2.1. It will be the practice throughout this thesis to calculate k_1^+ from these relationships.

c. Accuracy of the k^+ Approximation

Stein[22] has investigated the accuracy of the k^+ approximation by computing entrance-region Nusselt numbers in a uniform-wall-temperature parallel-plate channel and comparing them with the turbulent-flow solution of Poppendiek.[59] The entrance-region computation represents a stringent test of the approximation since k^+ is used in computing Nusselt numbers which are functions of axial distance. Figure 3.4 compares the k^+ solution with that of Poppendiek. Agreement between the two solutions is quite good everywhere but at the beginning of the thermal-entrance region. In the thermal-entrance region, temperature gradients are localized near the duct wall, where the principal mode of heat transfer is molecular conduction and eddy conduction plays a minor, if not insignificant, role. Thus, specification of an effective conductivity, kk^+, which includes eddy-conduction heat transfer, results in an overestimation of the heat transfer coefficient.

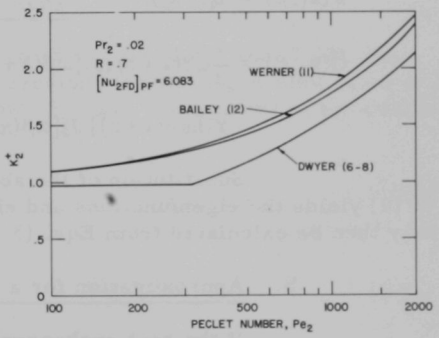

Fig. 3.3. k_2^+ vs. Peclet Number for Various Nusselt Number Relations

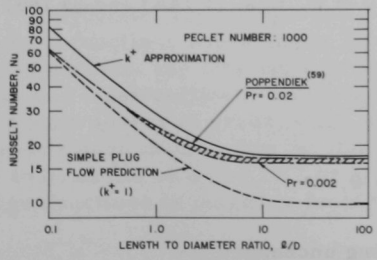

Fig. 3.4

Nusselt Number vs. Length Predictions, Uniform Surface Temperature in Parallel Plane Channel (from Ref. 22)

2. Plug-flow Solutions

The expression for the temperature distribution of the heat-exchanger fluids is given by Eqs. (3.8a) and (3.8b), in which the terms are defined in terms of the functions $F(x_1,\lambda)$, $\tilde{F}(x_1,\beta)$, $G(x_2,\lambda)$, and $\tilde{G}(x_2,\beta)$. These functions are given by the solution of Eqs. (3.13a) to (3.16a). For a plug-flow model, the functions $f_i(x_i)$ and $g_i(x_i)$ are unity, and a solution in terms of known functions is possible.

a. Nonnarrow Annular Space

The solutions of Eqs. (3.13a) to (3.16a) for a plug-flow model are

$$F(x_1,\lambda) = J_0(\lambda x_1); \tag{3.77}$$

$$G(x_2,\lambda) = \omega\lambda(1+\sigma)\{K_1[\omega\lambda(1+\sigma)]\, I_0[\omega\lambda(x_2+\sigma)] + I_1[\omega\lambda(1+\sigma)]\, K_0[\omega\lambda(x_2+\sigma)]\}; \tag{3.78}$$

$$\tilde{F}(x_1,\beta) = I_0(\beta x_1); \tag{3.79}$$

$$\tilde{G}(x_2,\beta) = \frac{\pi}{2}\omega\beta(1+\sigma)\{J_1[\omega\beta(1+\sigma)]\, Y_0[\omega\beta(x_2+\sigma)] - Y_1[\omega\beta(1+\sigma)]\, J_0[\omega\beta(x_2+\sigma)]\}. \tag{3.80}$$

Substitution of the above expressions into Eqs. (3.10) and (3.11) yields the eigenfunctions and eigenvalues. The expansion coefficients may then be calculated from Eqs. (3.17) and (3.18).

b. Approximation for a Narrow Annular Space

If the heat exchanger to be considered has a narrow annular space, that is, $R \approx 1$, Eqs. (3.14a) and 3.16a) may be further simplified by letting $R = 1$ and solving the resulting expression.

For $R = 1$, and $\sigma \to \infty$, Eqs. (3.14A) and (3.16a) reduce to the following:

$$\frac{d^2G(x_2,\lambda)}{dx_2^2} - \omega^2\lambda^2 G(x_2,\lambda) = 0; \tag{3.81}$$

$$\frac{d^2\tilde{G}(x_2,\beta)}{dx_2^2} + \omega^2\beta_n^2\,\tilde{G}(x_2,\beta) = 0, \tag{3.82}$$

with the initial conditions remaining unchanged.

Solutions of these equations are

$$G(x_2,\lambda) = \cosh [\omega\lambda(1 - x_2)] \tag{3.83}$$

and

$$\tilde{G}(x_2,\beta) = \cos [\omega\beta(1 - x_2)], \tag{3.84}$$

with $F(x_1,\lambda)$ and $\tilde{F}(x_1,\beta)$ the same as for the nonnarrow annular space.

The approximation for the narrow annular space affords a considerable simplification in the form of the expressions for $G(x_2,\lambda)$ and $\tilde{G}(x_2,\beta)$. In addition, the geometrical parameter R has been eliminated from the equations and is only accounted for in the parameter K. The narrow-annulus approximation is, of course, exact only for the physically impossible case that R = 1, but it will be shown that for practical computations, it can be used for values of R as low as 0.5.

C. Computation for Plug-flow Case

1. Eigenvalues and Eigenfunctions

Substitution of Eqs. (3.77) to (3.80), or (3.83) and (3.84), into Eqs. (3.10a) and (3.10b) yields the expressions for the eigenvalue equations $\psi(\lambda)$ and $\tilde{\psi}(\beta)$. The eigenvalues λ_n^2 and β_n^2, are the squares of the positive roots of the equations

$$\psi(\lambda) = 0 \tag{3.9a}$$

and

$$\tilde{\psi}(\beta) = 0. \tag{3.9b}$$

The roots of the above equations were found through use of a simple half-interval iteration procedure. The eigenfunctions were then easily calculated from Eqs (3.11a) to (3.11d).

Polynomial approximations given by Ref. 60 were used to calculate the Bessel functions appearing in Eqs. (3.77) to (3.80). Since it was not necessary to perform any long multiplications or additions in computing the eigenvalues and eigenfunctions, round-off errors were probably at a minimum. The main source of error, then, was the error in the polynomial approximations used to calculate the Bessel functions. This error is given in Ref. 60 to be of the order of 10^{-6} or smaller. The error in the eigenvalues and eigenfunctions is judged to be of the same order, namely, 10^{-6}.

2. Expansion Coefficients

The expansion coefficients are defined by the infinite set of linear algebraic equations, Eqs. (3.17a) and (3.17b). Solution of this system of equations for all values of n is, of course, impossible. In practical computational work for moderately long heat exchangers, however, only a few of the lower-ordered coefficients are needed to describe adequately the temperature distribution of the heat-exchanger fluids.

Specifically, only one term is retained in the series solution for the fully developed region of heat transfer, and only the zeroth-order coefficient, C_0, is needed to compute the efficiency. For short heat exchangers and for computations in the thermal-entrance regions, the large number of terms required in the solution could impose a serious restriction on the applicability of the present method.

Equations (3.17a) and (3.17b) may be solved for the lower-ordered coefficients by truncating the higher-ordered terms and equations, and solving the remaining finite set. For computational purposes, the summation in Eqs. (3.17a) and (3.17b) was from 1 to M, where M was equal to one-half the order of the resulting system of equations. This finite set of equations constitutes an approximation to the infinite set and may be solved for the coefficients C_n and A_n for n = 1,2,3, ..., M. The accuracy of the coefficients calculated in this manner must be judged by inspection of the values obtained for the coefficients as the number of equations is increased. As M is increased, the coefficients should asymptotically approach the value for "M = ∞." Table 3.1 illustrates the convergence of the coefficients as the number of equations retained in the solution is increased. Note that the zeroth-order coefficient is not calculated directly from the solution of the set of equations, but is calculated separately from A_n and C_n by Eq. (3.18).

TABLE 3.1. Convergence of Expansion Coefficients for Narrow Annular Space

H = 0.5; K = 0.1; K_w = 0; Z = 0.1

No. of Equations, 2M	C_0	C_1	C_2	A_1	A_2
2	-0.21264	-0.07151	-	0.57158	-
4	-0.20540	-0.06768	0.04173	0.55710	-0.03821
6	-0.20308	-0.06669	0.04086	0.55164	-0.03496
8	-0.20195	-0.06624	0.04050	0.54880	-0.03283
10	-0.20128	-0.06599	0.04031	0.54712	-0.03130
20	-0.20010	-0.06556	0.04001	0.54405	-0.02748
40	-0.19967	-0.06541	0.03990	0.54290	-0.02542
60	-0.19957	-0.06538	0.03988	0.54262	-0.02484
80	-0.19953	-0.06536	0.03987	0.54251	-0.02460
100	-0.19950	-0.06535	0.03987	0.54245	-0.02448
120	-0.19950	-0.06535	0.03986	0.54242	-0.02441

The number of equations necessary to produce the desired convergence varied from case to case. In general, more equations were necessary for small values than for large values of Z. In computing low values of heat-exchanger efficiency, for which only C_0 was required, it was necessary in some cases to use 60 equations to insure convergence in the third decimal place. For computations in the thermal-entrance region, 120 equations were used.

When Eqs. (3.17a) and (3.17b) are arranged so that the coefficients A_k and C_k are interlaced, and the unknowns are taken as $\left(1 - e^{-\beta_k^2 Z}\right) A_k$ and $\left(1 - e^{-\lambda_k^2 Z}\right) C_k$, then the coefficient matrix of the resulting system of equations possesses the following properties:

1. symmetry;

2. as the order of the off-diagonal terms is increased, they decrease in absolute value;

3. as the order of the diagonal terms is increased, they approach a constant value of order unity.

Table 3.2 illustrates the behavior of the elements of the coefficient matrix. Systems of equations whose coefficient matrix does not have terms which vary widely in magnitude and whose determinant is not close to zero are well-conditioned[70] with respect to computation. As a result, round-off errors, though always present, are not considered a major source of error. For the computations performed in this thesis, even though as many as 120 equations were solved in some cases, the coefficients converged uniformly and did not display the erratic behavior to be expected if serious round-off errors were present.

TABLE 3.2. Behavior of Coefficient Matrix Elements[a]

H = 0.5; K = 0.1; K_w = 0; Z = 0.1; M = 60

Column:	1	2	3	4	117	118	119	120	Nonhomogeneous Part
Row:									
1	3.12+0	-7.329-1	-2.639-1	4.593-1	5.941-3	-1.856-2	-5.841-3	1.825-2	1.102+0
2		1.350+0	1.294-1	-1.423-1	-2.303-3	6.987-3	2.264-3	-6.873-3	-3.336-1
3			1.124+0	-1.169-1	-4.882-3	1.634-2	4.801-3	-1.606-2	-1.426-1
4				1.094+0	1.838-3	-5.437-3	-1.806-3	5.350-3	2.100-1
117					1.002+0	-1.915-3	-2.451-3	1.920-3	2.924-3
118						1.002+0	1.878-3	-2.400-3	-9.043-3
119							1.002+0	-1.883-3	-2.874-3
120								1.002+0	8.893-3

[a]By an entry such as 5.941-3 we mean 5.941×10^{-3}.

Equations (3.17a) and (3.17b) were solved by two independent methods, Gauss elimination and Gauss-Seidel iteration. In the Gauss elimination scheme, the largest coefficient of the reduced matrix was used as the "pivot" in order to reduce round-off errors. Further support for the contention that large round-off errors were not present is the fact that use of the largest coefficient as the pivot had virtually no effect on the result. The Gauss-Seidel iteration scheme was used to check the results of the Gauss elimination. For the 36 cases tested, the two methods yielded identical results. All numerical results presented in this thesis were computed by Gauss elimination.

3. Effectiveness Coefficient

Once the eigenvalues, eigenfunctions, and expansion coefficients have been calculated, computation of Nusselt numbers and heat-exchanger efficiency is straightforward and poses no problem. In computing the effectiveness coefficient $\phi(Z)$ for large Z, however, the accuracy obtainable is severely limited by the form of the expression for $\phi(Z)$. For the computations, $\phi(Z)$ must be computed from the following equations:

$H < 1$:

$$\phi(Z) = \frac{1 - \epsilon}{1 - \epsilon H} e^{\beta_1^2 Z}; \tag{3.85a}$$

$H > 1$:

$$\phi(Z) = \frac{H(1 - \epsilon)}{H - \epsilon} e^{\lambda_1^2 Z}. \tag{3.85b}$$

For large Z, and hence ϵ close to unity, the preceding equations lead to inaccuracies in computing $\phi(Z)$ because of a loss of significant digits in computing the quantity $(1 - \epsilon)$. For some cases, ϵ must be known accurately to several significant digits in order to calculate $\phi(Z)$ accurately. To investigate what effect the error in ϵ has on the accuracy of $\phi(Z)$, Eqs. (3.85a) and (3.85b) may be written in finite difference form:

$H < 1$:

$$\frac{\Delta\phi}{\phi} \approx \frac{(H - 1)\,\epsilon}{(1 - \epsilon)(1 - \epsilon H)} \frac{\Delta\epsilon}{\epsilon}; \tag{3.86a}$$

$H > 1$:

$$\frac{\Delta\phi}{\phi} \approx \frac{(1 - H)\,\epsilon}{(1 - \epsilon)(H - \epsilon)} \frac{\Delta\epsilon}{\epsilon}. \tag{3.86b}$$

These equations reveal that as ϵ approaches unity, the percent of error in $\phi(Z)$ becomes much larger than the percent of error in ϵ. For $\epsilon = 0.9$, the percent error in ϕ is an order of magnitude larger than that in ϵ.

Since extensive computations for high efficiencies are necessary in order to establish the fact that $\phi(Z)$ reaches a fully developed value, the limitation on accuracy is a serious one for the prediction of ϕ_{FD}.

Figure 3.5 illustrates the behavior of $\phi(Z)$ as $\epsilon \rightarrow 1$. As the number of equations retained in the computation of the expansion coefficients is increased, $\phi(Z)$ seems to be asymptotically approaching a fully developed value for large ϵ. Values of ϕ_{FD} reported in this thesis are obtained by assuming that the minimum point of the curve corresponds to ϕ_{FD} and then extrapolating the left-hand portion of the curve to $\epsilon = 1$.

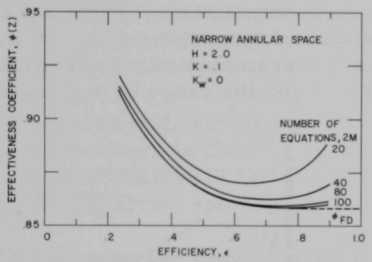

Fig. 3.5

Effectiveness Coefficient vs. Efficiency for Various Values of M

D. Comparison of Plug-flow Solutions for Narrow and Nonnarrow Annular Spaces

Due to the considerable simplification offered by the narrow-annulus approximation, it is of interest to know for what ranges of R the approximation yields accurate results. Extensive computations for various values of H, K, K_w, and Z were performed for both narrow and nonnarrow annular spaces.

The ranges of the parameters were as follows:

$$H = \frac{c_2 W_2}{c_1 W_1}: \ 0.1 \rightarrow 10.0;$$

$$K = \frac{k_1 k_1^+}{k_2 k_2^+} \frac{1 - R}{R}: \ \frac{k_1 k_1^+}{k_2 k_2^+} = 0.5, \ 1.0, \ 2.0; \text{ value of K determined by R;}$$

$$K_w = \frac{k_1 k_1^+}{k_w} \ln\left(\frac{r_{21}}{r_{12}}\right): \ 0 \rightarrow 0.1;$$

$$R = \frac{r_{21}}{r_{22}}: \quad 0.1 \rightarrow 0.9;$$

$$Z = \frac{4}{Pe_1} \frac{\ell}{2r_{12}} k_1^+: \quad 0.001 \rightarrow 1.0.$$

The percent difference between the two solutions was greatest for H = 0.1 and 10.0 and for $K_w = 0$. The magnitude of Z or $k_1 k_1^+ / k_2 k_2^+$ did not affect the agreement between the solutions to any significant degree.

Figures 3.6 to 3.9 compare results obtained by computations for both narrow and nonnarrow annular spaces. The Nusselt numbers in these figures have been "normalized," i.e., divided by their corresponding uniform heat-flux value. The graphs indicate that for a large range of R the approximation for the narrow annular space yields numerical results which are in agreement with the exact computations. Table 3.3 lists the percent difference between the solutions for various values of R. Since the values shown are for the "worst" cases obtained, the percent differences may be taken as the "maximum error" for the range of parameters tested.

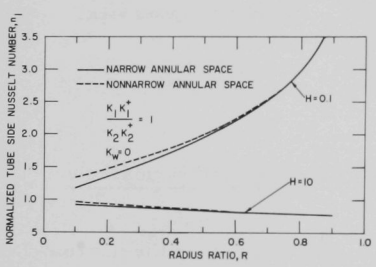

Fig. 3.6. Comparison of Tube-side Nusselt Numbers Computed from Solutions for Narrow and Nonnarrow Annular Spaces

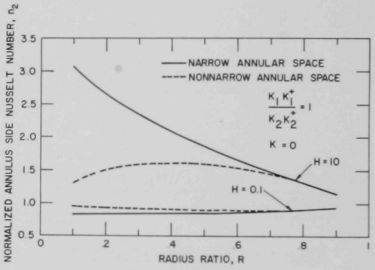

Fig. 3.7. Comparison of Annulus-side Nusselt Numbers Computed from Solutions for Narrow and Nonnarrow Annular Spaces

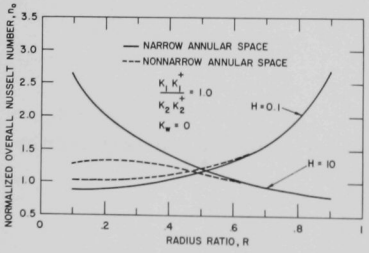

Fig. 3.8. Comparison of Overall Nusselt Numbers Computed from Solutions for Narrow and Nonnarrow Annular Spaces

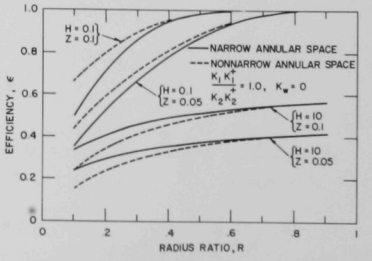

Fig. 3.9. Comparison of Efficiencies Computed from Solutions for Narrow and Nonnarrow Annular Spaces

TABLE 3.3. Maximum Error of Narrow-annular-space Approximation for Range of Parameters Investigated, %

	η_0		η_1		η_2		ϵ	
R	H < 1	H > 1	H < 1	H > 1	H < 1	H > 1	H < 1	H > 1
0.1	14.0	109.5	12.2	1.6	12.5	134.0	24.4	51.9
0.3	9.1	27.4	6.4	1.0	7.9	47.5	6.2	12.5
0.5	5.0	7.2	2.9	0.8	4.4	18.2	1.5	3.6
0.7	2.0	1.4	1.0	0.2	2.0	6.0	0.2	1.0
0.9	0.2	0.0	0.1	0.1	0.3	0.8	0.0	0.0

The error is seen to be quite small in most cases for R as low as 0.5. Since most practical heat exchangers have radius ratios which are greater than 0.5, the narrow-annular-space approximation yields results which are accurate in the area of practical interest.

Computations with $k_1k_1^+/k_2k_2^+ = 0.5$ and 2.0 gave nearly the same range of accuracy shown in Table 3.3. Apparently, this small a change in the relative fluid-conductivity ratio does not affect the agreement between the narrow and nonnarrow solutions to any significant degree.

E. Numerical Results for Plug-flow Model

Numerical computations in the range of practical interest are useful in investigating the effect of the operating conditions on the heat transfer characteristics of a heat exchanger. The operating conditions are specified by the parameters H, K, K_w, R, and Z. It has been shown that the narrow-annular-space approximation yields sufficiently accurate results for $R > 0.5$, where the value of R is accounted for in K. Therefore, all results presented are for computations using the narrow-annulus approximation.

1. Fully Developed Nusselt Numbers

Figures 3.10 through 3.15 illustrate the behavior of the fully developed overall, tube, and annulus Nusselt numbers for a wide range of the parameters H, K, and K_w. The Nusselt numbers have been "normalized" with respect to their corresponding uniform heat-flux value. The plug-flow Nusselt number for uniform heat flux in a tube is 8.0. For uniform heat flux from the inner wall of a concentric annulus with a narrow annular space, the plug-flow Nusselt number is 6.0. Also shown is the plug-flow Nusselt number for a uniform-wall-temperature boundary condition normalized with respect to the uniform heat-flux value.

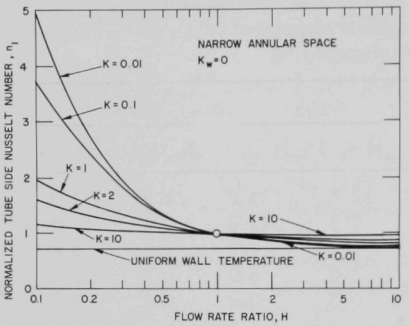

Fig. 3.10. Normalized Tube-side Nusselt Number vs. Flowrate Ratio

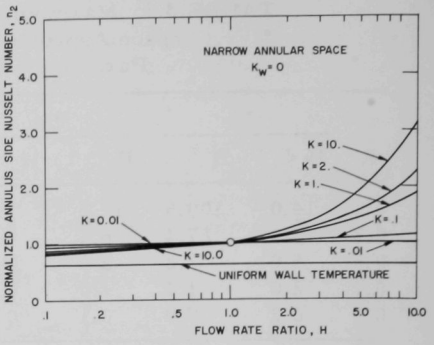

Fig. 3.11. Normalized Annulus-side Nusselt Number vs. Flowrate Ratio

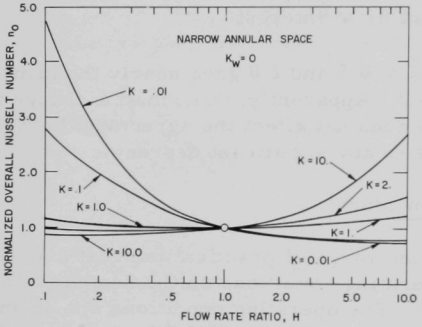

Fig. 3.12. Normalized Overall Nusselt Number vs. Flowrate Ratio

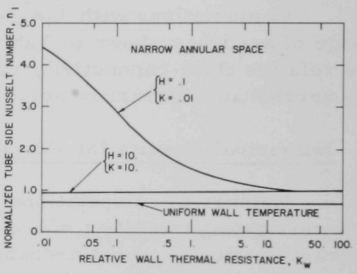

Fig. 3.13. Normalized Tube-side Nusselt Number vs. Relative Wall Thermal Resistance

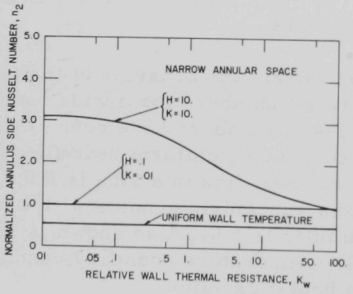

Fig. 3.14. Normalized Annulus-side Nusselt Number vs. Relative Wall Thermal Resistance

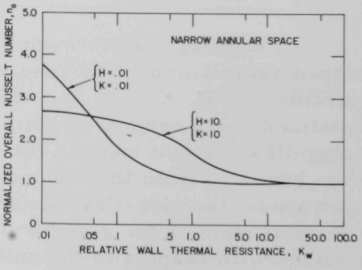

Fig. 3.15. Normalized Overall Nusselt Number vs. Relative Wall Thermal Resistance

In Figs. 3.10, 3.11, and 3.12, the tube, annulus, and overall Nusselt numbers are plotted against the heat capacity-flowrate ratio, H. Although the mathematical solution is indeterminate at H = 1, the values computed for the case $H \neq 1$ clearly show that the fully developed Nusselt numbers for H = 1 correspond to a uniform-heat-flux boundary condition, i.e., $\eta_0 = \eta_1 = \eta_2 = 1.0$.

For $H < 1$, the annulus-side Nusselt numbers lie between the values for uniform wall temperature and uniform heat flux, whereas the tube-side Nusselt numbers are always greater than the uniform heat-flux value. For $H > 1$, the annulus-side Nusselt numbers are always greater than the uniform heat-flux value, and the tube-side Nusselt numbers lie between the values for uniform heat flux and uniform wall temperature. In general, increasing the flowrate in either tube or annulus increases its respective heat transfer coefficient. This is different from existing plug-flow solutions for single channels, which predict Nusselt numbers that are independent of flowrate.

The behavior of the overall Nusselt number for H greater than or less than unity depends on the value of K. For large K, the heat transfer is controlled by the annulus-side heat transfer coefficient, and the overall Nusselt number displays the same characteristics as the annulus Nusselt number. For small values of K, the preceding statement applies to the tube-side heat transfer coefficient, and the overall Nusselt number behaves like the tube-side Nusselt number. The effect which the individual channel heat transfer coefficients have on the overall heat transfer coefficient can also be determined from Eq. (3.39). For values of K close to unity, the overall Nusselt number is fairly close to the uniform heat-flux value. One interesting point about the fully developed overall Nusselt number is that it has a minimum point which occurs at large values of H when K is small, and at small values of H when K is large. If the range of H in Fig. 3.12 were extended, the curves for K = 0.01 and 0.1 would reach a minimum at some value of H greater than 10.0 and then begin to rise. A similar statement applies to the curves for K = 2.0 and 10.0 for $H < 0.1$.

It is important to note that the fully developed overall, tube, and annulus Nusselt numbers are never less than the value for uniform wall temperature, but can be significantly larger than values corresponding to a uniform-heat-flux boundary condition. The Nusselt numbers display the largest deviation from the uniform heat-flux value at both ends of the ranges of H and K. For small H and K, the tube and overall Nusselt numbers are much larger than the uniform heat-flux value. For large H and K, the annulus and overall Nusselt numbers are much larger than their uniform heat-flux values.

In general, for $H < 1$, increasing K decreases the heat transfer coefficients, whereas for $H > 1$, increasing K increases them.

In Figs. 3.13, 3.14, and 3.15 the Nusselt numbers are plotted against K_W for two extreme sets of the parameters H and K. The Nusselt numbers display the greatest deviation from the uniform heat-flux value for small values of K_W and approach the uniform heat-flux value as K_W increases. For $K_W > 10.0$, all the Nusselt numbers are approximately equal to their corresponding values for uniform heat flux. This occurs because a wall with a high thermal resistance controls the heat transfer and "smooths out" variations in heat flux along its length.

Since the cases presented are extreme, it may be stated that for $K_W > 10.0$ the fully developed Nusselt numbers are equivalent to the values for uniform heat flux, regardless of the value of H and K. For liquid metal heat exchangers in which structural considerations require the use of a thick wall, and hence large K_W, heat transfer coefficients based on a uniform wall flux are sufficiently accurate. In many applications, however, heat exchangers are designed with a very low thermal resistance of the wall. The uniform heat-flux coefficients can be seriously inaccurate for applications in which the range of K_W is from 0 to 2.0.

2. Effectiveness Coefficient

The effectiveness coefficient, $\phi(Z)$, represents a potentially useful quantity for practical design computations. For a given set of operating conditions, the heat-exchanger efficiency may be computed from Eqs. (3.49a) and (3.49b) provided the values of $\phi(Z)$ and Nu°_{1FD} are known. The effectiveness coefficient is, in effect, a correction factor which accounts for the heat transfer in the thermal-entrance regions. Of particular importance is the fact that $\phi(Z)$ reaches a fully developed value as the heat-exchanger length is increased. Thus, for long heat exchangers, the only source of Z dependence for the efficiency is in the exponential terms in Eqs. (3.49a) and (3.49b).

As discussed in Section C, computations for the fully developed effectiveness coefficient were subject to error. Figure 3.16 shows the effectiveness coefficient plotted against heat-exchanger efficiency for various values of H and a fixed value of K. For H close to unity the computed values for $\phi(Z)$ reach a fully developed value, ϕ_{FD}. However, for H not close to unity, the fully developed values had to be obtained by extrapolating the left-hand portion of the curve to $\epsilon = 1.0$.

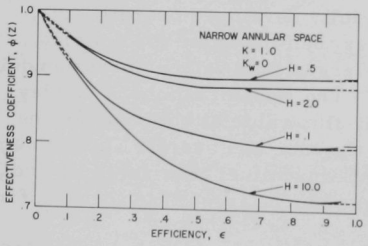

Fig. 3.16. Effectiveness Coefficient vs. Heat-exchanger Efficiency

Table 3.4 gives the results of the computations for ϕ_{FD} and Nu°_{1FD}, where Nu°_{1FD} has been normalized

with respect to the corresponding uniform heat-flux value. Because of the limitation of the accuracy of ϕ_{FD}, the accuracy in the third decimal place is suspect. The values presented in Table 3.4 are useful as a general indication of the importance of the thermal-entrance regions and also for practical computations for which accuracy to two decimal places in ϕ_{FD} is sufficient. The table is complete enough to permit graphical interpolation for values of H, K, and K_W intermediate to the values presented. Heat exchangers in which the thermal-entrance regions are unimportant are characterized by values of ϕ_{FD} close to unity. For heat exchangers in which thermal-entrance regions play a major role, the values of ϕ_{FD} are much smaller than unity. It is evident from Table 3.4 that ϕ_{FD} can be much smaller than unity. In general, the computations reveal that the thermal-entrance regions are important for small values of K_W, and for both large and small values of H.

TABLE 3.4. Computations for ϕ_{FD} and η_0 for a Narrow Annular Space

		$\Omega^a = 0$		$\Omega = 0.1$		$\Omega = 0.2$		$\Omega = 0.4$		$\Omega = 0.6$		$\Omega = 0.8$	
K	H	ϕ_{FD}	η_0	ϕ_{FD}	η_0	ϕ_{FD}	η_0	ϕ_{FD}	η_0	ϕ_{FD}	η_0	ϕ_{FD}	η_0
0.01	0.1	0.567	4.736	0.701	2.902	0.770	2.191	0.853	1.544	0.911	1.238	0.962	1.070
	0.5	0.772	1.368	0.818	1.277	0.857	1.207	0.917	1.109	0.961	1.047	0.989	1.012
	2.5	0.822	0.824	0.838	0.851	0.866	0.878	0.920	0.928	0.964	0.967	0.991	0.992
	5.0	0.770	0.774	0.785	0.807	0.819	0.840	0.889	0.903	0.950	0.955	0.988	0.989
	10.0	0.747	0.750	0.760	0.785	0.795	0.821	0.873	0.890	0.942	0.949	0.986	0.988
0.10	0.1	0.671	2.762	0.751	2.186	0.802	1.833	0.871	1.422	0.922	1.193	0.967	1.058
	0.5	0.811	1.269	0.850	1.207	0.882	1.158	0.931	1.085	0.967	1.038	0.991	1.010
	2.5	0.832	0.855	0.856	0.879	0.883	0.902	0.932	0.943	0.970	0.974	0.993	0.994
	5.0	0.777	0.813	0.802	0.842	0.837	0.871	0.904	0.924	0.957	0.966	0.990	0.992
	10.0	0.747	0.795	0.771	0.826	0.810	0.858	0.886	0.916	0.950	0.962	0.988	0.991
1.0	0.1	0.798	1.147	0.827	1.132	0.860	1.115	0.915	1.079	0.955	1.043	0.985	1.014
	0.5	0.898	1.015	0.919	1.013	0.937	1.011	0.965	1.007	0.985	1.004	0.996	1.001
	2.5	0.850	1.039	0.883	1.033	0.910	1.027	0.951	1.017	0.979	1.008	0.995	1.002
	5.0	0.763	1.115	0.810	1.099	0.851	1.083	0.916	1.052	0.961	1.026	0.989	1.007
	10.0	0.717	1.218	0.768	1.191	0.816	1.163	0.891	1.106	0.945	1.055	0.983	1.016
10.0	0.1	0.838	0.862	0.857	0.885	0.883	0.907	0.932	0.946	0.969	0.976	0.992	0.994
	0.5	0.910	0.918	0.925	0.933	0.940	0.946	0.966	0.969	0.985	0.986	0.996	0.997
	2.5	0.799	1.283	0.842	1.217	0.876	1.164	0.929	1.088	0.966	1.038	0.991	1.010
	5.0	0.672	1.798	0.743	1.566	0.797	1.408	0.877	1.208	0.937	1.090	0.980	1.024
	10.0	0.625	2.684	0.717	2.095	0.776	1.754	0.856	1.370	0.914	1.163	0.969	1.046

[a] $K_W = 2\left[\frac{1}{8}+\frac{K}{6}\right]\frac{\Omega}{1-\Omega}$

3. Heat-exchanger Efficiency

The heat-exchanger efficiency is a simple function of the heat-capacity-mass flowrate ratio, H, and the number of transfer units, NTU, as given by Eqs. (3.47a) and (3.47b). Use of these equations to compute the efficiency is complicated, however, by the difficulty of computing NTU, since the computation of NTU requires knowledge of the average overall Nusselt number. A more convenient and useful way of presenting ϵ is to

present it as a function of NTU_{UHF}, where NTU_{UHF} is the number of transfer units based on a fully developed, uniform-heat-flux overall Nusselt number. Figure 3.17 shows ϵ plotted vs. NTU_{UHF} for fixed values of H and K. For a specific set of operating conditions, the value of NTU_{UHF} may be computed quite easily, and the efficiency can then be taken directly from the graph. In order to cover a wide range of the parameters H and K, graphs other than the one shown in Fig. 3.17 are needed. A possibility for a future contribution would be the presentation of such graphs.

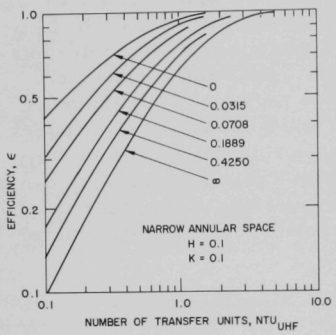

Fig. 3.17. Heat-exchanger Efficiency vs. Number of Transfer Units--Based on Nu^{o}_{1UHF} (labels on the curve correspond to values of K_w)

The curve labeled $K_w = \infty$ in Fig. 3.17 is obtained directly from Eqs. (3.47a) and (3.47b), and corresponds to the condition for which $NTU = NTU_{UHF}$. The computations have indicated that this is a limiting case for large K_w. It was previously shown that for large K_w the fully developed overall Nusselt number approached the value appropriate to a uniform-heat-flux boundary condition. Figure 3.17 indicates that another effect of a large K_w is to suppress the thermal-entrance regions so that the average overall Nusselt number is equivalent to the fully developed overall Nusselt number. The often-made assumption that $NTU = NTU_{FD} = NTU_{UHF}$ is therefore valid for heat exchangers with very large values of K_w. For values of K_w in the range of practical interest ($0 \leq K_w \leq 2.0$), it is clear from Fig. 3.17 that the assumption $NTU = NTU_{FD} = NTU_{UHF}$ can lead to a serious underspecification of the heat-exchanger efficiency for a given heat-exchanger length. In practical heat-exchanger design, the underspecification of efficiency leads to an oversizing of the heat exchanger. Figure 3.18 compares the heat exchanger length predicted by assuming a uniform-heat-flux boundary condition with that predicted by the present analysis. It is evident that large differences exist.

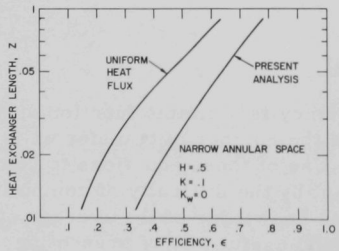

Fig. 3.18

Comparison of Heat-exchanger Lengths Computed from Present Analysis and from Uniform-heat-flux Analysis

4. Local Nusselt Number Distributions

Figure 3.19 shows the local Nusselt numbers, normalized with respect to their value for a uniform heat flux, plotted as a function of axial position along the heat exchanger. The scale for the axial position variable was chosen to better illustrate the behavior of the Nusselt numbers in the thermal-entrance regions. Also, for a given tube-side Peclet number the abscissa of the graph may be interpreted as a multiple of tube diameters. For a Peclet number of 400 the multiple is unity. Figure 3.19 clearly shows that thermal-entrance regions exist at both ends of the heat exchanger. For the particular case shown, the thermal-entrance regions comprise about 40% of the total length of the heat exchanger even though the efficiency is very high. As Z, and hence efficiency, is decreased, the thermal-entrance regions comprise more and more of the total length of heat exchanger. For the values of H, K, and K_W shown, the fully developed portion disappears at an efficiency of about 0.7, and all heat transfer then occurs in the thermal-entrance regions. As stated before, the assumption that NTU = NTU_{FD} or Nu_{iAV}° = Nu_{iFD}° can lead to serious inaccuracies for cases such as this.

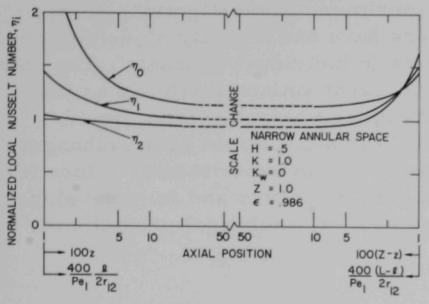

Fig. 3.19. Local Nusselt Number vs. Axial Position

Nusselt numbers at the thermal-entrance region are always higher than their fully developed values. For this reason, neglect of thermal-entrance effects always leads to an underestimate of heat-exchanger efficiency and subsequent oversizing of the heat exchanger. Although this procedure always results in a "safe" design, it is not desirable when space and economic factors are considered. Incorporation of a "safety" factor into design computations is standard engineering practice; however, neglect of the high heat fluxes occurring in the thermal-entrance regions can, in some cases, result in a safety factor which is unreasonably high.

CHAPTER IV

EXPERIMENTAL PROGRAM

The experimental program was initiated to study the effect of operating conditions on the overall performance of the heat exchanger. As mentioned in the literature survey, other experimental investigations with double-pipe, liquid-metal heat exchangers have had as their objective the measurement of heat transfer coefficients in individual channels. The only experimental investigation known to the present author which had as its objective the investigation of the performance of a double-pipe, liquid-metal heat exchanger is that of Merriam[23] for a cocurrent heat exchanger. The goal of the present investigation was to obtain experimental values for countercurrent, liquid-metal heat-exchanger efficiency and fully developed overall Nusselt numbers for comparison with the analytical predictions obtained through the k^+ approximation.

A. Experimental Approach

The quantities most descriptive of the performance of a heat exchanger are the efficiency and fully developed overall Nusselt number. These quantities may be presented as heat-exchanger performance curves, which are curves of efficiency or Nu°_{iFD} plotted as functions of the flowrates in the heat-exchanger channels. Experimental data for such performance curves were obtained in the following manner.

A method first suggested by Stein[45] was used to measure the fully developed overall Nusselt numbers. This method, which comes directly from the mathematical analysis, requires detailed measurements of the temperature distribution along the outer wall of the heat exchanger, as well as measurements of flowrate and inlet and outlet bulk fluid temperatures. The method is described in detail below.

The fully developed overall Nusselt number, as given by Eqs. (3.42a) or (3.42b), is

$H < 1$:

$$Nu^{\circ}_{iFD} = \frac{H}{1 - H}\,\beta_1^2, \tag{3.42a}$$

$H > 1$:

$$Nu^{\circ}_{iFD} = \frac{H}{H - 1}\,\lambda_1^2. \tag{3.42b}$$

The above expressions may be used to compute Nu°_{iFD} if the values of H and λ_1^2 or β_1^2 are known. The value of H is an easily determined quantity,

requiring only knowledge of the flowrates in the tube and annulus of the heat exchanger. The value of the first-order eigenvalue, λ_1^2 or β_1^2, may be determined from the temperature distribution of the outer wall of the heat exchanger in the following way. For the fully developed region, the temperature distribution of the heat-exchanger fluid in the annulus is given by Eqs. (3.41b) or (3.41d). At the outer wall of the annular space ($x_2 = 1$), Eqs. (3.41b) and (3.41d) are

$H < 1$:

$$\xi_2(1,z) = \frac{H}{H-1}(1-\epsilon) + A_1\tilde{E}_{2,1}(1)e^{-\beta_1^2(Z-z)};$$

$H > 1$:

$$\xi_2(1,z) = \frac{(H-\epsilon)}{H-1} + C_1E_{2,1}(1)e^{-\lambda_1^2 z},$$

where Eqs. (3.29a) and (3.29b) have been used to eliminate the zeroth-order expansion coefficient.

Taking the log of the above quantities yields

$H < 1$:

$$\ell n\left[\xi_2(1,z) - \frac{H}{H-1}(1-\epsilon)\right] = \ell n\,[A_1E_{2,1}(1)] - \beta_1^2(Z-z); \qquad (4.1a)$$

$H > 1$:

$$\ell n\left[\xi_2(1,z) - \frac{(H-\epsilon)}{H-1}\right] = \ell n\,[C_1E_{2,1}(1)] - \lambda_1^2 z. \qquad (4.1b)$$

These expressions provide a convenient way of measuring the first-order eigenvalue.

The left-hand portions of the expressions are easily measurable, requiring only flowrates, inlet and outlet bulk temperatures, and the temperature distribution of the outer wall of the heat exchanger. A plot of this experimentally determined quantity vs. z yields a curve which is linear in the region of fully developed heat transfer and whose slope is equal to either β_1^2 or λ_1^2, depending on the value of H. The fully developed overall Nusselt number may then be computed from Eqs. (3.42a) and (3.42b).

The method not only yields experimental values of Nu_{1FD}°, but also reveals the extent of the fully developed region of heat transfer, since the fully developed region may be determined by the extent of the linear portion of the curve.

Since the temperature distribution for the outer wall may be conveniently and accurately measured, the method is potentially superior to other methods which determine only average Nusselt numbers or require local fluid-temperature measurements or measurements of the radial temperature distribution for the inner wall.

Merriam[23] has successfully used an equivalent method to measure Nusselt numbers for cocurrent heat exchangers.

B. Experimental Apparatus

In order to obtain experimental data for countercurrent liquid-metal heat-exchanger performance, a liquid-metal-circulating apparatus or "loop" was needed. The design and construction of such an apparatus was considerably simplified by the availability of an existing liquid-metal loop used by Merriam[23] for cocurrent heat-exchanger experiments. The basic features of the cocurrent loop were:

(1) use of mercury as the heat transfer fluid;

(2) variable flowrates in both tube and annulus of the test section;

(3) heating and cooling of mercury streams to produce the desired inlet temperatures in the test section.

The above basic features were retained in the modification of the loop for countercurrent flow, although general changes and improvements in some of the individual components were made. The loop, modified for countercurrent flow, is described in detail below.

1. Schematic of Flow Circuit

A diagram of the flow circuit is given in Fig. 4.1. The liquid leaves the pump and splits into three streams, one of which is directed through a bypass valve back into the suction line of the pump. The other two streams flow through the tube and annulus of the heat exchanger (denoted as test section in the figure).

The annulus-side stream flows through a cooler and into a mixing chamber from which it flows upward through the test section. Upon exit from the test section, the annulus stream flows through another mixing chamber into the flow-measurement assembly, which consists of an orifice and electromagnetic flowmeter in series. The annulus stream is then directed back into the suction line of the pump.

The tube stream goes through a similar circuit, passing through a heater and mixing chamber, downward through the test section, and into a second mixing chamber from which it passes through a flow-measurement assembly into the suction line of the pump.

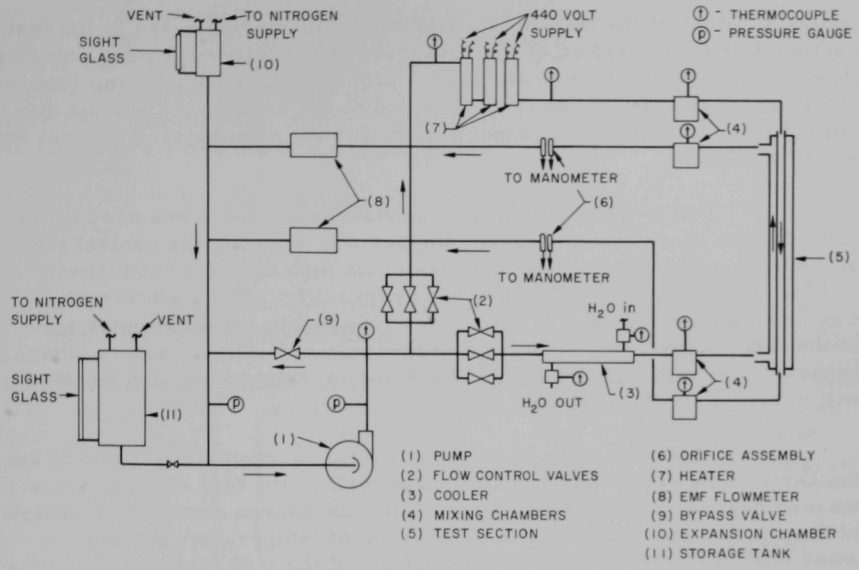

Fig. 4.1. Diagram of Flow Circuit

An expansion chamber located at the top of the loop was included to permit thermal expansion of the mercury. The storage tank proved useful when draining or filling the loop. Thermocouples were located in the mixing chambers and at various points of the loop as indicated in Fig. 4.1. The operating conditions for each experimental run were determined by the flowrate setting, the rate of heat input from the heater, and the rate of heat removal by the cooler.

A detailed description of the construction of the experimental apparatus is given in Appendix D.

2. Design of Test Section

With the heat transfer fluid chosen, the design of the test sections involved a choice of heat-exchanger materials and dimensions which gave values of K, K_w, R, and Z which were in the range of practical interest. The values of H, k_1^+, and k_2^+ were determined by the flowrates in the tube and annulus of the test section. Since the same fluid was flowing in both tube and annulus of the test section, the parameter K was determined solely by R and the values of k_1^+ and k_2^+. The values of k_1^+ and k_2^+ were computed by means of Eqs. (2.1a) and (2.1b). The three major design parameters, then, were R, K_w, and Z. Also of prime importance was the necessity of designing a test section which realized as many as possible of the physical idealities which were incorporated into the mathematical

analysis. Most of the idealities could easily be approximated in the test section with the exception of the requirement for fully developed entering flow. The tube-side flow presented no problem since an entering flow development length could easily be included in the design. As will be discussed later, a flow-development section for the annulus side was not so easily attainable.

Two materials, copper and stainless steel, were used in the construction of each test section. Copper was used for the central tube of the test sections primarily because of its high thermal conductivity and the fact that it is easily "wetted" by mercury. The stainless steel was used to clad portions of the copper tube and to form the outer wall of the test section. Although flowing mercury will erode copper, other experimental investigations[34,53,54] have shown that no detrimental effects will occur in short-term use.

Care was taken in the construction of the test sections to keep the center tube concentric with the outer wall of the test section, since a marked degree of eccentricity would cause an uneven distribution of flow in the annular space, leading to a variation of temperature around the outer wall of the test section. Although all of the test sections had some degree of eccentricity, temperature measurements taken during heat transfer tests showed a circumferential temperature variation which was generally less than 2°F.

Three test sections, of varying design, were built and tested. The first, 20 L/D_1 in length, had adiabatic entrance lengths at either end to aid in establishing a fully developed annular flow. Because of difficulties with the first test section, the second and third, 47 L/D_1 and 10 L/D_1, respectively, were designed without adiabatic entrance lengths. Because of the high thermal conductivity of liquid metals, the shape of the velocity profile is of lesser importance than with nonmetallic fluids. Because of this, the absence of a fully developed entering-velocity profile for the annulus was not considered to be a serious limitation.

All test sections were installed in the loop with stainless steel ring-joint flanges.

a. 20-L/D_1 Test Section

The first consideration in the design of the 20-L/D_1 test section was the inclusion of flow-development sections for the entering fluids. Various estimates of flow development lengths are found in the literature,[3] ranging from 10 to 20 equivalent diameters for pressure-gradient development to 50 to 100 equivalent diameters for velocity-profile development. The flow-development sections consisted of adiabatic sleeves forced onto either end of the copper tube, as shown in Fig. 4.2. Computations indicated that the rate of heat flow across the

air gap of the adiabatic sleeves would be less than 1% of the total heat transferred by the test section. Due to space limitations, the flow-development section for the tube was made 20 tube diameters in length and that for the annulus 17 annulus equivalent diameters in length. The manifold at the annulus fluid entrance was designed to distribute evenly the flow into the annular space to further aid in its development.

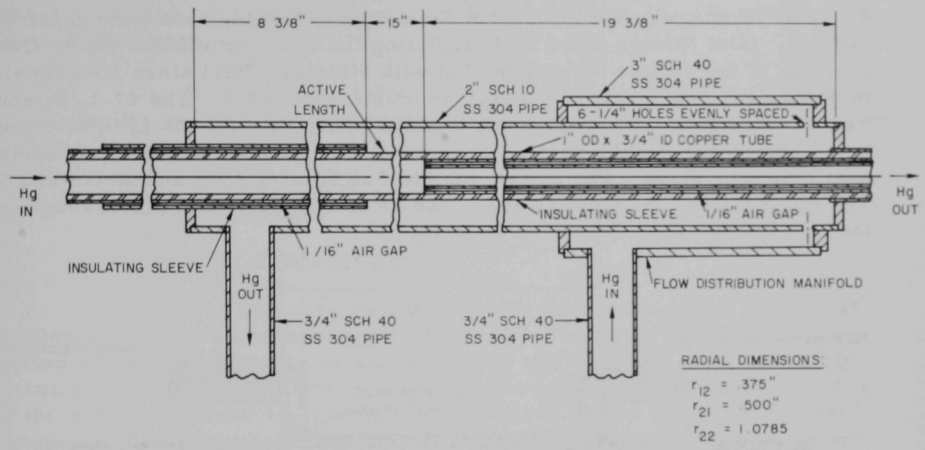

Fig. 4.2. Design of 20-L/D_1 Test Section

Dimensions of the test section were dictated largely by commercially available pipe sizes. The central copper tube had an internal diameter of 3/4 in. and an outside diameter of 1 in. The outer wall of the annular space had an internal diameter of 2.157 in. The active length of the test section was 15 in. or 20 L/D_1.

Radiographs of the completed section showed that the width of the annular space had a maximum deviation of 5% from the value for zero eccentricity.

Problems were encountered in the construction of the 20-L/D_1 section primarily because of the difficulty of fitting the long adiabatic sleeves to the copper tube. After several unsuccessful attempts to shrink fit the pieces together, it was decided to use a force fit instead. The force-fit method accomplished the purpose of fitting the pieces together, but in applying the necessary force to shove the tube-entrance adiabatic sleeve over the copper tube, the weld at the end of the sleeve was cracked. This crack went unnoticed until the actual heat transfer tests were begun.

When the section was filled with mercury, the mercury leaked through the crack into the intended air gap. The effect which the mercury-filled sleeve had on the data will be discussed in a later section.

b. 47-L/D_1 Test Section

The primary consideration in the design of a second test section was the construction of a heat exchanger which would have a fully developed thermal field over much of its length. Figure 4.3 is a sketch of the 47-L/D_1 test section. Because of the difficulty encountered in fitting the long adiabatic sleeves onto the copper tube in the first test section, the 47-L/D_1 section was constructed without a flow-development section for the annulus. Inlet fittings aided in distributing the entering annulus fluid. Outer portions of the copper tube were clad with stainless steel since it was desired to reduce the possibility of leakage as much as possible. The 47-L/D_1 section was designed with a narrower annular space than the 20-L/D_1 test section. Dimensions of the heat exchanger were dictated largely by commercially available pipe sizes. The copper tube had an ID of 3/4 in. and an OD of 1 in. The outer wall of the annular space had an ID of $1\frac{3}{8}$ in. The active length of the test section was $35\frac{1}{2}$ in. or 47 L/D_1.

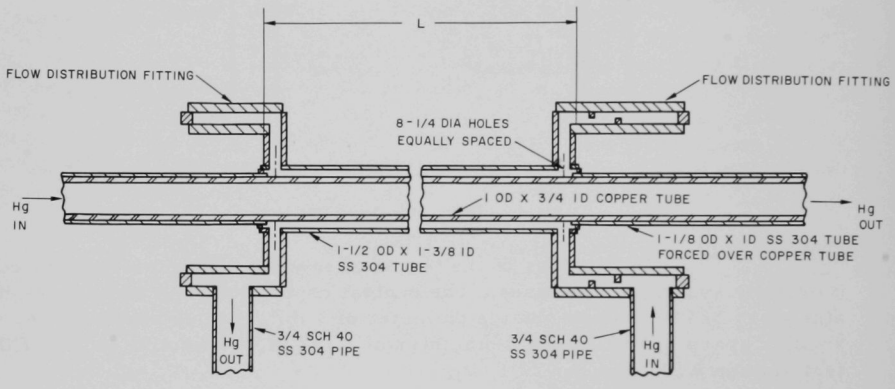

TEST SECTION	r_{12}	r_{21}	r_{22}	L
47 L/D	0.375	0.5	0.6875	35.5
10 L/D	0.375	0.5	0.6875	7.5

Fig. 4.3. Design of 47- and 10-L/D_1 Test Sections

Since the test section was fairly long, extra care had to be taken to keep the center tube concentric with the outer wall of the annular space.

Radiographs taken of the completed test section showed that the point of maximum eccentricity occurred in the middle of the heat exchanger. At this point the width of the annular space had a deviation of 7% from the value expected for zero eccentricity.

c. 10-L/D_1 Test Section

The third test section was of the same design and dimensions as the 47-L/D_1 test section except that it was much shorter, being only $7\frac{1}{2}$ in. in length. The prime consideration in the design of this section was to provide a heat exchanger in which no fully developed region of heat transfer existed. Figure 4.3 shows the designs of both the 47- and the 10-L/D_1 test sections.

Radiographs of the completed section showed that the width of the annular space had a maximum deviation of 5% from the value expected for zero eccentricity.

3. Instrumentation

a. Flow Measurement

The mercury flowrates in the tube and annulus of the test section were each measured by two methods. The first, in which a calibrated orifice and manometer assembly was utilized, was used primarily to calibrate the second, employing an electromagnetic flowmeter. The use of the electromagnetic flowmeter was preferred to that of the orifice arrangement for actual heat transfer tests, since its range was virtually unlimited compared to that of the orifice assembly. The flowmeter emfs were read on a Hewlett-Packard Model 2401C integrating digital voltmeter. The accuracy of the electromagnetic flowmeters is estimated to be within $\pm 5\%$ of the actual flowrate.

Details of the construction and calibration of the flow-measurement devices are given in Appendix D.

b. Temperature Measurements

All temperature measurements were made with select-grade copper-constantan thermocouples. All thermocouples which were in direct contact with mercury or water were sheathed in stainless steel jackets and inserted through compression fittings into the loop. The locations of the sheathed thermocouples are shown in Fig. 4.1. Thermocouples which were used to measure the temperature distribution of the outer wall of the test section were bare-bead thermocouples. These thermocouples were affixed to the outer wall of the test section by fiber glass tape for the experimental runs with the 20-L/D_1 test section and for a portion of the runs with the 47-L/D_1 test section. Inspection of the thermocouples midway through the series of tests with the 47-L/D_1 test section revealed that the high temperatures had caused the fiber glass tape to stretch and that some of the thermocouples had pulled away from the wall of the test section. The thermocouples

were then fastened to the test section with epoxy cement, a method which proved vastly superior to merely taping them.

The thermocouples for the measurement of the temperature distribution of the outer wall were spaced at equal intervals along the active length of the test section. For the 20- and 47-L/D_1 test sections, 31 thermocouples were used to measure the outer wall temperatures, and for the 10-L/D_1 section 16 were used. Thermocouples were also placed along the entrance lengths of the 20-L/D_1 section and at various locations around the circumference of all three test sections.

All the thermocouples were calibrated in a well-stirred, heated silicon oil bath prior to installation in the loop. Between the temperature limits of 70 to 230°F the thermocouples gave readings which were within 1/2°F of each other. This was judged to be accurate enough for the purposes of the experiment. No attempt was made to calibrate the thermocouples absolutely since only differential measurements were required for the experiment.

After installation in the loop, the thermocouple leads were fed through an insulated switchbox with an ice-junction reference to the Hewlett-Packard digital voltmeter. The switches used in the switchbox were high-quality double-pole, nonshorting thermocouple switches.

C. Experimental Procedure

1. Cleaning of Loop Components

Prior to the series of experimental runs with the first test section, the loop was given a thorough cleaning. Portions of the loop which could be dismantled and removed were pickled in a dilute solution of citric acid. This procedure removed any visible trace of surface impurities, and left the surfaces clean and shiny. Portions of the loop which could not be removed were scrubbed and flushed with acetone. To remove possible grease and impurities from the heat transfer surface of the test section and to promote wetting of the copper by mercury, the entire section was treated with a 12.5% solution of hydrochloric acid. After reassembly, the entire system was purged with nitrogen. Similar, although not quite as thorough, cleaning procedures were followed before installation of the second and third test sections.

Mercury used for the experiment was cleaned in a Bethlehem Oxifier and filtered through a Gold Seal filter. The loop was filled with a fresh charge of mercury for each test section.

Of special concern was the wetting of the copper heat transfer surface by the flowing mercury as well as the extent to which the mercury

eroded the copper surface. Inspection of the heat transfer surfaces after completion of the runs with each test section revealed that the mercury did wet the copper and that the only visible evidence of erosion was a slight pitting of the surface. Contamination of the mercury itself was probably so slight as to have no effect on the experimental measurements. Samples of mercury taken from the loop during heat transfer tests were clean and bright in appearance and had no visible contamination.

2. Operation for Data

With the loop filled with mercury and all safety controls in readiness, the circulating pump was energized and the flowrates adjusted to the desired setting. The water supply for the cooler was then turned on and adjusted to the proper flowrate. If required, the heater was energized and set at the desired power level. (For some of the runs with the canned rotor pump, the pump itself supplied a sufficient amount of heat to the system and the heater was not used.)

The loop was operated until stable conditions were reached. The loop was considered to be "stable" when the inlet and outlet temperatures of the test section varied less than 1/2°F over a period of 30 min. The inlet and outlet temperatures of the test section were read and recorded at 15-min intervals during the stabilization of the loop. It generally took at least 4 hr from startup for the loop to stabilize and about 2 hr for each successive run.

With the loop at stable operating conditions, the flowmeter and thermocouple emfs were read and recorded. Also read and recorded were the voltages across the heaters and the cooling water manometer differential. The readings were then rechecked for possible errors in the reading or recording of the data. Each experimental run was assigned a run number.

After tabulation of the data, the loop was adjusted to the operating conditions for the next run.

After completion of the desired number of runs, the loop was shut down by turning off the heaters, cooling water, and pump, in that order. The safety controls were then turned off, and the main power switch for the loop was opened.

3. Reduction of Data

The computations of most importance in the analysis of the data were the calculations for heat-exchanger efficiency and fully developed overall Nusselt number. Other computations, such as heat balances across the cooler, are of lesser importance and are not described here. A detailed description of the entire method of data reduction may be found in Appendix B.

a. Calculation of Efficiency

The heat-exchanger efficiency was calculated from measurements of both tube and annulus heat flux.

H < 1:

$$\epsilon_1 = \frac{c_1 W_1[\overline{T}_1(0) - \overline{T}_1(L)]}{c_2 W_2 \Delta T_0}; \qquad \text{Tube}$$

$$\epsilon_2 = \frac{\overline{T}_2(0) - \overline{T}_2(L)}{\Delta T_0}; \qquad \text{Annulus}$$

H > 1:

$$\epsilon_1 = \frac{\overline{T}_1(0) - \overline{T}_1(L)}{\Delta T_0}; \qquad \text{Tube}$$

$$\epsilon_2 = \frac{c_2 W_2[\overline{T}_2(0) - \overline{T}_2(L)]}{c_1 W_1 T_0}, \qquad \text{Annulus}$$

where

$$\Delta T_0 = \overline{T}_1(0) - \overline{T}_2(L).$$

In the ideal case, $\epsilon_1 = \epsilon_2$ in the above equations. Because of experimental error, however, the measured values of ϵ_1 and ϵ_2 usually differed from each other by a few percent. The percent difference between ϵ_1 and ϵ_2 is equivalent to the heat-balance error in the test section. The main cause of the heat-balance error is thought to be heat losses from the lines leading from the test section to the mixing chambers, where the fluid temperatures were measured. These extraneous heat losses affect the measured heat fluxes in a consistent manner and may be corrected to some extent. Since part of the heat transferred to the annulus fluid in the test section was lost in the entrance and exit lines, the measured heat flux was lower than the actual heat flux in the test section. For the tube side, the measured heat flux was larger than the actual heat flux in the test section since an additional amount of heat was lost in the entrance and exit lines. The result of these extraneous heat losses was that ϵ_2 was lower than the actual test-section efficiency, while ϵ_1 was higher. The error may be reduced to some extent by taking the efficiency to be the average of ϵ_1 and ϵ_2. The error of the average value is equal to one-half of the difference in the errors of ϵ_1 and ϵ_2. The experimental heat-exchanger efficiencies presented in this thesis are the averages of ϵ_1 and ϵ_2. A more complete discussion of the expected maximum experimental error is given in Appendix E.

b. Calculation of Nu°_{iFD}

The fully developed overall Nusselt number was computed by the method outlined in the first part of this chapter. The left-hand sides of Eqs. (4.1a) and (4.1b) were plotted against axial position as follows:

$H < 1$:

$$\ell n \left[\xi_2(1,z) - H \frac{1 - \epsilon}{H - 1} \right] \text{ vs. } z;$$

$H > 1$:

$$\ell n \left[\frac{H - \epsilon}{H - 1} - \xi_2(1,z) \right] \text{ vs. } z,$$

where

$$\xi_2(1,z) = \frac{T_2(r_{22},\ell) - \overline{T}_1(0)}{-\Delta T_0},$$

$$H = c_2 W_2 / c_1 W_1,$$

and

ϵ is the efficiency.

The curves so obtained were linear in regions of fully developed heat transfer. The linear portion of each curve was determined by inspection, and a least-squares method was then used to fit a straight line to the experimental points in the linear region. The slope of this straight line was then used to compute the fully developed overall Nusselt number according to Eqs. (3.42a) and (3.43a).

The value of ϵ used in the computation was the average of ϵ_1 and ϵ_2. A discussion of the expected maximum experimental error is given in Appendix E.

D. Analysis of Experimental Measurements

1. Tests with the 20-L/D_1 Test Section

The accuracy of the experimental data for comparison with the results of the mathematical analysis depends, in part, on the degree to which the experiment realizes the physical idealizations upon which the mathematical analysis is based. It was for the purpose of providing fully developed entering flow that the adiabatic entrance lengths were included in the design

of the 20-L/D_1 test section. As mentioned before, the "adiabatic" sleeve for the entering tube flow was filled with mercury for the entire series of runs with the 20-L/D_1 test section. The effect which the mercury-filled sleeve had on the data is discussed below.

The data taken with the first test section was reduced to yield heat-exchanger efficiencies and fully developed overall Nusselt numbers. These quantities are determined by the operating conditions of the heat exchanger as specified by the parameters H, K, K_w, R, and Z. With the test-section materials and dimensions fixed and the heat transfer fluid chosen, the efficiencies and Nusselt numbers should be dependent only on the flowrates in the tube and annulus of the test section. In addition to a dependence on flowrates, however, the initial series of runs with the 20-L/D_1 section revealed that the efficiencies and Nusselt numbers were strongly dependent on ΔT_0, the inlet temperature difference of the fluids. This dependence is illustrated in Figs. 4.4 and 4.5 for runs in which the flowrates were held constant and only ΔT_0 was varied. The dependence on ΔT_0 suggested the presence of a mode of heat transfer other than that occurring in the active length of the test section. The fact that this extraneous heat transfer occurred through the tube-entrance sleeve was partially confirmed by the observation that the outer wall temperature of the test section rose steadily along the length of the sleeve, indicating a significant amount of heat transfer through the sleeve. Similar measurements along the sleeve at the opposite end of the test section showed very little temperature rise. It was not known for certain, however, that the tube-entrance sleeve was filled with mercury until the test section was removed and torn apart.

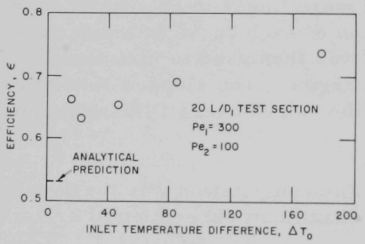

Fig. 4.4. Effect of Fluid Inlet Temperature Difference on Efficiency for the 20-L/D_1 Test Section

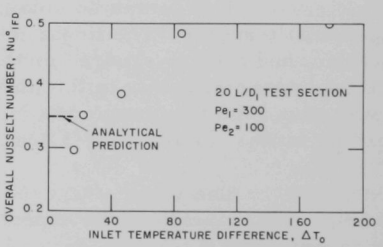

Fig. 4.5. Effect of Fluid Inlet Temperature Difference on Fully Developed Overall Nusselt Number for the 20-L/D_1 Test Section

With the ΔT_0 dependence present in the results from the 20-L/D_1 test section, a meaningful comparison with the analytical prediction could not be made. Attempts to produce a satisfactory analytical model to explain the ΔT_0 dependence failed. Merriam[23] encountered the same problem in his co-current experiments and concluded that the extraneous heat transfer was due

to conduction through the end plates of the heat exchanger. The method which Merriam used to analyze his data was to first plot ϵ or Nu°_{iFD} vs. ΔT_0, as in Figs. 4.4 and 4.5. He then extrapolated the data to the value for $\Delta T_0 = 0$ and took that value as the correct one. Merriam's assumption was that the extraneous heat transfer effect was dependent only on ΔT_0 and that the ΔT_0 dependence would vanish at $\Delta T_0 = 0$. Merriam achieved moderate success with this method of analysis, so the present experimental program with the 20-L/D_i test section was conducted to obtain data for the plots of ϵ or Nu°_{iFD} vs. ΔT_0. Values of ϵ and Nu°_{iFD} obtained in this manner showed a great deal of scatter, particularly for high flowrates in the annulus. Inasmuch as the method of analysis was subject to large errors, particularly errors of judgment in the extrapolation of the data to $\Delta T_0 = 0$, the results from the 20-L/D_i test section were considered unreliable and were discarded.

2. Tests with the 47-L/D_i Test Section

Because of the difficulties encountered with the adiabatic sleeves on the first test section, the 47-L/D_i test section was constructed without flow-development lengths in order to reduce the occurrence of extraneous heat transfer as much as possible. Initial operation of the 47-L/D_i test section was for the purpose of determining the effect of the inlet temperature difference, ΔT_0, on the efficiency and overall Nusselt number. The results of this initial series of tests showed that the ΔT_0 effect had been eliminated.

As the tests continued, however, the temperature distribution of the outer wall began to exhibit a considerable amount of distortion. This distortion eventually became so pronounced that the temperature distribution of the outer wall could not be used for determining the Nusselt number. Inspection of the thermocouples on the outer wall revealed that the tape which held them in place had stretched and that most of the thermocouples had pulled away from the wall, thereby giving erroneous readings. The thermocouples were then cemented in place with extra care taken to keep the bead in contact with the wall. A resistance meter was used to check the contact. The data taken with the thermocouples cemented in place showed much improvement over the data taken with the thermocouples taped in place. The accuracy of the data taken with the taped thermocouples was uncertain, and the data were discarded.

The actual operation of the 47-L/D_i test section "for data" began after the thermocouples were cemented in place. A total of 40 usable experimental runs were made for flowrates corresponding to Peclet numbers in the range from 100 to 1500 for the tube and from 50 to 300 for the annulus. The plots of temperature for the outer wall for all of the test showed a well-defined linear portion whose slope was proportional to the

fully developed overall Nusselt number. Figure 4.6 is a representative sample of such a temperature plot for the 47-L/D_1 test section. Heat-balance deviations for the test section were generally less than ±5%. The heat-balance deviation was used as a general indication of the error of the experimental results. The data for the 47-L/D_1 test section are tabulated in Appendix C.

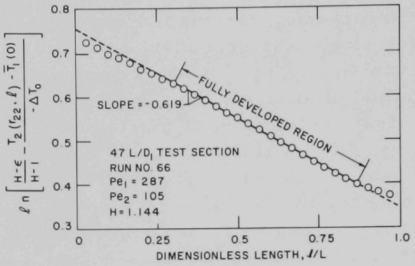

Fig. 4.6. Outer-wall Temperature Plot for Test Section in Which Heat Transfer Is Fully Developed

3. Tests with the 10-L/D_1 Test Section

The 10-L/D_1 test section was tested over the same ranges of flowrates as the 47-L/D_1 test section. Initial tests in which the flowrates were held constant and only ΔT_0 was varied gave efficiencies which were independent of ΔT_0. The plots obtained from the outer-wall temperatures did not have a linear region corresponding to fully developed heat transfer. Figure 4.7 is a typical temperature plot for the outer wall for the tests with the 10-L/D_1 test section. All of the plots for the various runs produced the "S" shaped curve.

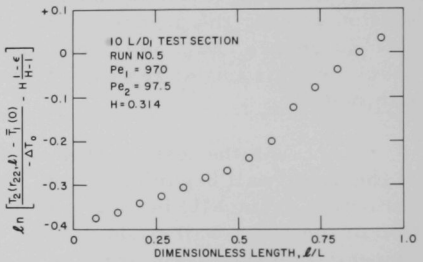

Fig. 4.7. Outer-wall Temperature Plot for Test Section in Which Heat Transfer Is Not Fully Developed

Since a fully developed region was not present in any of the tests, only heat-exchanger efficiencies were calculated. Heat-balance deviations for the 10-L/D_1 test section were somewhat higher than those for the 47-L/D_1 test section, probably because of the difference in the lengths of the two test sections. Less heat was transferred in the 10-L/D_1 section, so the error due to losses in the lines leading to the mixing chambers, which should have remained approximately the same, contributed to a larger deviation of heat balance. The data for the 10-L/D_1 test section are tabulated in Appendix C.

CHAPTER V

RESULTS AND DISCUSSION

Operating curves for the heat exchangers used in the experiments were computed from the present mathematical analysis and from the traditional method of heat-exchanger design. The theoretical operating curves are compared with the experimental results.

A. Heat-exchanger Calculations

Computations were performed to obtain theoretical operating curves for the heat exchangers used in the experiment. Efficiencies and fully developed overall Nusselt numbers were computed from the present mathematical analysis by means of the k^+ approximation. The nonnarrow annular-space form was used for the computations. The values of the major parameters for the 47- and 10-L/D_1 test sections are given in Table 5.1. Computations for the 20-L/D_1 test section are not given because no reliable experimental data were obtained and a comparison between theory and data was not possible.

TABLE 5.1. Dimensionless Parameters for the Test Sections

Parameter	Test Section	
	47 L/D_1	10 L/D_1
$H = \frac{c_2 W_2}{c_1 W_1} = \frac{k_2}{k_1} \frac{r_{22} + r_{21}}{r_{12}} \frac{Pe_2}{Pe_1}$	$3.15 \frac{Pe_2}{Pe_1}$	$3.15 \frac{Pe_2}{Pe_1}$
$K = \frac{1 - R}{R} \frac{k_1 k_1^+}{k_2 k_2^+}$	$0.38 \frac{k_1^+}{k_2^+}$	$0.38 \frac{k_1^+}{k_2^+}$
$K_w = \frac{k_1 k_1^+}{k_w} \ln\left(\frac{r_{21}}{r_{12}}\right)$	$0.00679\ k_1^+$	$0.00679\ k_1^+$
$R = \frac{r_{21}}{r_{22}}$	0.727	0.727
$Z = \frac{4}{Pe_1} \frac{L}{2r_{12}} k_1^+$	$189.5 \frac{k_1^+}{Pe_1}$	$40 \frac{k_1^+}{Pe_1}$

The values of the thermal conductivities used in Table 5.1 are given in Appendix B. The values of k_1^+ and k_2^+ were calculated from the uniform-heat-flux correlations of Buleev[5] and Dwyer,[6-8] Eqs. (2.1a) and (2.1b). For the 47- and 10-L/D_1 test sections, Eqs. (2.1a) and (2.1b) reduce to the following:

Buleev[5]--Uniform Heat Flux in Tube:

$$Nu_{1UHF} = 4.69 + 0.0303Pe_1^{0.779}; \tag{5.1a}$$

Dwyer[6-8]--Uniform Heat Flux at Inner Wall of Annulus:

$$Nu_{2UHF} = 5.890; \quad Pe_2 \leq 325;$$

$$Nu_{2UHF} = 5.779 + 0.0222\left[Pe_2 - \frac{79.5Pe_2}{\left(4 + 0.0936Pe_2^{0.919}\right)^{1.4}}\right]^{0.771}; \quad Pe > 325. \tag{5.1b}$$

The corresponding fully developed plug-flow Nusselt numbers are: for a uniformly heated tube, Eq. (3.1c), Nu = 8; for a uniformly heated annulus Eq. (2.1e), Nu = 6.06 for both test sections, since their radial dimensions were identical.

The expressions for k_1^+ and k_2^+ are

$$k_1^+ = \tfrac{1}{8}Nu_{1UHF} \tag{5.2a}$$

and

$$k_2^+ = \frac{1}{6.06}Nu_{2UHF} \tag{5.2b}$$

With the above relations for k_1^+ and k_2^+ chosen, the results of the computations depend only on the tube and annulus Peclet numbers. Computations were made for tube-side Peclet numbers in the range 100-1500 and for annulus-size Peclet numbers of 50, 100, 200, and 300. For the computations for efficiency where only the zeroth-order expansion coefficient was needed, 40 equations of the infinite set were used.

The traditional method of heat-exchanger design was also used to predict operating curves for the heat exchangers. The individual-channel Nusselt numbers were assumed to be uniform over the entire length of the heat exchanger and were those appropriate to a uniform-heat-flux boundary condition as given by Eqs. (5.1a) and (5.1b). The overall Nusselt number, Nu_{1UHF}°, was then computed from the individual-channel Nusselt numbers by means of Eq. (3.39). The heat-exchanger efficiency, ϵ_{UHF}, was computed by means of Eqs. (3.47a) and (3.47b). The results of all the heat-exchanger computations are given in Table 5.2.

TABLE 5.2. Results of Computations for Test Sections

									Test Section					
									47 L/D_1			10 L/D_1		
Pe_1	Pe_2	k_1^+	k_2^+	H	K	K_w	Nu^0_{1FD}	Nu^0_{1UHF}	Z	ε	ε_{UHF}	Z	ε	ε_{UHF}
100	50	0.723	0.971	1.577	0.282	0.00491	3.914	4.154	1.369	0.977	0.979	0.2893	0.719	0.696
200	50	0.821	0.971	0.788	0.321	0.00557	4.719	4.543	0.777	0.921	0.911	0.1643	0.625	0.566
400	50	0.990	0.971	0.394	0.387	0.00672	6.045	5.148	0.468	0.994	0.986	0.0989	0.767	0.666
600	50	1.139	0.971	0.263	0.445	0.00773	7.017	5.630	0.359	0.999	0.995	0.0759	0.829	0.717
800	50	1.278	0.971	0.197	0.499	0.00867	7.736	6.035	0.302	0.999	0.998	0.0639	0.862	0.751
1000	50	1.410	0.971	0.158	0.551	0.00957	8.285	6.386	0.267	0.999	0.999	0.0564	0.883	0.776
1500	50	1.716	0.971	0.105	0.671	0.01164	9.216	7.103	0.216	0.999	0.999	0.0457	0.910	0.818
100	100	0.723	0.971	3.154	0.282	0.00491	3.726	4.154	1.369	0.995	0.997	0.2893	0.774	0.755
200	100	0.821	0.971	1.577	0.321	0.00557	4.305	4.543	0.777	0.912	0.911	0.1643	0.573	0.519
400	100	0.990	0.971	0.788	0.387	0.00672	5.317	5.148	0.468	0.837	0.817	0.0989	0.492	0.412
600	100	1.139	0.971	0.526	0.445	0.00773	6.149	5.630	0.359	0.923	0.896	0.0759	0.565	0.459
800	100	1.278	0.971	0.394	0.499	0.00867	6.827	6.035	0.302	0.957	0.931	0.0639	0.612	0.493
1000	100	1.410	0.971	0.315	0.551	0.00957	7.381	6.386	0.267	0.973	0.951	0.0564	0.644	0.520
1500	100	1.716	0.971	0.210	0.671	0.01164	8.390	7.103	0.216	0.988	0.974	0.0457	0.694	0.568
100	200	0.723	0.971	6.308	0.282	0.00491	3.670	4.154	1.369	0.996	0.999	0.2893	0.803	0.784
200	200	0.821	0.971	3.154	0.321	0.00557	4.125	4.543	0.777	0.959	0.963	0.1643	0.620	0.557
400	200	0.990	0.971	1.577	0.387	0.00672	4.922	5.148	0.468	0.807	0.796	0.0989	0.445	0.362
600	200	1.139	0.971	1.051	0.445	0.00773	5.601	5.630	0.359	0.670	0.648	0.0759	0.355	0.275
800	200	1.278	0.971	0.788	0.499	0.00867	6.183	6.035	0.302	0.724	0.692	0.0639	0.377	0.285
1000	200	1.410	0.971	0.631	0.551	0.00957	6.683	6.386	0.267	0.778	0.740	0.0564	0.407	0.304
1500	200	1.716	0.971	0.421	0.671	0.01164	7.660	7.103	0.216	0.854	0.811	0.0457	0.456	0.340
100	300	0.723	0.971	9.461	0.282	0.00491	3.676	4.154	1.369	0.996	0.999	0.2893	0.815	0.793
200	300	0.821	0.971	4.731	0.321	0.00557	4.088	4.543	0.777	0.969	0.973	0.1643	0.639	0.570
400	300	0.990	0.971	2.365	0.387	0.00672	4.808	5.148	0.468	0.850	0.842	0.0989	0.471	0.375
600	300	1.139	0.971	1.577	0.445	0.00773	5.421	5.630	0.359	0.735	0.713	0.0759	0.383	0.287
800	300	1.278	0.971	1.183	0.499	0.00867	5.952	6.035	0.302	0.643	0.614	0.0639	0.325	0.236
1000	300	1.410	0.971	0.946	0.551	0.00957	6.415	6.386	0.267	0.607	0.573	0.0564	0.300	0.214
1500	300	1.716	0.971	0.631	0.671	0.01164	7.343	7.103	0.216	0.701	0.655	0.0457	0.344	0.241

B. Experimental Results

The experimental data were reduced according to the procedure given in Appendix B. The heat-exchanger efficiencies and fully developed overall Nusselt numbers which were obtained were functions of the flowrates in the tube and annulus of the test sections. The experiment covered a range of flowrates corresponding to Peclet numbers of 100 to 1500 for the tube side and of 50 to 300 for the annulus side of the test sections. The operating conditions and results for each experimental run for the 47- and 10-L/D_1 test sections are given in Tables 5.3 and 5.4, respectively. As mentioned previously, the data for the 20-L/D_1 section were considered unreliable and were discarded. In addition, only the last 40 runs with the 47-L/D_1 test section are tabulated, since the data taken in the first 42 runs had to be discarded because of errors in the measurements of the outer wall temperature. These errors were discussed in Chapter IV.

The accuracy of the experimental results in Tables 5.3 and 5.4 can be judged by the magnitude of the "expected maximum error" given in Appendix E. This expected maximum error is considered to be the upper limit for experimental error. The actual experimental error is probably considerably less than the values reported in Appendix E.

TABLE 5.3. Experimental Results with the 47-L/D_1 Test Section

Run	Pe_1	Pe_2	H	Nu_{FD}°	ε	Test Section Heat Balance Deviation, %	ΔT_0	Run	Pe_1	Pe_2	H	Nu_{FD}°	ε	Test Section Heat Balance Deviation, %	ΔT_0
43	290	199	2.144	4.838	0.888	1.719	46.7	63	98	98	3.107	4.092	0.974	4.780	67.7
44	389	199	1.597	5.060	0.795	2.289	49.3	64	143	98	2.145	4.456	0.963	3.644	82.3
45	488	199	1.275	5.385	0.717	3.280	48.9	65	194	99	1.597	4.638	0.910	4.991	82.4
46	582	199	1.067	5.542	0.653	2.490	51.1	66	287	105	1.144	5.031	0.798	1.396	84.9
47	781	199	0.798	6.192	0.690	2.728	50.6	67	394	103	0.821	5.365	0.796	2.110	88.9
48	975	199	0.639	6.677	0.744	3.132	51.3	68	488	99	0.633	5.575	0.862	2.684	90.2
49	1171	199	0.532	7.072	0.779	1.095	53.3	69	588	99	0.526	5.873	0.899	3.246	92.1
50	1373	199	0.454	7.324	0.808	2.114	53.8	70	783	103	0.411	6.320	0.931	4.326	89.2
51	104	199	5.926	3.939	0.990	0.664	29.6	71	981	103	0.328	6.717	0.957	4.785	90.4
52	146	199	4.233	3.988	0.998	4.636	36.8	72	1176	102	0.272	7.137	0.962	1.888	91.1
53	193	199	3.216	4.588	0.953	6.165	40.3	73	1373	101	0.231	7.518	0.973	2.778	87.7
54	193	300	4.861	4.903	0.953	7.609	23.9	74	108	49	1.438	4.234	0.972	1.289	110.3
55	289	300	3.243	4.816	0.905	3.297	29.4	75	204	49	0.758	5.603	0.900	7.617	133.5
56	384	300	2.445	5.080	0.844	1.154	32.4	76	300	49	0.520	5.204	0.968	2.172	138.0
57	476	300	1.974	5.128	0.785	1.265	33.9	77	394	49	0.396	5.233	0.993	4.893	138.0
58	587	300	1.598	5.574	0.719	0.988	34.6	78	598	49	0.256	5.934	1.006	5.670	143.0
59	783	300	1.197	6.070	0.625	1.873	34.9	79	979	49	0.159	7.131	1.002	3.983	142.9
60	975	298	0.957	6.859	0.576	2.299	35.9	80	780	51	0.205	6.572	0.980	0.021	142.5
61	1171	300	0.802	7.235	0.616	1.764	36.6	81	1157	49	0.135	7.495	0.994	2.454	146.4
62	1364	300	0.689	7.327	0.649	1.814	35.3	82	1379	48	0.109	7.837	1.019	7.125	146.9

TABLE 5.4 Experimental Results with the 10-L/D_1 Test Section

Run	Pe_1	Pe_2	H	ε	Test Section Heat Balance Deviation, %	ΔT_0	Run	Pe_1	Pe_2	H	ε	Test Section Heat Balance Deviation, %	ΔT_0
1	488	100	0.641	0.516	2.584	55.5	24	1281	196	0.478	0.439	2.926	35.9
2	485	99	0.637	0.529	5.247	74.7	25	1574	198	0.393	0.465	6.962	35.9
3	483	100	0.651	0.521	3.178	99.4	26	187	299	4.992	0.721	2.882	32.8
4	971	99	0.320	0.627	1.522	64.2	27	288	298	3.226	0.546	12.518	34.4
5	970	97	0.313	0.641	4.946	79.5	28	389	300	2.409	0.473	6.137	18.7
6	970	100	0.324	0.631	3.969	96.0	29	481	299	1.943	0.427	1.534	21.6
7	98	99	3.163	0.809	11.063	13.9	30	596	298	1.565	0.383	3.406	23.9
8	145	99	2.133	0.695	3.113	27.6	31	774	299	1.209	0.323	2.527	26.5
9	198	100	1.580	0.586	2.444	37.0	32	966	298	0.966	0.292	1.773	25.0
10	292	99	1.067	0.461	7.661	43.8	33	1278	300	0.735	0.315	3.687	26.9
11	391	99	0.791	0.484	4.723	50.3	34	1551	302	0.608	0.337	7.775	26.0
12	585	98	0.527	0.552	5.273	61.3	35	95	49	1.625	0.790	0.698	55.6
13	775	100	0.404	0.590	5.660	61.8	36	148	49	1.046	0.615	2.307	71.6
14	1278	99	0.242	0.671	6.547	66.5	37	194	49	0.789	0.642	2.262	81.9
15	1589	101	0.199	0.687	5.067	64.2	38	291	49	0.533	0.701	3.004	92.8
16	148	199	4.214	0.688	31.352	20.1	39	385	49	0.398	0.753	4.512	96.8
17	195	198	3.168	0.628	18.667	25.3	40	483	48	0.315	0.793	5.987	100.4
18	292	199	2.134	0.516	14.363	33.3	41	582	49	0.263	0.817	6.661	100.2
19	385	199	1.611	0.450	7.538	26.7	42	775	48	0.194	0.862	7.938	101.7
20	487	199	1.276	0.390	9.437	28.9	43	965	49	0.161	0.881	9.516	97.8
21	585	198	1.060	0.349	9.294	31.0	44	1271	49	0.121	0.908	9.454	100.3
22	783	200	0.798	0.367	7.654	33.6	45	1551	48	0.097	0.930	10.101	101.6
23	974	199	0.638	0.402	10.838	32.8							

C. Comparison of Theory and Experiment

1. Results with the 47-L/D_1 Test Section

a. Fully Developed Overall Nusselt Number

The fully developed overall Nusselt numbers determined experimentally were compared with theoretical operating curves computed from the present analysis and from the traditional method, assuming a uniform-heat-flux boundary condition. Figures 5.1 to 5.4 show the results

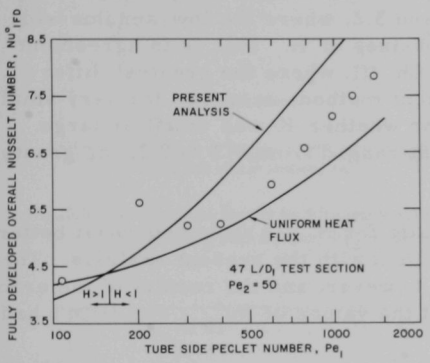

Fig. 5.1. Experimental Results for Overall Nusselt Number with the 47-L/D_1 Test Section, $Pe_2 = 50$

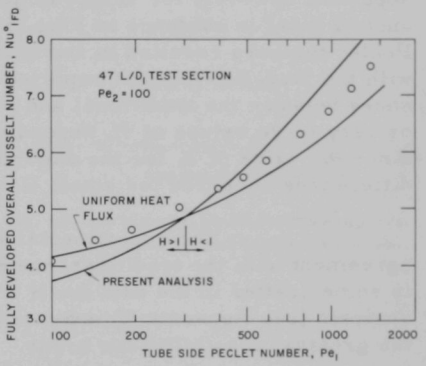

Fig. 5.2. Experimental Results for Overall Nusselt Number with the 47-L/D_1 Test Section, $Pe_2 = 100$

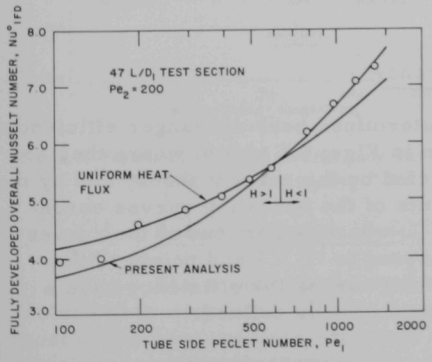

Fig. 5.3. Experimental Results for Overall Nusselt Number with the 47-L/D_1 Test Section, $Pe_2 = 200$

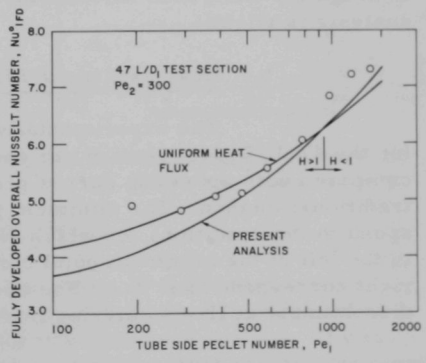

Fig. 5.4. Experimental Results for Overall Nusselt Number with the 47-L/D_1 Test Section, $Pe_2 = 300$

for runs in which the annulus flowrate was held constant and the tube-side flowrate was varied. The point at which the theoretical curves cross on the graphs is the condition for H = 1. The portions of the curves for $H > 1$ lie to the left of the intersection and the portions for $H < 1$ lie to the right.

The operating curves computed by the present theory and the traditional method did not exhibit significant differences for values of H greater than unity. Significant differences between the results of the present theory and the traditional method of heat-exchanger design are apparent, however, for values of H much smaller than unity. The difference is most in evidence in Figs. 5.1 and 5.2, where the low-annulus-side Peclet numbers resulted in fairly low values of H. This is in agreement with the plug-flow results reported in Ch. III, where the greatest differences between the traditional and present methods occurred for very small or very large values of H, depending on whether K was small or large. Since the value of K for the experiment ranged from 0.3 to 0.7, the greatest differences occurred for small H.

The experimental results for $H > 1$ show somewhat better agreement with the traditional method than with the present analysis. There is some scatter in the data for $H > 1$, however, and the results of the error analysis (see Appendix E) indicate that the values of Nu°_{1FD} for $H > 1$ had the greatest possibility for error.

The experimental results for $H < 1$ in Figs. 5.1 and 5.2 fall approximately equidistant between the curves computed from the present theory and the traditional method. For the operating curves shown in Figs. 5.3 and 5.4, the data for $H < 1$ agree better with the present analysis, although the difference between the present analysis and the traditional analysis is slight.

b. Heat-exchanger Efficiency

The experimentally determined heat-exchanger efficiencies for the 47-L/D_1 test section are shown in Figs. 5.5 to 5.8, where they are compared with operating curves predicted by the present theory and by the traditional method. The minimum points of the operating curves correspond to the conditions for which H = 1, whereas portions of the curves to the left of the minimum point correspond to $H > 1$ and points to the right correspond to $H < 1$. The operating curves for efficiency have a discontinuity at H = 1, arising from the way ϵ is defined.

Differences between the theoretical operating curves in Figs. 5.5 to 5.8 are seen to be quite small for values of H greater than unity. For values of H less than unity the difference is more pronounced, although either operating curve would probably be accurate enough for practical design computations. The experimental data show good agreement

with the theoretical operating curves over the entire range of operating conditions for which data were obtained. The data exhibit somewhat better agreement with the curve computed from the traditional method than with that computed from the present theory.

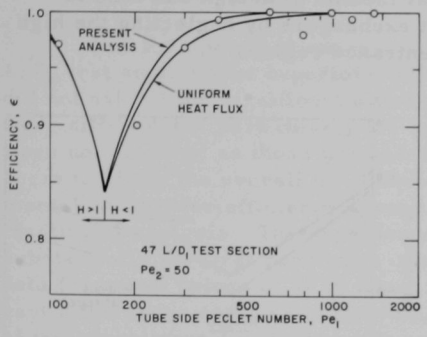

Fig. 5.5. Experimental Results for Efficiency with the 47-L/D_1 Test Section, Pe_2 = 50

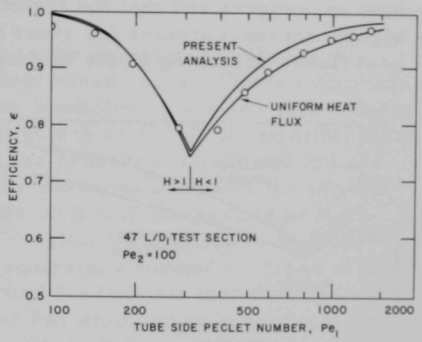

Fig. 5.6. Experimental Results for Efficiency with the 47-L/D_1 Test Section, Pe_2 = 100

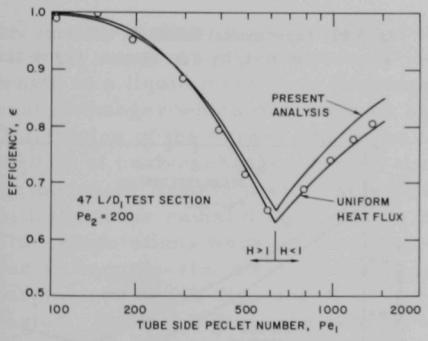

Fig. 5.7. Experimental Results for Efficiency with the 47-L/D_1 Test Section, Pe_2 = 200

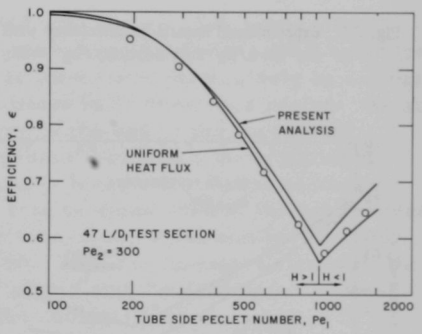

Fig. 5.8. Experimental Results for Efficiency with the 47-L/D_1 Test Section, Pe_2 = 300

2. Results with the 10-L/D_1 Test Section

The experimental data for the short, 10-L/D_1 test section yielded heat-exchanger efficiencies for a heat exchanger in which all or most of the heat transfer occurred in thermal entrance regions. It was mentioned previously that no fully developed region could be detected from the temperature distribution of the outer wall. The experimental results with the 10-L/D_1 test section are shown in Figs. 5.9 to 5.12 where they are compared with operating curves computed by the present analysis and

by the traditional method. It is evident from the figures that significant differences exist between the differently predicted operating curves. The experimental results from the 10-L/D_1 test section agree quite well with the curve computed from the present analysis. The data strongly support the contention that entrance-region effects are important for liquid metal heat exchangers and that the traditional method of design can lead to significant inaccuracies for short heat exchangers by neglecting the high heat fluxes occurring in the thermal-entrance regions.

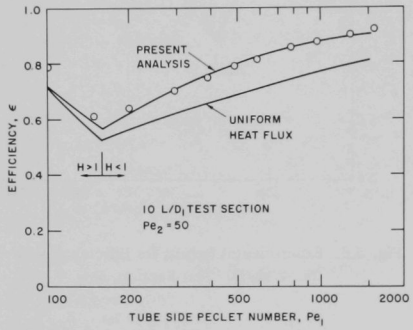

Fig. 5.9. Experimental Results for Efficiency with the 10-L/D_1 Test Section, Pe_2 = 50

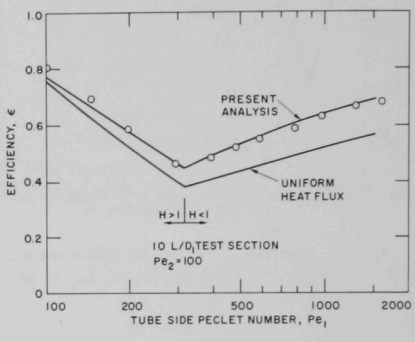

Fig. 5.10. Experimental Results for Efficiency with the 10-L/D_1 Test Section, Pe_2 = 100

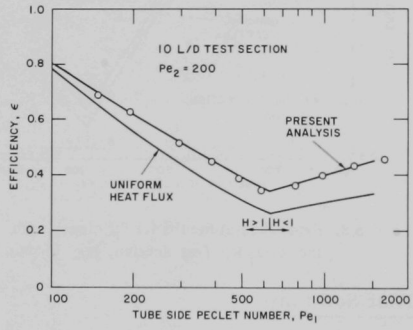

Fig. 5.11. Experimental Results for Efficiency with the 10-L/D_1 Test Section, Pe_2 = 200

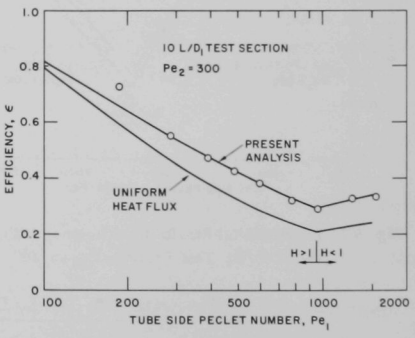

Fig. 5.12. Experimental Results for Efficiency with the 10-L/D_1 Test Section, Pe_2 = 300

D. Discussion

The present analysis has indicated that significant errors can result from use of the traditional analysis for heat-exchanger design because:

1) The actual fully developed overall Nusselt number may be quite different from that assumed in the traditional analysis.

2) The high heat fluxes occurring in the thermal-entrance regions of liquid metal heat exchangers are not negligible and may cause serious errors if ignored.

For the operating range covered in the experiment with the 47-L/D_1 test section, the experimentally determined overall Nusselt numbers did not exhibit the significant differences predicted by the analysis. There were differences, particularly for small values of H, but these differences were not as large as those predicted by the present analysis and did not seem to affect the overall heat-exchanger performance since the experimental results for efficiency agreed quite well with the results of the traditional analysis. The experimental results, then, failed to support substantially the first prediction of the analysis, although the trend of the data for small values of H in Figs. 5.3 and 5.4 indicate that these significant differences could exist for values of Pe_1 which were beyond the range of the experimental apparatus. It seems likely that the differences predicted by the analysis could occur for heat exchangers which have very small annular spaces and which therefore must be operated at very small values of H.

The experimental results obtained with the 10-L/D_1 test section strongly support the present analytical prediction that the thermal-entrance length in a liquid metal heat exchanger is important, particularly in a short heat exchanger which may have no significant fully developed region. As an illustration of the errors which can occur in the use of the traditional method of heat-exchanger design, the present theory and the traditional method were used to predict heat-exchanger lengths for a heat exchanger with the same radial dimensions as the test sections used in the experiment. The computations were performed for a tube-side Peclet number of 1000 and an annulus-side Peclet number of 100. With the flowrates constant, the parameters H, K, K_w, and R were calculated and the parameter Z was varied. Table 5.5 gives the results of the computations.

TABLE 5.5. Heat-exchanger Lengths Predicted by Present and Traditional Analyses

$Pe_1 = 1000$; $Pe_2 = 100$; $H = 0.315$; $K = 0.551$; $K_w = 0.00957$; $R = 0.727$; $Z = \frac{L(\text{in.})}{133}$

Efficiency of Heat Exchanger	Length Predicted by Present Analysis (in.)	Length Predicted by Traditional Analysis (in.)
0.2	0.75	2.15
0.4	2.80	5.10
0.6	6.35	9.20
0.8	13.20	17.50

It is evident from these results that the traditional method overestimates the length required for a given efficiency by a substantial amount for the lower efficiencies. The differences between the present and traditional methods become smaller as the efficiency increases, although the traditional method still overestimates the length by more than 30% for the fairly high efficiency of 0.8.

The experimental evidence was partially successful in supporting the results of the present analysis. The large differences in Nu°_{1FD} were not in evidence in the data, but trends indicated that they might occur for larger values of Pe_1. More experimental data for different test sections and widely varying values of H are needed before a definite statement can be made about the validity of the traditional assumption regarding the heat transfer coefficients.

The experimental evidence regarding the importance of the thermal-entrance regions gives strong support for the present analysis in suggesting that significant errors can arise when such regions are ignored. In view of the experimental results for the $10\text{-}L/D_1$ test section, the analysis gives results which are quite accurate for the design of short heat exchangers.

CHAPTER VI

SUMMARY

Heat transfer in countercurrent, liquid metal, double-pipe heat exchangers was investigated both analytically and experimentally. None of the traditional simplifying assumptions regarding the heat transfer coefficients of individual channels were incorporated into the mathematical analysis. The analysis, in its most general form, was applicable to both laminar and turbulent flow. An approximation was introduced which permitted the use of a plug-flow model for turbulent, liquid metal heat exchangers. The approximation was accurate for Peclet numbers up to and possibly greater than 1000. Since practical heat exchangers may be operated at Peclet numbers of 1000 or less, the approximation provides a considerable simplification for a physically important range. For application to heat exchangers which operate at Peclet numbers much larger than 1000, the accuracy of the approximation is doubtful.

Numerical results for the plug-flow model have been presented. Computations were made using the narrow-annular-space approximation as well as for a nonnarrow annular space. In general, the numerical results showed that:

1. For a fluid conductivity ratio of the order of unity, the narrow-annular-space approximation yields overall heat-exchanger results which are quite accurate for radius ratios as low as 0.5.

2. The fully developed Nusselt numbers are never lower than the value corresponding to a uniform-wall-temperature boundary condition, but can be significantly higher than that corresponding to a uniform-heat-flux boundary condition.

3. The heat transfer characteristics of a countercurrent heat exchanger depend upon its operating conditions as specified by the parameters, H, K, K_w, R, and Z. In some cases, serious inaccuracies can result from a prior assumption about the boundary condition at the wall separating the fluids.

4. Neglect of the high heat fluxes occurring in the thermal-entrance regions of a heat exchanger can, in some cases, result in a serious underestimate of the efficiency.

An experimental investigation was conducted to provide experimental data for comparison with the results of the mathematical analysis. A new technique, requiring measurement of the temperature distribution of the outer wall of the heat exchanger, was successfully used to measure fully developed overall heat transfer coefficients. The technique proved to be

simpler to use and potentially more accurate than techniques requiring measurements of fluid or temperature distributions of the inner wall.

The experimental data partially supported the results of the mathematical analysis. The experimentally determined overall Nusselt numbers were different from those computed using the traditional analysis. The magnitude of the difference was not as great as that predicted by the present analysis, but the trend of the data indicated that large difference would occur for large tube-side flowrates. The experimentally determined heat-exchanger efficiencies showed that neglect of the thermal-entrance regions in short heat exchangers leads to significant errors. For long heat exchangers, the data indicated that the thermal-entrance region was of lesser importance.

Heat-exchanger performance has been shown to depend in a very complicated manner on the parameters H, K, K_w, R, and Z. For turbulent flow the situation is further complicated by the dependence of the above parameters on the quantities k_1^+ and k_2^+. Because of the complicated nature of the problem, no simplified formulae have been presented for use in practical design work. For the design of liquid metal heat exchangers, in regions where the accuracy of the traditional method is doubtful, the present analysis may be used with reasonable confidence for predicting performance of heat exchangers.

CHAPTER VII

RECOMMENDATIONS

1. Although the present method of computing the expansion coefficients yields sufficiently accurate results, the solution of the large sets of equations necessary for accuracy is laborious and time-consuming. The investigation of improved methods of computing the expansion coefficients is, therefore, recommended.

2. Application of the analysis to obtain detailed wall-heat-flux and fluid-temperature distributions would be of interest, and is suggested as a possible future contribution.

3. The results presented in this thesis are intended to illustrate the regions in which the traditional method of design may lead to inaccuracies. In a more practical vein, the presentation of detailed design curves or simplified design formulae, based on the present analysis, would be a contribution.

4. The application of the analysis to a true turbulent flow with the appropriate velocity and eddy-diffusivity distribution would constitute a significant extension of the work presented here. The results of such an analysis would be valid for all values of the Peclet number and would not be restricted to liquid metals. The results could also be used as a further check on the accuracy of the k^+ approximation.

5. The technique used for measuring the fully developed overall Nusselt number is recommended for use in other experimental investigations of heat transfer. The method is applicable for both laminar and turbulent flow, and can be used for configurations other than the double-pipe configuration.

APPENDIX A

Details of Mathematical Analysis

1. Mathematical Basis of the Analysis

The theorem upon which the analysis is based is that regarding the existence of the negative eigenvalues. This theorem, which is an extension of the classical Sturmian theory, will be stated now for later reference. A rigorous mathematical treatment of the following system may be found in Refs. 62 and 63.

Consider the system:

$$\frac{d}{dx}\left(k\,\frac{dy}{dx}\right) + (\lambda^2 g - \ell)\,y = 0; \tag{A.1a}$$

$$\alpha' y(a) - \alpha y'(a) = 0; \tag{A.1b}$$

$$\gamma' y(b) + \gamma y'(b) = 0, \tag{A.1c}$$

where k, g, and ℓ are real continuous functions of x in the interval

$$a \leq x \leq b,$$

and

$$k > 0;\quad g > 0;\quad \ell \geq 0;$$

$\alpha\alpha' \geq 0$, with α and α' not both zero;

$\gamma\gamma' \geq 0$, with γ and γ' not both zero.

The above system constitutes the familiar Sturm-Liouville system for which characteristic solutions, called eigenfunctions, exist for a set of real, discrete, positive characteristic numbers, called eigenvalues, λ_0^2, λ_1^2, λ_2^2, ..., which have no limit point except $\lambda^2 = +\infty$. If the eigenfunctions are denoted as y_0, y_1, y_2, ..., corresponding to the index of their corresponding eigenvalue, then y_m has exactly m zeros in the interval $a < x < b$.

If, on the other hand, the function g changes sign in the interval $a < x < b$ and all other conditions remain the same, then the preceding result has to be modified as follows.

For the case that g changes sign in the interval $a < x < b$, there exists an infinite set of real eigenvalues that has the limit points $+\infty$ and $-\infty$. If the positive and negative eigenvalues are arranged each in order of

increasing absolute value, and are denoted by

$$\lambda^2_{+0}, \lambda^2_{+1}, \lambda^2_{+2}, \ldots, \lambda^2_{+m}, \ldots;$$

$$\lambda^2_{-0}, \lambda^2_{-1}, \lambda^2_{-2}, \ldots, \lambda^2_{-m}, \ldots,$$

and the corresponding eigenfunctions by

$$y_{+0}, y_{+1}, y_{+2}, \ldots, y_{+m}, \ldots;$$

$$y_{-0}, y_{-1}, y_{-2}, \ldots, y_{-m}, \ldots,$$

then y_{+m} and y_{-m} have exactly m zeros in the interval $a < x < b$.

For the special case that $\ell \equiv 0$, $\alpha' = \gamma' = 0$, and g changes sign in the interval $a < x < b$, Bocher[62] has shown that the values of λ^2_{-0} or λ^2_{+0} depend on the integral of the function g:

$$\int_a^b g\,dx < 0; \quad \lambda^2_{-0} = 0; \quad \lambda^2_{+0} \neq 0; \tag{A.2a}$$

$$\int_a^b g\,dx > 0; \quad \lambda^2_{+0} = 0; \quad \lambda^2_{-0} \neq 0; \tag{A.2b}$$

$$\int_a^b g\,dx = 0; \quad \lambda^2_{-0} = \lambda^2_{+0} = 0. \tag{A.2c}$$

Note that g is the "weight" function for the orthogonal relationship

$$\int_a^b g y_m y_n dx \begin{cases} = 0 & m \neq n \\ \neq 0 & m = n. \end{cases} \tag{A.2d}$$

2. Separation of Variables

The temperature distribution of the heat-exchanger fluids is obtained from the solution of the nondimensional governing equations:

Tube:

$$\frac{1}{x_1} \frac{\partial}{\partial x_1}\left[f_1(x_1)\, x_1 \frac{\partial \xi_1(x_1, z)}{\partial x_1}\right] = g_1(x_1) \frac{\partial \xi_1(x_1, z)}{\partial z}; \tag{A.3a}$$

Annulus:

$$\frac{1}{x_2+\sigma}\frac{\partial}{\partial x_2}\left[f_2(x_2)(x_2+\sigma)\frac{\partial \xi_2(x_2,z)}{\partial x_2}\right] = -g_2(x_2)\,\omega^2\,\frac{\partial \xi_2(x_2,z)}{\partial z}. \qquad (A.3b)$$

The above equations are subject to the following boundary conditions:

Entrance:

$$\xi_1(x_1,0) = 0; \qquad (A.3c)$$

$$\xi_2(x_2,Z) = 1; \qquad (A.3d)$$

Interior:

$$\frac{\partial \xi_1(0,z)}{\partial x_1} = 0; \qquad (A.3e)$$

$$K\,\frac{\partial \xi_1(1,z)}{\partial x_1} \qquad \frac{\partial \xi_2(0,z)}{\partial x_2}; \qquad (A.3f)$$

$$K_w\,\frac{\partial \xi_1(1,z)}{\partial x_1} + \xi_1(1,z) = \xi_2(0,z); \qquad (A.3g)$$

$$\frac{\partial \xi_2(1,z)}{\partial x_2} = 0. \qquad (A.3h)$$

Separation of the variables in the form

$$\xi_1(x_i,z) = E_i(x_i)\;\theta(z) \qquad (A.4)$$

when applied to the preceding equations results in the following:

Tube:

$$\frac{1}{\theta(z)}\frac{d\theta(z)}{dz} = \frac{1}{g_1(x_1)\;E_1(x_1)\;x_1}\frac{d}{dx_1}\left[f_1(x_1)\;x_1\;\frac{dE_1(x_1)}{dx_1}\right]; \qquad (A.5a)$$

Annulus:

$$\frac{1}{\theta(z)}\frac{d\theta(z)}{dz} = \frac{-1}{g_2(x_2)\;\omega^2 E_2(x_2)(x_2+\sigma)}\frac{d}{dx_2}\left[(x_2+\sigma)\,f_2(x_2)\;\frac{dE_2(x_2)}{dx_2}\right]. \qquad (A.5b)$$

The left-hand sides of the above equations are functions of z only, whereas the right-hand sides are functions of x only; consequently, they can be equal only if they each equal a constant, $-\lambda^2$.

Equations (A.5a) and (A.5b) may be separated as follows:

$$\frac{1}{\theta(z)} \frac{d\theta(z)}{dz} = -\lambda^2, \tag{A.6}$$

which has the solution

$$\theta(z) = e^{-\lambda^2 z}. \tag{A.7}$$

The right-hand sides of Eqs. (A.5a) and (A.5b) may be written

$$\frac{d}{dx_1}\left[f_1(x_1)\, x_1 \frac{dE_1(x_1)}{dx_1}\right] + \lambda^2 g_1(x_1)\, x_1 E_1(x_1) = 0; \tag{A.8a}$$

$$\frac{d}{dx_2}\left[f_2(x_2)(x_2+\sigma) \frac{dE_2(x_2)}{dx_2}\right] - \lambda^2 \omega^2 g_2(x_2)(x_2+\sigma)\, E_2(x_2) = 0. \tag{A.8b}$$

The interior boundary conditions become

$$\frac{dE_1(0)}{dx_1} = 0; \tag{A.8c}$$

$$K \frac{dE_1(1)}{dx_1} = \frac{dE_2(0)}{dx_2}; \tag{A.8d}$$

$$K_w \frac{dE_1(1)}{dx_1} + E_1(1) = E_2(0); \tag{A.8e}$$

$$\frac{dE_2(1)}{dx_2} = 0. \tag{A.8f}$$

3. Two-region Sturm-Liouville Problem

a. Application of Theory to Present System

Equations (A.8a) and (A.8b) correspond to what may be called a two-region Sturm-Liouville problem and may be written as a single differential equation:

$$\frac{d}{dx}\left(k \frac{dy}{dx}\right) + \lambda^2 g y = 0; \quad 0 \leq x \leq 2; \tag{A.9a}$$

$$y'(0) = 0; \quad y'(2) = 0, \tag{A.9b}$$

where $x = 0$ and $x = 2$ correspond to $x_1 = 0$ and $x_2 = 1$, respectively.

The functions y, k, and g are defined over both regions, tube and annulus, of the heat exchanger by

Tube: $(x = x_1; 0 \leq x_1 \leq 1)$

$$y = E_1(x_1); \tag{A.10a}$$

$$k = x_1 f_1(x_1); \tag{A.10b}$$

$$g = x_1 g_1(x_1); \tag{A.10c}$$

Annulus: $(x = x_2 + 1; 0 \leq x_2 \leq 1)$

$$y = E_2(x_2); \tag{A.11a}$$

$$k = (x_2 + \sigma) f_2(x_2); \tag{A.11b}$$

$$g = -\omega^2 (x_2 + \sigma) g_2(x_2), \tag{A.11c}$$

where the function y must meet the compatibility conditions at the inner wall of the heat exchanger, Eqs. (A.8d) and (A.8e), and the functions k and g have finite discontinuities at the inner wall of the heat exchanger.

Equation (A.9a) is of the same type as that considered in Section 1 of this appendix. Specifically, if $\ell \equiv 0$ and $\alpha' = \gamma' = 0$ in Eq. (A.1a), then they are identical for the case treated by Bocher[62] in which the weighting function, g, changes sign in the interval $a < x < b$. The difficulty in applying the theorem to the present system lies in the fact that the theorem specifies that the functions k and g be continuous in the interval $a < x < b$, whereas these functions have finite discontinuities at the inner wall in the system being considered. Because of the fact that the functions are continuous in their respective regions, i.e., piecewise continuous, Stein[64] has been able to show that the theorem applies to the present system.

According to the theorem, then, there is an infinite set of eigenvalues, having the limit points $+\infty$ and $-\infty$, for which solutions to Eq. (A.9a) exist. Their corresponding eigenfunctions, y_{-m} and y_{+m}, have exactly m zeros in the interval $a < x < b$.

b. Orthogonality of the Eigenfunctions

According to the theorem, Eqs. (A.8a) and (A.8b) represent a two-region Sturm-Liouville system for which infinite sets of positive and negative eigenvalues exist. The equations may be written in the form

$$\frac{d}{dx_1}\left[f_1(x_1)\, x_1 \frac{dE_{1,n}(x_1)}{dx_1}\right] + \lambda_n^2 x_1 g_1(x_1)\, E_{1,n}(x_1) = 0; \qquad \text{(A.12a)}$$

$$\frac{d}{dx_2}\left[f_2(x_2)(x_2+\sigma) \frac{dE_{2,n}(x_2)}{dx_2}\right] - \lambda_n^2 \omega^2 g_2(x_2)(x_2+\sigma)\, E_{2,n}(x_2) = 0. \qquad \text{(A.12b)}$$

Boundary Conditions:

$$\frac{dE_{1,n}(0)}{dx_1} = 0; \qquad \text{(A.12c)}$$

$$K \frac{dE_{1,n}(1)}{dx_1} = \frac{dE_{2,n}(0)}{dx_2}; \qquad \text{(A.12d)}$$

$$K_w \frac{dE_{1,n}(1)}{dx_1} + E_{1,n}(1) = E_{2,n}(0); \qquad \text{(A.12e)}$$

$$\frac{dE_{2,n}(1)}{dx_2} = 0; \qquad \text{(A.12f)}$$

$n = \pm 0, \pm 1, \pm 2, \pm 3, \ldots,$

where $E_{i,n}$ is the eigenfunction corresponding to λ_n^2.

The orthogonal property of the eigenfunctions may be derived in the following way. Equation (A.12a) is first multiplied by $E_{1,m}$ to obtain a relation containing different ordered eigenfunctions. A second relation is obtained by interchanging m and n in the first relation. The two expressions are then integrated between 0 and 1, subtracted, and simplified to yield Eq. (A.13) below. A similar treatment of Eq. (A.12b) yields Eq. (A.14):

$$(\lambda_n^2 - \lambda_m^2)\, B_1\{E_{1,n}(x_1)\, E_{1,m}(x_1)\} = 2E_{1,n}(1)\left[\frac{dE_{1,m}(1)}{dx_1} - E_{1,m}(1) \frac{dE_{1,n}(1)}{dx_1}\right]; \qquad \text{(A.13)}$$

$$(\lambda_n^2 - \lambda_m^2)\, HB_2\{E_{2,n}(x_2)\, E_{2,m}(x_2)\} = \frac{2}{K}\left[E_{2,m}(0)\,\frac{dE_{2,n}(0)}{dx_2} - E_{2,n}(0)\,\frac{dE_{2,m}(0)}{dx_2}\right]; \tag{A.14}$$

$n = \pm 0, \pm 1, \pm 2, \ldots$.

The above equations may be combined by applying the inner-wall boundary condition to yield

$$(\lambda_n^2 - \lambda_m^2)[B_1\{E_{1,n}(x_1)\, E_{1,m}(x_1)\} - HB_2\{E_{2,n}(x_2)\, E_{2,m}(x_2)\}] = 0; \tag{A.15}$$

$\begin{matrix} m \\ n \end{matrix} = \pm 0, \pm 1, \pm 2, \ldots$.

This gives the desired orthogonality condition:

$$B_1\{E_{1,n}(x_1)\, E_{1,m}(x_1)\} - HB_2\{E_{2,n}(x_2)\, E_{2,m}(x_2)\} = 0; \quad n \neq m; \tag{A.16}$$

$$B_1[E_{1,n}(x_1)]^2 - HB_2[E_{2,n}(x_2)]^2 = N_n; \quad n = m; \tag{A.17}$$

$n = \pm 0, \pm 1, \pm 2, \ldots$.

Recalling the definition of the bulk average operation [see Eqs. (3.22a) and (3.22b)], it is easily verified that the eigenfunctions are orthogonal with respect to the weight function g, where g is defined for both regions of the heat exchanger by

Tube:

$$g = x_1 g_1(x_1); \tag{A.18a}$$

Annulus:

$$g = -\frac{H}{1 + 2\sigma}(x_2 + \sigma)\, g_2(x_2). \tag{A.18b}$$

An alternative form for the normalizing factor N_n may be obtained by multiplying Eqs. (A.12a) and (A.12b) by $E_{1,n}$ and $E_{2,n}$, respectively, and integrating the resulting expressions between 0 and 1. These expressions contain the quantities $B_i\{[E_{i,n}(x_i)]^2\}$ and are used in Eq. (A.17) to obtain an integral expression for N_n. This resulting integral expression is integrated by parts to yield

$$\lambda_n^2 N_n = 2 \int_0^1 x_1 f_1(x_1) \left[\frac{dE_{1,n}(x_1)}{dx_1} \right]^2 dx_1$$

$$+ \frac{2}{\sigma K} \int_0^1 (x_2 + \sigma) f_2(x_2) \left[\frac{dE_{2,n}(x_2)}{dx_2} \right]^2 dx_2$$

$$+ 2K_w \left[\frac{dE_{1,n}(1)}{dx_1} \right]^2 . \qquad (A.19)$$

The sign of N_n may be determined from the above expression. Since the right-hand side is always positive, $\lambda_n^2 N_n$ must always be greater than zero.

Therefore, for

$n < 0$: $N_n < 0$ since $\lambda_n^2 < 0$;

$n > 0$: $N_n > 0$ since $\lambda_n^2 > 0$.

c. Zeroth-order Eigenvalues

According to the theorem of Bocher,[62] the zeroth-order eigenvalues have values which depend on the sign of the integral of the weighting function g.

For the two-region problem, the weighting function is defined over both tube and annulus, and

$$\int_a^b g dx$$

corresponds to

$$\int_0^1 x_1 g_1(x)\, dx_1 - \frac{H}{1 + 2\sigma} \int_0^1 (x_2 + \sigma)\, g_2(x_2)\, dx_2 .$$

Writing the above in terms of the bulk operator $B_i\{\ \}$ gives

$$\int_a^b g dx = \frac{1}{2} B_1\{1\} - \frac{H}{2} B_2\{1\}; \qquad \int_a^b g dx = \frac{1}{2}(1 - H) \qquad (A.20)$$

since $B_i\{1\} = 1$.

Therefore, for

H < 1:

$$\lambda^2_{+0} = 0 \quad \text{since} \int_a^b g\,dx > 0; \tag{A.21a}$$

H > 1:

$$\lambda^2_{-0} = 0 \quad \text{since} \int_a^b g\,dx < 0; \tag{A.21b}$$

H = 1:

$$\lambda^2_{-0} = \lambda^2_{+0} = 0 \quad \text{since} \int_a^b g\,dx = 0. \tag{A.21c}$$

For H = 1, two zero eigenvalues exist, corresponding to a "double root" of the eigenvalue equation. This case requires special treatment and has been excluded from the analysis. As mentioned in the literature survey, Stein[28] has presented a solution for the case H = 1.

For $H \neq 1$ only one zero eigenvalue exists, and it belongs to the positive set of eigenvalues for $H < 1$ and to the negative set for $H > 1$.

For convenience, let the eigenvalues be denoted

$$\ldots, \lambda^2_{-m}, \ldots, \lambda^2_{-2}, \lambda^2_{-1}, \lambda^2_0, \lambda^2_{+1}, \lambda^2_{+2}, \ldots, \lambda^2_{+m}, \ldots,$$

where $\lambda^2_0 = 0$ for both H greater than and less than unity.

Note that for $H < 1$ the λ^2_0 above corresponds to the previous λ^2_{+0} and for $H > 1$ λ^2_0 above corresponds to the previous λ^2_{-0}. The corresponding eigenfunctions are denoted

$$\ldots, E_{i,-m}, \ldots, E_{i,-2}, E_{i,-1}, E_{i,0}, E_{i,+1}, \ldots, E_{i,+2}, E_{i,+m}, \ldots .$$

The above notation is more convenient for the purposes of the present analysis than that used in the previous part of this appendix, and is used exclusively in the remainder of this appendix and in the main body of the thesis.

d. Eigenfunctions

The solution of Eqs. (A.12a) and (A.12b) for $\lambda_0^2 = 0$ are $E_{1,0} = E_{2,0} =$ constant. No generality is lost by assuming that this constant is unity:

$$E_{1,0} = E_{2,0} = 1. \tag{A.22a}$$

Note that with $E_{1,0} = E_{2,0} = 1$ the zeroth-order normalizing factor as given by Eq. (A.17) is

$$N_0 = 1 - H. \tag{A.22b}$$

Solution of Eqs. (A.12a) and (A.12b) for $n \neq 0$ is best effected by defining auxiliary functions $F(x_1,\lambda)$ and $G(x_2,\lambda)$. Let

$$E_{1,n}(x_1) = A_n' F(x_1,\lambda_n); \tag{A.23a}$$

$$E_{2,n}(x_2) = B_n' G(x_2,\lambda_n); \tag{A.23b}$$

$$n = \pm 1, \pm 2, \pm 3, \ldots,$$

where $F(x_1,\lambda)$ and $G(x_2,\lambda)$ satisfy

$$\frac{d}{dx_1}\left[f_1(x_1)\, x_1 \frac{dF(x_1,\lambda)}{dx_1}\right] + \lambda^2 x_1 g_1(x_1)\, F(x_1,\lambda) = 0 \tag{A.24a}$$

and

$$\frac{d}{dx_2}\left[f_2(x_2)(x_2+\sigma) \frac{dG(x_2,\lambda)}{dx_2}\right] - \lambda^2\omega^2 g_2(x_2)(x_2+\sigma)\, G(x_2,\lambda) = 0. \tag{A.24b}$$

Initial Conditions:

$$\frac{dF(0,\lambda)}{dx_1} = 0; \qquad \frac{dG(1,\lambda)}{dx_2} = 0;$$

$$F(0,\lambda) = 1; \qquad G(1,\lambda) = 1.$$

The constants A_n' and B_n' are defined such that they satisfy the first inner-wall boundary condition, Eq. (A.12d):

$$K \frac{dE_{1,n}(1)}{dx_1} = \frac{dE_{2,n}(0)}{dx_2}; \tag{A.25a}$$

$$KA_n' \frac{dF(1,\lambda_n)}{dx_1} = B_n' \frac{dG(0,\lambda_n)}{dx_2}. \tag{A.25b}$$

Therefore, let

$$A_n' = \frac{dG(0,\lambda_n)}{dx_2}; \tag{A.26a}$$

$$B_n' = K \frac{dF(1,\lambda_n)}{dx_1}; \tag{A.26b}$$

$n = \pm 1, \pm 2, \pm 3, \ldots .$

e. Eigenvalue Equation

The eigenvalues are determined by the second inner-wall boundary condition, Eq. (A.12e):

$$K_w \frac{dG(0,\lambda_n)}{dx_2} \frac{dF(1,\lambda_n)}{dx_1} + \frac{dG(0,\lambda_n)}{dx_2} F(1,\lambda_n) = K \frac{dF(1,\lambda_n)}{dx_1} G(0,\lambda_n);$$

$n = \pm 1, \pm 2, \pm 3, \ldots .$

The eigenvalue equation, $\psi(\lambda)$, is defined as

$$\psi(\lambda) = K_w \frac{dG(0,\lambda)}{dx_2} \frac{dF(1,\lambda)}{dx_1} + \frac{dG(0,\lambda)}{dx_2} F(1,\lambda) - K \frac{dF(1,\lambda)}{dx_1} G(0,\lambda), \tag{A.27}$$

and the eigenvalues λ_n^2 are obtained from the roots of the equation

$$\psi(\lambda) = 0 \tag{A.28}$$

with

$$\lambda_0^2 = 0.$$

4. Expansion Coefficient

The general solution of Eqs. (A.3a) and (A.3b) is the sum of all particular solutions. The expressions for the temperature distribution of the heat exchanger fluids are

$$\xi_1(x_1,z) = \sum_{n=-\infty}^{+\infty} C_n E_{1,n}(x_1)\, e^{-\lambda_n^2 z} \tag{A.29a}$$

and

$$\xi_2(x_2,z) = \sum_{n=-\infty}^{+\infty} C_n E_{2,n}(x_2)\, e^{-\lambda_n^2 z}. \tag{A.29b}$$

Relations defining the expansion coefficients, C_n, are obtained from the entrance and exit temperature profiles of the heat exchanger fluids:

z = 0:

$$\xi_1(x_1,0) = 0; \tag{A.30a}$$

$$\xi_2(x_2,0) = p_2(x_2) \quad \text{(unknown)}; \tag{A.30b}$$

z = Z:

$$\xi_1(x_1,Z) = p_1(x_1) \quad \text{(unknown)}; \tag{A.30c}$$

$$\xi_2(x_2,Z) = 1. \tag{A.30d}$$

The end temperature distributions may be written in terms of the series solution:

z = 0:

$$0 = \sum_{n=-\infty}^{+\infty} C_n E_{1,n}(x_1); \tag{A.31a}$$

$$p_2(x_2) = \sum_{n=-\infty}^{+\infty} C_n E_{2,n}(x_2); \tag{A.31b}$$

z = Z:

$$p_1(x_1) = \sum_{n=-\infty}^{+\infty} C_n E_{1,n}(x_1)\, e^{-\lambda_n^2 Z}; \tag{A.31c}$$

$$1 = \sum_{-\infty}^{+\infty} C_n E_{2,n}(x_2)\, e^{-\lambda_n^2 Z}. \tag{A.31d}$$

Manipulation of the above equations yields expressions for the expansion coefficients. For example, Eqs. (A.31a) and (A.31b) are multiplied by $E_{1,n}$ and $HE_{2,n}$, respectively, and the bulk average operation $B_i\{\ \}$ is applied to the result. The expressions are then subtracted and the orthogonality condition, Eqs. (A.16) and (A.17), applied to give Eq. (A.32a) below. A similar treatment of Eqs. (A.31c) and (A.31d) yields Eq. (A.32b).

$$C_n N_n = -HB_2\{p_2(x_2)\ E_{2,n}(x_2)\}; \tag{A.32a}$$

$$C_n N_n e^{-\lambda_n^2 Z} = B_1\{p_1(x_1)\ E_{1,n}(x_1)\} - HB_2\{E_{2,n}(x_2)\}. \tag{A.32b}$$

The above expressions cannot be used directly to calculate the expansion coefficients since they contain the unknown outlet temperature distributions, $p_1(x)$ and $p_2(x)$. The unknown functions may be eliminated from Eqs. (A.32a) and (A.32b), however, by expressing the functions in terms of their series solution and substituting this series into the equations. After the substitution, Eqs. (A.32a) and (A.32b) are added to give

$$C_n N_n\left(1 + e^{-\lambda_n^2 Z}\right) = \sum_{k=-\infty}^{+\infty} C_k\left[e^{-\lambda_k^2 Z}\ B_1\{E_{1,n}(x_1)\ E_{1,k}(x_1)\} - HB_2\{E_{2,n}(x_2)\ E_{2,k}(x_2)\}\right] - HB_2\{E_{2,n}(x_2)\}; \tag{A.33}$$

$n = 0, \pm 1, \pm 2, \ldots$.

For $n \neq 0$, the term for $k = 0$ drops out of the above summation and C_0 does not appear in the expression. An explicit relation for C_0 in terms of higher-ordered expansion coefficients may be obtained for $n = 0$.

For $n = 0$ Eq. (A.33) becomes

$$C_0 N_0 = \sum_{k=-\infty}^{+\infty} C_k\left(e^{-\lambda_k^2 Z} - 1\right) B_1\{E_{1,k}(x_1)\} - H. \tag{A.34}$$

A fairly straightforward manipulation of Eq. (A.33) yields the following simplified form:

$$\sum_{k=-\infty}^{+\infty} C_k\left(1 - e^{-\lambda_k^2 Z}\right) Q_{n,k} = B_1\{E_{1,n}(x_1)\}, \tag{A.35a}$$

where

$$Q_{n,k} = -B_1\{E_{1,n}(x_1)\ E_{1,k}(x_1)\}; \quad k \neq n; \tag{A.35b}$$

$$Q_{n,n} = -\left[B_1\{[E_{1,n}(x_1)]^2\} + \frac{e^{-\lambda_n^2 Z}}{\left(1 - e^{-\lambda_n^2 Z}\right)} N_n \right]; \quad k = n; \qquad \text{(A.35c)}$$

$n = \pm 1, \pm 2, \pm 3, \ldots .$

The zeroth-order expansion coefficient does not appear in the above equation and must be calculated by Eq. (A.34).

The expansion coefficients must be calculated from the infinite set of linear algebraic equations defined by Eq. (A.35a). Computation is done by truncating higher-ordered terms and equations, and solving the remaining finite set. Convergence of the solution must be judged by inspection of the results as more terms are added, since no usable convergence test for this type of system is known. The accuracy and convergence of the computational procedure is discussed in the main body of this thesis.

5. Normalized Eigenfunctions

At this point, it becomes desirable from a practical viewpoint to normalize the eigenfunctions with the square root of the absolute value of N_n, the normalizing factor. The absolute value is used because of the fact that N_n is negative for $n < 0$. This normalization is desirable for computational considerations, since it was found that unnormalized eigenfunctions become unmanageably large as their order is increased.

Let

$$E_{1,n}(x_1) \rightarrow \frac{E_{1,n}(x_1)}{\sqrt{|N_n|}};$$

$$E_{2,n}(x_2) \rightarrow \frac{E_{2,n}(x_2)}{\sqrt{|N_n|}};$$

$n = \pm 1, \pm 2, \pm 3, \ldots .$

Throughout the remainder of this appendix and in the main body of this thesis, all eigenfunctions are normalized with the exception of the zeroth-order eigenfunctions, which remain

$$E_{1,0} = E_{2,0} = 1.$$

Using normalized eigenfunctions, the orthogonality condition becomes

$$B_1\{E_{1,n}(x_1)\, E_{1,m}(x_1)\} - HB_2\{E_{2,n}(x_2)\, E_{2,m}(x_2)\} = 0; \quad n \neq m; \qquad \text{(A.36a)}$$

$$B_1\{[E_{1,n}(x_1)]^2\} - HB_2\{[E_{2,n}(x_2)]^2\} = \begin{matrix} +1 & n > 0 \\ -1 & n < 0 \end{matrix}; \quad n = m. \tag{A.36b}$$

The relationships which were derived in the preceding sections of this appendix also apply to normalized eigenfunctions if the value of N_n is taken to be +1 for $n > 0$ and -1 for $n < 0$, and N_0 remains the same.

6. Definitions to Avoid Use of Negative Indices

The necessity of summing a series with exponentially increasing terms can be eliminated by defining an auxiliary eigenvalue, β_n^2. Let

$$\lambda_{-n}^2 \rightarrow -\beta_n^2. \tag{A.37}$$

The eigenfunctions associated with negative eigenvalues may also be redefined with positive indices:

$$E_{1,-n}(x_1) = \tilde{E}_{1,n}(x_1); \tag{A.38a}$$

$$E_{2,-n}(x_2) = \tilde{E}_{2,n}(x_2). \tag{A.38b}$$

The expansion coefficients associated with the negative eigenvalues may be redefined in terms of an auxiliary expansion coefficient, A_n:

$$C_{-n} = e^{-\beta_n^2 Z} A_n. \tag{A.39}$$

The above definitions serve the dual purpose of eliminating negative indices and ensuring that the exponential terms in the series solution "decay" for large arguments.

In terms of the above redefined eigenvalues, eigenfunctions, and expansion coefficients, the temperature distributions of the heat-exchanger fluids are given by Eqs. (3.8a) and (3.8b), where the zeroth-order term has been separated from the summation which is now from one to $+\infty$. In Eqs. (3.8) to (3.19) the terms associated with negative eigenvalues have been separated from those with positive eigenvalues so that the set of functions defining $E_{i,n}$ and β_n^2 is separate from the set defining $E_{i,n}$ and λ_n^2.

APPENDIX B

Reduction of Data

The tabulated data for each experimental run were the flowmeter emfs, the cooling water manometer differential, and the thermocouple emfs. In the early stages of the experimental program, the voltage supplied to the heaters was also recorded for the purpose of making a heat balance across the heaters. This practice was abandoned because the voltmeters proved to be too inaccurate for anything more than a general indication of the power level.

The first step in the reduction of the data was the conversion of the tabulated data to physically meaningful quantities by means of flowmeter-calibration curves and standard thermocouple conversion tables. The basic data obtained were denoted as follows:

Flowrates (lb/hr)

W_1 - tube-side mercury flowrate

W_2 - annulus-side mercury flowrate

W_{H_2O} - cooling-water flowrate

Bulk Temperatures (°F)

TA_1 - test-section tube inlet

TA_2 - test-section tube outlet

TA_3 - test-section annulus inlet

TA_4 - test-section annulus outlet

TA_5 - heater inlet

TA_6 - heater outlet

TA_7 - cooler mercury inlet

TA_8 - cooler mercury outlet

TA_9 - cooler water inlet

TA_{10} - cooler water outlet

Measurements of the temperature of the outer wall were made with both 47- and 10-L/D_1 test sections, but since the 10-L/D_1 test section had no fully developed region, only the temperature measurements for the 47-L/D_1 test section were useful for computing Nu_{1FD}°. The data for the outer wall temperature for the 47-L/D_1 test section were denoted as follows:

Outer Wall Temperatures (°F) of the
47-L/D_1 Test Section

Thermocouple	Distance from Tube Inlet, ℓ (in.)
TB_1	0
TB_2	$L/30 = 1.18$
.	.
.	.
.	.
TB_{30}	$29(L/30) = 34.32$
TB_{31}	$L = 35.5$

1. Operating Conditions for the Test Section

Quantities defining the operating conditions of the test section for each experimental run were calculated in the following manner:

$$H = \frac{c_2 W_2}{c_1 W_1} = 1.005 \frac{W_2}{W_1};$$

$$Pe_1 = \frac{24\, c_1}{\pi k_1 r_{12}} W_1 = 0.127\, W_1;$$

$$Pe_2 = \frac{24\, c_2}{\pi k_2 (r_{22} + r_{21})} W_2 = 0.041\, W_2;$$

$$\Delta T_0 = TA_1 - TA_3.$$

The physical properties used in the computations were taken from Ref. 65. Because of the relatively small temperature range obtained in the experiments, the mercury properties used were taken to be average values appropriate to an average temperature of 150°F for the tube side and 130°F for the annulus side. The values used were:

Tube*	Annulus
$k_1 = 5.27$ Btu/hr-ft-°F	$k_2 = 5.20$ Btu/hr-ft-°F
$c_1 = 0.0329$ Btu/lb-°F	$c_2 = 0.0331$ Btu/lb-°F
$Pr_1 = 0.0205$	$Pr_2 = 0.0215$

For the temperature range of the experiment, the maximum deviation of the properties in Ref. 65 from the above average values was less than ±3% for k_i, ±1% for c_i, and ±5% for Pr_i.

*Thermal conductivity of copper tube: $k_W = 223$ Btu/hr-ft-°F.

2. Heat Balance for Water Cooler

The heat flux computed from the water-cooler data was given by

$$Qc_{H_2O} = c_{H_2O} W_{H_2O} (TA_{10} - TA_9); \quad c_{H_2O} = 1.0;$$

$$Qc_{Hg} = c_2 W_2 (TA_7 - TA_8).$$

The heat-balance deviation for the water cooler was calculated from

$$\delta_c = 100 \left[1 - \frac{Qc_{H_2O}}{Qc_{Hg}} \right] \quad (\%).$$

3. Heat Balance for Test Section

The heat flux computed from the test-section data was given by

$$Q_1 = c_1 W_1 (TA_1 - TA_2);$$

$$Q_2 = c_2 W_2 (TA_4 - TA_3);$$

The heat-balance deviation for the test section was calculated from

$$\delta_H = 100 \left[1 - \frac{Q_2}{Q_1} \right] \quad (\%).$$

4. Efficiency of the Heat Exchanger

The heat flux for a heat exchanger of infinite length was computed by the relations in Section III.A.6.c.

$H < 1$:

$$Q_{max} = c_2 W_2 \Delta T_0.$$

$H > 1$:

$$Q_{max} = c_1 W_1 \Delta T_0.$$

The efficiencies computed from the tube and annulus data were

$$\epsilon_1 = Q_1/Q_{max}; \quad \epsilon_2 = Q_2/Q_{max}.$$

The actual efficiency was taken to be the average of these values

$$\epsilon = \tfrac{1}{2}(\epsilon_1 + \epsilon_2).$$

5. Fully Developed Overall Nusselt Number

The outer-wall temperatures were expressed in the form:

$H < 1$:

$$S_i = \ell n\left[\frac{TB_i - TA_1}{-\Delta T_0} - H\frac{1-\epsilon}{H-1}\right];$$

$H > 1$:

$$S_i = \ell n\left[\frac{H-\epsilon}{H-1} - \frac{TB_i - TA_1}{-\Delta T_0}\right].$$

The above values were plotted against z_i, where

$$z_i = \frac{4}{Pe_1}\frac{\ell_i}{2r_{12}} = 5.333\frac{\ell_i}{Pe_1},$$

ℓ_i being the location of the thermocouple on the test section.

The S_i vs. z_i plots were linear in regions where the heat transfer was fully developed. An example of the S_i vs. z_i plot is given in Fig. 4.6. The extent of the linear region was determined by inspection, and the standard least-squares method was used to fit a straight line to these points. The slope of the line was then used to compute the fully developed overall Nusselt number by

$$Nu^{\circ}_{iFD} = \left|\frac{H}{1-H}\right| \times \left|\text{slope}\right|.$$

A simple FORTRAN program was written to perform the actual computations involved in the reduction of the data. The program reduced the data in two stages. In the first, the outer-wall temperature plot was obtained. The extent of the linear portion was then determined by inspection and used as input for the second stage, which reduced the bulk of the data according to the procedure just described. Inputs to the program were the mercury and water flowrates and the thermocouple emfs. The program converted the thermocouple emfs to temperatures and then proceeded to reduce the data.

APPENDIX C

Tabulation of Experimental Data

The basic experimental data taken with the 47- and 10-L/D_1 test sections are tabulated in Tables C-1, C-2, and C-3. The data are denoted as in Appendix B with the weight flowrates in lb/hr and the temperatures in °F. It has been stated previously that the data taken in the first 42 runs with the 47-L/D_1 test section were discarded.

TABLE C-1. Basic Experimental Data for 47-L/D_1 Test Section

RUN	W_1	W_2	W_{H2O}	TA_1	TA_2	TA_3	TA_4	TA_5	TA_6	TA_7	TA_8	TA_9	TA_{10}
43	2285.	4870.	1490.	156.3	114.4	109.6	128.8	167.0	157.8	167.0	109.6	51.6	58.0
44	3060.	4860.	1500.	159.0	119.4	109.7	134.0	167.4	160.0	167.4	109.7	51.4	57.8
45	3840.	4870.	1490.	158.7	123.0	109.8	136.8	165.3	159.7	165.3	109.8	51.2	57.4
46	4580.	4860.	1510.	159.8	125.9	108.6	139.6	165.3	160.5	165.3	108.6	51.1	57.0
47	6149.	4880.	1440.	161.2	132.9	110.5	145.0	165.2	161.7	165.2	110.5	51.8	58.0
48	7671.	4874.	1445.	162.6	137.7	111.2	148.8	165.9	163.0	165.9	111.2	51.7	58.0
49	9210.	4870.	1458.	162.4	140.2	109.1	150.4	165.0	162.7	165.0	109.1	52.0	58.2
50	10800.	4880.	1465.	162.3	142.2	108.4	151.5	164.7	162.6	164.7	108.4	51.7	57.9
51	825.	4860.	1462.	138.6	109.2	109.0	113.9	164.8	141.6	164.8	109.0	51.6	57.8
52	1155.	4860.	1457.	147.0	111.0	110.1	119.0	167.1	149.5	167.1	110.1	51.3	57.6
53	1520.	4860.	1470.	152.4	112.7	112.0	123.6	168.0	154.3	168.0	112.0	51.2	57.5
54	1521.	7350.	1409.	140.7	116.9	116.7	121.2	153.9	142.3	153.9	116.7	52.0	58.5
55	2280.	7350.	1461.	145.5	118.4	116.1	124.2	154.4	146.8	154.4	116.1	51.6	58.2
56	3020.	7340.	1475.	148.3	120.7	115.8	126.9	154.1	149.0	154.1	115.8	51.7	58.3
57	3745.	7350.	1460.	150.2	123.6	116.2	129.8	155.2	150.9	155.2	116.2	53.5	60.1

TABLE C-1 (Contd.)

RUN	W_1	W_2	W_{H2O}	TA_1	TA_2	TA_3	TA_4	TA_5	TA_6	TA_7	TA_8	TA_9	TA_{10}
58	4620.	7340.	1465.	151.0	125.9	116.3	131.8	155.7	151.5	155.7	116.3	52.8	59.4
59	6160.	7335.	1470.	149.9	127.9	115.0	133.0	153.3	150.3	153.3	115.0	52.4	58.9
60	7670.	7300.	1468.	151.8	131.7	115.9	136.4	154.5	152.2	154.5	115.9	52.8	59.4
61	9210.	7340.	1475.	153.1	134.9	116.5	138.9	155.4	153.4	155.4	116.5	52.5	59.1
62	10730.	7350.	1475.	151.3	135.3	116.0	138.7	153.1	151.5	153.1	116.0	52.2	58.5
63	777.	2400.	1405.	161.2	93.6	93.4	114.2	200.1	166.5	200.1	93.4	53.9	60.3
64	1130.	2410.	1460.	177.0	96.2	94.6	130.9	202.8	181.0	202.8	94.6	53.4	59.7
65	1530.	2430.	1420.	178.6	101.6	96.2	141.9	199.3	181.1	199.3	96.2	55.6	61.7
66	2260.	2570.	1420.	180.4	112.0	95.4	154.3	194.7	182.3	194.7	95.4	55.5	61.6
67	3100.	2530.	1420.	183.9	125.1	94.9	165.0	194.3	185.2	194.3	94.9	55.3	61.2
68	3845.	2420.	1410.	180.9	130.9	90.6	167.4	188.9	182.1	188.9	90.6	53.9	59.5
69	4625.	2420.	1420.	183.8	139.4	91.6	173.1	190.5	184.7	190.5	91.6	54.1	59.8
70	6160.	2520.	1415.	179.9	144.9	90.7	172.0	185.0	180.6	185.0	90.7	51.6	57.4
71	7720.	2520.	1420.	180.1	151.0	89.7	174.1	184.2	180.7	184.2	89.7	51.0	56.7
72	9250.	2500.	1420.	182.4	158.3	91.3	178.2	185.6	182.8	185.6	91.3	54.9	60.5

TABLE C-1 (Contd.)

RUN	W_1	W_2	W_{H2O}	TA_1	TA_2	TA_3	TA_4	TA_5	TA_6	TA_7	TA_8	TA_9	TA_{10}
73	10800.	2480.	1420.	178.5	158.5	90.8	175.0	181.2	178.8	181.2	90.8	54.5	59.6
74	850.	1215.	1415.	176.9	70.2	66.5	141.6	225.9	183.6	225.9	66.5	54.4	58.8
75	1605.	1210.	1415.	200.0	112.1	66.4	191.1	223.6	203.4	223.6	66.4	54.4	58.7
76	2360.	1220.	1410.	207.1	136.8	69.0	201.3	224.3	209.1	224.3	69.0	54.0	58.5
77	3100.	1220.	1410.	207.9	152.3	69.9	203.6	221.0	42.5	221.0	69.9	54.3	58.7
78	4710.	1200.	1405.	212.0	174.0	68.9	208.7	220.7	213.3	220.7	68.9	54.3	58.7
79	7700.	1220.	1415.	212.4	189.1	69.5	209.9	217.8	213.0	217.8	69.5	54.4	58.8
80	6140.	1250.	1405.	210.0	181.4	67.5	207.3	216.5	210.9	216.5	67.5	52.8	57.3
81	9100.	1220.	1410.	214.9	195.0	68.4	212.2	219.2	215.4	219.2	68.4	52.5	57.0
82	10850.	1180.	1415.	216.4	199.4	69.4	213.7	220.1	216.8	220.1	69.4	54.0	58.5

TABLE C-2. Outer-wall Temperature Data for 47-L/D_1 Test Section

RUN	43	44	45	46	47	48	49	50	51	52	53	54	55	56	57
TB_1	129.4	134.7	137.6	140.4	145.8	149.6	151.1	152.4	114.0	119.2	124.2	121.6	124.8	127.6	130.8
TB_2	124.8	130.2	133.4	136.3	142.4	146.6	148.4	150.0	111.4	115.8	120.1	119.4	121.9	124.4	127.5
TB_3	123.7	129.1	132.3	135.1	141.4	145.6	147.4	149.1	110.8	115.0	119.1	119.0	121.3	123.7	126.8
·	122.3	127.6	130.8	133.7	139.9	144.2	146.1	147.7	110.5	114.4	118.4	118.7	120.9	123.1	125.9
·	121.8	127.0	130.3	133.1	139.4	143.9	145.8	147.5	110.2	113.9	117.7	118.4	120.5	122.6	125.7
·	121.0	126.0	129.4	132.1	138.5	142.9	144.9	146.7	109.9	113.4	117.1	118.2	120.1	122.1	125.1
·	119.9	124.8	128.1	130.8	137.2	141.7	143.6	145.5	109.7	112.8	116.2	117.9	119.5	121.4	124.4
·	119.3	124.2	127.3	130.2	136.6	141.0	143.1	144.9	109.7	112.6	115.9	117.7	119.3	121.1	124.1
·	118.4	123.2	126.3	129.0	135.4	139.8	141.9	143.8	109.5	112.2	115.2	117.5	118.9	120.5	123.4
·	117.7	122.3	125.4	127.9	134.3	138.7	140.9	142.8	109.5	111.9	114.8	117.3	118.6	120.1	122.9
·	117.0	121.4	124.3	126.8	133.3	137.6	139.8	141.7	109.4	111.7	114.3	117.1	118.2	119.7	122.4
·	116.2	120.3	123.2	125.5	132.0	136.3	138.3	140.3	109.3	111.4	113.8	116.8	117.8	119.1	121.7
·	115.6	119.5	122.2	124.4	130.9	135.1	137.1	139.1	109.1	111.2	113.4	116.6	117.5	118.6	121.2
·	115.0	118.7	121.3	123.4	129.8	134.0	135.9	137.9	109.1	111.1	113.1	116.6	117.2	118.2	120.8
·	114.4	117.8	120.3	122.3	128.5	132.6	134.4	136.4	109.1	110.9	112.8	116.5	117.0	117.9	120.3
·	114.1	117.2	119.7	121.6	127.7	131.7	133.6	135.5	109.1	110.9	112.7	116.5	116.9	117.7	120.0
·	113.6	116.4	118.8	120.6	126.5	130.4	132.3	134.3	109.1	110.9	112.5	116.4	116.8	117.4	119.7
·	113.2	115.7	118.0	119.6	125.3	129.1	131.0	132.8	109.1	110.9	112.3	116.3	116.6	117.1	119.3
·	112.7	115.0	117.1	118.5	123.9	127.6	129.4	131.2	109.1	110.9	112.2	116.3	116.5	116.9	118.9
·	112.2	114.3	116.3	117.5	122.7	126.1	127.9	129.4	109.1	110.5	112.0	116.2	116.3	116.5	118.5
·	111.8	113.7	115.5	116.5	121.3	124.6	126.2	127.7	109.1	110.9	111.8	116.1	116.1	116.3	118.0
·	111.4	113.1	114.7	115.6	120.0	123.1	124.4	125.9	109.1	110.9	111.7	116.0	115.9	116.1	117.7
·	111.0	112.3	113.8	114.6	118.7	121.4	122.5	124.0	109.1	110.9	111.5	116.0	115.8	115.9	117.4
·	110.8	111.8	113.2	113.7	117.5	119.9	120.9	122.2	109.1	110.9	111.4	116.0	115.7	115.7	117.1
·	110.4	111.4	112.4	112.7	116.3	118.5	119.1	120.4	109.1	110.9	111.3	116.0	115.7	115.5	117.0
·	110.2	110.9	111.9	111.8	115.1	117.1	117.4	118.5	109.1	110.9	111.3	116.0	115.7	115.4	116.8
·	109.9	110.5	111.3	111.1	114.2	115.7	115.9	116.7	109.1	110.9	111.3	116.0	115.7	115.4	116.5
·	109.8	110.3	110.9	110.4	113.3	114.7	114.5	115.1	109.1	110.9	111.3	116.0	115.7	115.3	116.5
·	109.6	109.9	110.3	109.7	112.2	113.4	112.8	113.1	109.1	110.9	111.3	116.0	115.7	115.2	116.3
·	109.4	109.5	109.9	109.1	111.2	112.0	111.1	111.1	109.1	110.9	111.3	116.0	115.7	115.1	116.2
TB_{31}	109.2	109.1	109.2	108.2	109.9	110.3	109.0	108.5	109.1	110.9	111.3	116.0	115.7	114.9	115.9

TABLE C-2 (Contd.)

RUN	58	59	60	61	62	63	64	65	66	67	68	69	70	71	72
TB_1	132.8	134.1	137.5	140.0	139.8	114.8	131.3	142.4	154.5	165.2	167.7	173.5	172.4	174.6	178.6
TB_2	129.7	131.0	134.6	137.1	137.2	106.0	122.0	138.9	148.8	160.7	164.4	170.8	170.5	173.2	177.6
TB_3	128.9	130.3	133.8	136.5	136.6	103.3	118.9	132.2	146.6	158.8	162.7	169.4	169.4	172.3	176.9
.	127.9	129.8	132.8	135.4	135.6	101.0	115.8	129.4	144.1	156.2	160.7	167.4	167.7	170.8	175.6
.	127.7	129.2	132.5	135.3	135.5	99.6	113.6	127.6	142.7	155.1	159.8	166.8	167.4	170.7	175.6
.	127.1	128.5	131.9	134.6	134.9	98.4	111.3	125.3	140.7	153.3	158.2	165.4	166.3	169.8	175.0
.	126.4	127.7	131.1	133.7	134.0	97.4	109.1	122.7	138.5	151.2	156.2	163.6	164.8	168.5	173.9
.	126.0	127.2	130.7	133.4	133.7	96.7	107.5	120.8	136.8	149.6	154.9	162.6	164.0	167.9	173.5
.	125.4	126.5	129.9	132.5	132.8	96.1	105.9	118.7	134.9	147.6	153.1	160.8	162.5	166.6	172.4
.	124.8	125.9	129.2	131.8	132.1	95.7	104.6	116.8	133.0	145.7	151.3	159.2	161.1	165.4	171.3
.	124.2	125.2	128.5	131.1	131.4	95.2	103.4	115.0	131.2	143.7	149.4	157.5	159.6	164.1	170.2
.	123.4	124.3	127.5	130.1	130.4	94.8	102.2	113.2	129.0	141.4	147.2	155.2	157.7	162.3	168.7
.	122.8	123.7	126.8	129.3	129.6	94.6	101.3	111.7	127.0	139.4	144.4	152.8	155.8	160.7	167.3
.	122.3	123.0	126.0	128.5	128.7	94.4	100.5	110.2	124.9	137.3	143.0	151.1	154.0	159.0	165.9
.	121.7	122.2	125.1	127.5	127.8	94.2	99.7	108.8	122.8	135.1	140.7	148.7	151.9	157.0	164.0
.	121.4	121.9	124.6	126.9	127.2	94.1	99.1	107.7	121.1	133.3	138.7	146.8	150.2	155.5	162.7
.	120.9	121.2	123.9	126.0	126.4	94.0	98.5	106.5	119.1	130.9	136.3	144.4	147.8	153.2	160.6
.	120.4	120.6	123.1	125.2	125.5	93.8	97.9	105.3	117.1	128.5	133.7	141.6	145.2	150.7	158.3
.	120.0	120.0	122.3	124.2	124.7	93.8	97.4	104.2	115.0	125.9	131.0	138.8	142.4	148.0	155.7
.	119.5	119.4	121.5	123.4	123.8	93.7	97.0	103.1	113.0	123.3	128.0	135.6	139.3	144.8	152.7
.	119.1	118.7	120.8	122.6	122.7	93.6	96.6	102.1	111.0	120.5	124.8	132.2	136.0	141.4	149.4
.	118.6	118.1	120.0	121.7	121.8	93.6	96.2	101.1	109.0	117.6	121.3	128.5	132.1	137.5	145.5
.	118.2	117.7	119.4	121.0	121.0	93.5	95.9	100.2	107.0	114.7	117.7	124.5	128.2	133.4	141.4
.	117.9	117.2	118.8	120.4	120.2	93.5	95.6	99.5	105.2	112.1	114.2	120.6	124.0	129.1	137.1
.	117.5	116.7	118.2	119.6	119.4	93.5	95.4	98.8	103.5	109.3	111.0	116.5	119.4	124.1	132.0
.	117.4	116.3	117.7	118.9	118.8	93.4	95.1	98.2	101.9	106.6	107.5	112.4	114.9	119.1	126.5
.	117.0	115.9	117.1	118.2	118.1	93.4	95.0	97.6	100.4	104.1	104.2	108.3	110.2	114.1	120.7
.	116.9	115.7	116.8	117.9	117.7	93.4	94.8	97.1	99.2	101.9	101.1	104.8	105.8	109.0	114.8
.	116.6	115.4	116.3	117.4	117.2	93.4	94.7	96.7	98.1	100.0	98.5	101.3	101.6	103.7	108.5
.	116.5	115.0	115.8	116.8	116.5	93.4	94.6	96.4	97.2	98.1	95.7	97.9	97.3	98.3	102.0
TB_{31}	116.1	114.5	115.0	115.7	115.3	93.4	94.4	95.7	95.2	94.5	90.6	91.6	90.1	89.6	91.4

TABLE C-2 (Contd.)

RUN	73	74	75	76	77	78	79	80	81	82
TB_1	175.4	142.4	192.2	202.1	204.7	210.1	211.3	208.7	213.8	215.4
TB_2	174.8	132.0	190.1	200.8	204.1	210.0	211.1	208.5	213.5	215.0
TB_3	174.1	126.2	188.4	199.7	203.4	209.6	210.9	208.3	213.4	215.0
.	173.1	119.9	186.1	197.8	201.9	208.4	209.8	207.2	212.4	214.0
.	173.2	115.0	185.4	197.5	202.0	208.9	210.5	207.8	213.1	214.7
.	172.6	110.1	183.8	196.4	201.3	208.7	210.4	207.7	213.0	214.7
.	171.7	105.7	181.7	194.8	200.1	207.9	209.8	207.0	212.5	214.2
.	171.4	102.3	180.3	193.9	199.6	208.0	210.1	207.3	212.9	214.5
.	170.5	99.1	178.1	192.2	198.4	207.2	209.7	206.8	212.4	214.2
.	169.6	96.2	175.9	190.7	197.2	206.6	209.4	206.4	212.2	214.0
.	168.7	93.6	173.5	188.7	195.8	205.8	208.9	205.8	211.8	213.6
.	167.4	91.1	170.9	186.5	194.1	204.8	208.3	205.1	211.2	213.2
.	165.9	88.8	168.2	184.3	192.3	203.7	207.7	204.3	210.7	212.7
.	164.9	86.7	165.5	182.1	190.7	202.8	207.4	203.8	210.5	212.6
.	163.2	84.6	162.5	179.5	188.5	201.4	206.6	202.8	209.8	212.2
.	162.1	83.0	159.8	177.2	186.7	200.5	206.4	202.4	209.8	212.2
.	160.1	81.3	156.5	173.9	184.0	198.6	205.4	201.1	208.9	211.5
.	158.1	79.7	153.0	170.6	181.2	196.6	204.2	199.7	208.0	210.8
.	155.7	78.2	149.3	167.0	177.9	194.3	202.9	197.9	206.8	210.0
.	153.0	76.8	145.2	162.9	174.1	191.4	201.0	195.5	205.1	208.6
.	149.7	75.5	140.7	158.4	169.7	187.8	198.5	192.5	202.7	206.7
.	145.9	74.3	135.9	153.3	164.6	183.6	195.5	188.8	199.8	204.5
.	141.9	73.1	130.6	147.7	158.9	178.6	191.7	184.3	195.9	201.2
.	137.6	72.1	124.6	141.6	152.4	172.4	187.0	178.6	191.0	197.1
.	132.8	71.1	117.9	134.4	144.6	164.6	180.6	171.3	184.4	190.4
.	127.5	70.2	110.8	126.3	135.9	155.4	172.3	162.9	176.5	182.2
.	121.7	69.3	103.1	116.5	125.7	144.5	161.4	152.4	166.6	171.5
.	115.7	68.5	95.5	106.6	114.5	131.3	147.8	138.8	153.9	161.2
.	109.3	68.0	87.0	95.9	101.6	113.9	128.5	121.1	132.8	141.1
.	102.2	67.3	79.1	85.6	89.7	95.6	106.3	100.8	109.9	117.7
TB_{31}	90.8	66.5	67.0	69.7	70.8	70.4	70.9	68.9	70.2	71.6

TABLE C-3. Basic Experimental Data for 10-L/D_1 Test Section

RUN	W_1	W_2	W_{H2O}	TA_1	TA_2	TA_3	TA_4	TA_5	TA_6	TA_7	TA_8	TA_9	TA_{10}
1	3840.	2450.	1340.	145.6	126.9	90.0	118.3	164.4	148.8	164.4	90.0	57.4	61.8
2	3820.	2420.	1335.	168.3	142.4	93.6	132.1	176.6	173.5	176.6	93.6	58.4	63.1
3	3805.	2465.	1345.	197.5	163.1	98.1	149.1	191.9	204.2	191.9	98.1	58.5	64.0
4	7640.	2435.	1420.	149.3	136.3	85.1	125.1	158.7	151.2	158.7	85.1	58.3	61.9
5	7630.	2380.	1420.	169.5	153.0	89.9	139.7	173.2	171.6	173.2	89.9	59.0	63.4
6	7630.	2460.	1430.	191.7	171.6	95.7	155.1	188.4	194.6	188.4	95.7	59.3	64.4
7	776.	2440.	1480.	104.4	92.4	90.4	93.8	178.1	113.0	178.1	90.4	57.3	61.7
8	1141.	2420.	1480.	116.8	97.3	89.1	98.0	173.6	161.4	173.6	89.1	57.1	61.5
9	1560.	2450.	1480.	125.0	103.0	87.9	101.5	169.0	131.9	169.0	87.9	57.2	61.6
10	2300.	2440.	1475.	131.9	110.9	88.1	106.3	162.6	137.3	162.6	88.1	57.1	60.9
11	3075.	2420.	1475.	137.5	117.7	87.1	111.0	161.2	142.0	161.2	87.1	57.4	61.3
12	4600.	2410.	1480.	149.7	131.3	88.3	121.3	165.8	152.2	165.8	88.3	57.4	61.3
13	6100.	2450.	1425.	151.1	135.9	89.2	124.7	163.1	152.4	163.1	89.2	57.9	61.8
14	10050.	2420.	1420.	155.6	144.4	89.0	132.2	163.0	156.7	163.0	89.0	57.9	61.8
15	12500.	2480.	1430.	153.8	144.7	89.5	132.5	159.5	154.5	159.5	89.5	58.2	61.9

TABLE C-3 (Contd.)

RUN	W_1	W_2	W_{H2O}	TA_1	TA_2	TA_3	TA_4	TA_5	TA_6	TA_7	TA_8	TA_9	TA_{10}
16	1165.	4880.	1420.	132.8	116.3	112.6	115.3	160.4	142.6	160.4	112.6	58.4	63.4
17	1540.	4850.	1430.	137.0	119.4	111.7	116.2	158.8	145.1	158.8	111.7	58.3	63.5
18	2300.	4880.	1440.	146.4	127.9	113.1	120.5	160.9	150.9	160.9	113.1	58.4	63.5
19	3035.	4860.	1425.	133.9	121.4	107.2	114.4	152.7	136.8	152.7	107.2	58.5	63.0
20	3830.	4860.	1420.	137.7	125.9	108.8	117.2	153.0	140.1	153.0	108.8	58.6	63.4
21	4600.	4850.	1430.	139.8	128.4	108.7	118.4	152.5	141.6	152.5	108.7	58.7	63.3
22	6160.	4890.	1430.	142.2	132.0	108.6	120.5	152.0	143.7	152.0	108.6	58.8	63.4
23	7660.	4860.	1430.	137.2	128.2	104.3	116.8	145.3	138.8	145.3	104.3	58.8	63.2
24	10080.	4790.	1475.	140.0	132.3	104.0	119.6	145.3	140.8	145.3	104.0	59.8	63.8
25	12380.	4840.	1480.	141.0	134.2	105.0	121.1	145.7	141.7	145.7	105.0	59.6	63.8
26	1475.	7320.	1710.	151.5	128.2	118.7	123.5	155.8	159.7	155.8	118.7	59.3	64.0
27	2270.	7280.	1720.	154.5	134.5	120.1	125.5	156.5	159.6	156.5	120.1	59.2	64.0
28	3060.	7330.	1710.	130.2	121.1	111.4	115.0	145.0	132.4	145.0	111.4	60.4	64.4
29	3790.	7320.	1720.	134.3	125.0	112.7	117.4	146.2	136.0	146.2	112.7	59.9	64.2
30	4690.	7300.	1725.	136.1	127.1	112.2	118.1	146.0	137.7	146.0	112.2	60.2	64.5

TABLE C-3 (Contd.)

RUN	W_1	W_2	W_{H2O}	TA_1	TA_2	TA_3	TA_4	TA_5	TA_6	TA_7	TA_8	TA_9	TA_{10}
31	6090.	7320.	1715.	139.3	130.8	112.8	119.9	146.6	140.5	146.6	112.8	60.7	64.9
32	7600.	7300.	1720.	135.0	128.0	109.9	117.4	141.4	136.3	141.4	109.9	61.3	65.4
33	10050.	7350.	1725.	139.9	133.5	112.9	121.3	144.2	140.6	144.2	112.9	60.6	64.7
34	12200.	7380.	1715.	136.4	130.9	110.4	118.8	140.3	136.9	140.3	110.4	60.0	63.8
35	750.	1212.	1420.	129.5	85.6	73.8	101.0	222.0	139.6	222.0	73.8	60.3	64.3
36	1165.	1212.	1425.	145.4	100.8	73.7	115.4	214.4	154.9	214.4	73.7	60.5	64.2
37	1530.	1200.	1420.	156.0	114.0	74.1	126.2	210.0	163.5	210.0	74.1	62.0	65.5
38	2290.	1215.	1430.	167.3	132.0	74.5	138.6	204.7	172.6	204.7	74.5	62.3	65.4
39	3030.	1200.	1420.	169.6	139.9	72.8	144.1	197.5	173.5	197.5	72.8	61.9	64.8
40	3800.	1190.	1420.	174.1	148.2	73.6	150.9	196.9	177.6	196.9	73.6	62.3	65.2
41	4580.	1200.	1420.	172.9	150.5	72.6	151.8	192.2	175.7	192.2	72.6	61.5	64.5
42	6100.	1180.	1425.	173.1	155.3	71.3	155.4	187.5	175.4	187.5	71.3	60.6	63.3
43	7590.	1220.	1385.	168.7	154.1	70.9	152.8	179.4	170.2	179.4	70.9	59.2	62.2
44	10000.	1210.	1380.	170.9	159.3	70.5	157.1	179.1	172.3	179.1	70.5	59.2	62.1
45	12200.	1180.	1390.	172.5	162.8	70.8	160.4	179.5	173.4	179.5	70.8	60.0	62.8

APPENDIX D

Construction of Experimental Apparatus

1. Description of Loop Components

a. Pump

Two pumps were used in the course of the experiment. The first, a Goulds Model 3196 centrifugal pump with a water-cooled, double mechanical seal, had a capacity of 15 gal of mercury per minute at a total dynamic head of 35 psi. This pump was used for the experimental runs with the first test section. After the experimental program with the first test section was completed, however, mercury began to leak past the mechanical seal, making further operation of the pump undesirable. A second pump, a Chem-Flow Model 1003 self-cooled canned rotor centrifugal pump, was then installed. After modifications, the Chem-Flow pump was capable of delivering 3 gal of mercury per minute to the test section. The Chem-Flow pump was operated for over 6 months without any difficulty.

Both of the above pumps were equipped with constant-speed motors.

Pressure gauges, located on the suction and discharge lines of the pump, aided in control of the pump-operating conditions.

b. Flow-control Assembly

Since the pumps were equipped with constant-speed motors, a flow-control and bypass-valve assembly was used to control the flow of mercury to the test section. The bypass valve was a 2-in., Teflon-packed, stainless steel needle-type valve. Three Teflon-packed, stainless steel needle-type valves were located in a parallel configuration in each of the lines leading to the test section. These flow-control valves varied in size from 1/4 to 3/4 in. to permit fine control of the mercury flowrate. All valves in the flow-control assembly were welded in place. The above system provided for extremely stable flowrates of mercury, with drifting from the desired setting generally less than ±1% during each experimental run.

c. Cooler

A counterflow, single-pass, double-pipe heat exchanger was located in the line leading to the annulus side of the test section. Mercury passing through the tube side of the cooler was cooled by water flowing through the annulus side. The water flow was provided by a small centrifugal pump which was supplied by a constant-head tank. This arrangement provided extremely steady flowrates of water in the range from

1 to 3 gal/min. The water flowrate was measured by a calibrated orifice-and-manometer assembly. Bulk temperature measurements at the water inlet and outlet were made in mixing chambers located close to the inlet and outlet of the cooler. The cooler was constructed entirely of commercially pure nickel.

d. Heaters

Three tubular immersion heaters with stainless steel sheaths heated the mercury flowing to the tube side of the test section. Each heater had a maximum power rating of $3\frac{1}{3}$ kW at 440 V, three-phase, giving a total maximum power rating of 10 kW for the assembly. The power input to the heaters was controlled by a powerstat. The power input was determined by a measurement of the voltage supplied to each heater, the heater resistances being known quantities.

e. Mercury-mixing Chambers

Fluid-mixing chambers were located close to the inlet and outlet of the tube and annulus sides of the test section to promote mixing of the mercury stream before the temperatures of the bulk fluid were measured. The fluid temperatures measured were steady, indicating that the baffle-plate arrangement of the mixing chambers provided for sufficient mixing of the mercury.

f. Assembly for Flow Measurement

The mercury flowrates in the tube and annulus of the test section were each measured by two methods. The first, a calibrated orifice-and-manometer assembly, was used primarily to calibrate the second, an electromagnetic flowmeter. The orifice assembly was calibrated with water prior to installation in the loop. This calibration procedure has been shown to be quite accurate for liquid metal flow measurements.[61] The pressure differential across the orifice plate was measured by means of an inverted mercury manometer. In order to cover the wide range of mercury flowrates desired for the experiment, the electromagnetic flowmeter was located in series with the orifice assembly. Simply constructed, it consisted of a permanent magnet, with a flux density of approximately 5000 G, located such that the magnetic field was perpendicular to the direction of flow. Copper pins were located by compression fittings, such that they were in direct contact with the flowing mercury. The mercury flow produced an emf across the copper pins which was directly proportional to the flowrate. The emf flowmeter was preferred to the orifice arrangement for actual heat transfer tests, since its range was virtually unlimited compared to that of the orifice assembly. Because of gradual drifting of the flux density of the permanent magnets, it was necessary to recalibrate the emf flowmeter from time to time. Frequent checks of the accuracy of the

emf flowmeter indicated that the drifting was quite gradual, and one calibration a week was more than sufficient. The accuracy of the emf flowmeters is estimated to be within ±5% of the actual flowrate.

g. Expansion Chamber

A vented expansion chamber, located at the highest point in the loop, provided for thermal expansion of the mercury as the operating temperature of the loop was increased. A sight glass was included to permit visual observation of the mercury level. A high-pressure nitrogen-supply line leading to the expansion chamber was used to force mercury out of the loop and into the storage tank.

h. Storage Tank

A vented storage tank of 1-cu ft capacity was located at the lowest point of the loop. A high-pressure nitrogen-supply line was used to force mercury out of the storage tank into the loop. A sight glass proved useful when filling the storage tank.

i. Piping and Connections

All parts of the loop in contact with the mercury were constructed of stainless steel with the exception of the emf flowmeter, copper pins, cooler, and test section. Conduit used was, for the most part, seamless stainless steel pipe or tubing. Due to the high tendency of mercury to leak, connections were welded whenever possible. In order to disassemble the loop easily for cleaning, however, some of the connections were flanged. Flanges used were, for the most part, stainless steel ring-joint flanges, although stainless flanges with "Flexitallic" gaskets were used for the pump and heater connections. Manometer connections as well as drain and vent-line connections were made with compression fittings and Teflon-wrapped threaded connectors.

j. Insulation and Support

For the experimental tests with the first test section, the entire loop was insulated with 1-in. fiber glass insulation. Since it was desired to disassemble the loop for cleaning from time to time, only the heater, cooler, and test section were insulated for the experimental runs with subsequent test sections.

The entire loop was supported by a framework of Unistrut adjustable metal framing.

2. Control of Experimental Apparatus

a. General Loop Control

The operating conditions for each experimental run depended on the mercury flowrates in the tube and annulus of the test section, the rate of heat input to the tube stream by the heater, and the rate of heat removal from the annulus stream by the cooler. The desired flowrates were obtained by careful adjustment of the valves in the flow-control assembly. The outputs of the emf flowmeters were read on a Hewlett-Packard Model 2401C integrating digital voltmeter accurate to $\pm 5\ \mu V$. The digital voltmeter permitted a continuous visual observation of the flowrates. The rate of heat input from the heater was determined by measuring the voltage supplied to the individual heating elements with the resistance of each a known quantity. A wattmeter gave an approximate value of the power level of the heater assembly. The rate of heat removal by the cooler was determined by the water flowrate, and measurements of the inlet and outlet water bulk temperature. The water flowrate was measured by the calibrated orifice-and-manometer assembly.

A general indication of the temperature level of the loop was obtained by periodic temperature measurements at various points of the flow circuit.

b. Safety Control

Because of the high toxicity of mercury vapor, the entire loop was built in a ventilated enclosure. An exhaust fan ducted to the outside of the building prevented mercury vapors from escaping from the enclosure. To catch spilled mercury, the entire apparatus was located over a leak-proof stainless steel pan. A mercury-vapor detector was used to monitor the level of mercury vapor present in the enclosure.

To prevent overheating and possible boiling of the mercury, the power supply for the heater was interlocked with the pump control so that the heaters would operate only when the pump was running. A temperature controller was included to shut the heater off if the heater wall temperature exceeded a predetermined value, usually in the neighborhood of 230°F.

A mercury-level probe located in the top of the expansion tank was interlocked with the pump control to shut off the pump, and hence the heaters, if the mercury dropped below its normal level. An alarm bell was also activated if the mercury level dropped.

Because of the necessity of providing a cooling water flow for the mechanical seal of the first pump, a flow switch was interlocked with the pump control. The pump and heaters could not be turned on unless a cooling water flow in excess of 1 gpm was delivered to the mechanical seal. The second pump was a self-cooled type, so the flow switch was disconnected when the first pump was removed.

APPENDIX E

Analysis of Experimental Errors

1. Expected Maximum Error

If a quantity is a function of several variables, it may be written

$$Q = f(x_1, x_2, x_3, \ldots x_n). \tag{E.1}$$

If Q is subject to error because of errors in the independent variables, this error may be expressed as

$$\delta_Q = \sum_{i=i}^{n} \left(\frac{\partial f}{\partial x_i}\right) \delta_i, \tag{E.2}$$

where

δ_i = error in x_i;

δ_Q = resultant error in Q.

Since some of the δ_i are likely to be positive and others negative, the resultant error in Q will generally be less than the sum of the absolute values of the terms in Eq. (E.2). This necessitates the use of the square of the errors as an indication of the magnitude of the resultant error:

$$\delta_Q^2 = \sum_{i=1}^{n} \left(\frac{\partial f}{\partial x_i}\right)^2 \delta_i^2 + \sum_{i=1}^{n} \left[\frac{\partial f}{\partial x_i} \delta_i \left(\sum_{\substack{j=1 \\ j \neq i}}^{n} \frac{\partial f}{\partial x_j} \delta_j\right)\right].$$

If the positive and negative errors are equally distributed, the term on the right will tend, on the average, to disappear, leaving the following expression as an estimate of the "expected maximum error":

$$\delta_Q = \left[\sum_{i=1}^{n} \left(\frac{\partial f}{\partial x_i}\right)^2 \delta_i^2\right]^{1/2}. \tag{E.3}$$

2. Errors in H and Temperature Differences

a. Errors in H

The accuracy of the emf flowmeters, as mentioned in Ch. IV, was estimated to be ±5%. This maximum error effects the completion of H in the following manner:

$$H = W_2/W_1;$$

$$\delta_H = \left[\left(\frac{\partial H}{\partial W_1}\right)^2 \delta^2_{W_1} + \left(\frac{\partial H}{\partial W_2}\right)^2 \delta^2_{W_2}\right]^{1/2}$$

$$= \left[\left(\frac{W_2}{W_1}\right)^2 \frac{\delta^2_{W_1}}{W_1^2} + \left(\frac{W_2}{W_1}\right)^2 \frac{\delta^2_{W_2}}{W_2^2}\right]^{1/2}$$

$$= \frac{W_2}{W_1}\left[(0.05)^2 + (0.05)^2\right]^{1/2}$$

$$= 0.0707\ H = \text{expected maximum error in H.} \qquad \text{(E.4)}$$

b. Errors in ΔT

The accuracy of the temperature measurements, as mentioned in Ch. IV, was estimated to be $\pm 1/2°F$. This maximum error effects the computation of temperature differences in the following manner:

$$\Delta T = T_i - T_j;$$

$$\delta_{\Delta T} = \left[\left(\frac{\partial \Delta T}{\partial T_i}\right)^2 \delta^2_{T_i} + \left(\frac{\partial \Delta T}{\partial T_j}\right)^2 \delta^2_j\right]^{1/2}$$

$$= \left(\delta^2_{T_i} + \delta^2_{T_j}\right)^{1/2}$$

$$= \left(0.5^2 + 0.5^2\right)^{1/2}$$

$$= 0.707 = \text{expected maximum error in } \Delta T. \qquad \text{(E.5)}$$

3. Errors in Efficiency

The heat-exchanger efficiency was calculated from the following relationships:

$H < 1$:

$$\epsilon = \frac{\Delta T_1 + H\Delta T_2}{2H\Delta T_0};$$

$H > 1$:

$$\epsilon = \frac{\Delta T_1 + H\Delta T_2}{2\Delta T_0},$$

where

$$\Delta T_0 = \overline{T}_1(0) - \overline{T}_2(L);$$

$$\Delta T_1 = \overline{T}_1(0) - \overline{T}_1(L);$$

$$\Delta T_2 = \overline{T}_2(0) - \overline{T}_2(L).$$

Application of Eqs. (E.3), (E.4), and (E.5) to the above yields the following for the expected maximum error in ϵ:

H < 1:

$$\delta_\epsilon = \pm \frac{[0.5(1 + H^2 + 4H^2\epsilon^2) + 0.005\Delta T_1]^{1/2}}{2H\Delta T_0} \tag{E.6a}$$

H > 1:

$$\delta_\epsilon = \pm \frac{[0.5(1 + H^2 + 4\epsilon^2) + 0.005H^2\Delta T_2^2]^{1/2}}{2\Delta T_0} \tag{E.6b}$$

The expected maximum error for ϵ in all of the experimental runs is tabulated in Table E-1.

4. Errors in Nu_{1FD}°

The fully developed overall Nusselt number was computed from

H < 1:

$$Nu_{1FD}^{\circ} = \frac{H}{1 - H}\beta_1^2; \tag{3.42a}$$

H > 1:

$$Nu_{1FD}^{\circ} = \frac{H}{H - 1}\lambda_1^2 \tag{3.42b}$$

where β_1^2 and λ_1^2 were the slopes of the linear portion of the graphs of S vs. Z. Now,

H < 1:

$$S = \ell n\left[\xi_2(1,z) + \frac{H(1 - \epsilon)}{1 - H}\right]; \tag{E.7a}$$

H > 1:

$$S = \ell n\left[\frac{H - \epsilon}{H - 1} - \xi_2(1,z)\right], \tag{E.7b}$$

TABLE E-1. Expected Maximum Error for Efficiency

Run	δ_ϵ	δ_ϵ/ϵ (%)	Run	δ_ϵ	δ_ϵ/ϵ (%)
		10-L/D_1 Test Section			
1	0.0230	4.4	24	0.0292	6.6
2	0.0219	4.1	25	0.0332	7.1
3	0.0203	3.9	26	0.0623	8.7
4	0.0297	4.7	27	0.0404	7.4
5	0.0284	4.4	28	0.0544	11.5
6	0.0263	4.1	29	0.0404	9.9
7	0.0967	11.9	30	0.0326	8.6
8	0.0423	6.1	31	0.0253	7.9
9	0.0292	5.0	32	0.0242	8.2
10	0.0209	4.5	33	0.0263	8.3
11	0.0221	4.5	34	0.0304	9.0
12	0.0246	4.4	35	0.0320	4.1
13	0.0273	4.6	36	0.0233	3.8
14	0.0343	5.1	37	0.0248	3.8
15	0.0386	5.6	38	0.0272	3.9
16	0.0816	11.8	39	0.0296	3.9
17	0.0532	8.5	40	0.0319	4.0
18	0.0319	6.2	41	0.0337	4.1
19	0.0316	7.0	42	0.0373	4.3
20	0.0255	6.6	43	0.0405	4.6
21	0.0217	6.2	44	0.0452	5.0
22	0.0230	6.2	45	0.0506	5.4
23	0.0267	6.6			
		47-L/D_1 Test Section			
43	0.0382	4.1	63	0.0389	4.0
44	0.0328	4.1	64	0.0357	3.7
45	0.0293	4.1	65	0.0331	3.6
46	0.0264	4.0	66	0.0293	3.7
47	0.0289	4.2	67	0.0300	3.7
48	0.0316	4.2	68	0.0327	3.8
49	0.0329	4.2	69	0.0343	3.8
50	0.0349	4.3	70	0.0363	3.9
51	0.0827	8.4	71	0.0378	3.9
52	0.0580	5.8	72	0.0384	4.0
53	0.0468	4.9	73	0.0402	4.1
54	0.0842	8.9	74	0.0354	3.6
55	0.0557	6.2	75	0.0315	3.5
56	0.0449	5.3	76	0.0356	3.7
57	0.0395	5.0	77	0.0372	3.7
58	0.0348	4.8	78	0.0385	3.8
59	0.0296	4.8	79	0.0400	4.0
60	0.0277	4.8	80	0.0373	3.8
61	0.0295	4.8	81	0.0405	4.1
62	0.0321	4.9	82	0.0440	4.4

where

$$\xi_2(1,z) = \frac{T_1(0) - T_2(r_{22},\ell)}{\Delta T_0}.$$

The standard least-squares fit was used to obtain the best fit for the data points, and the slope of the approximating line was taken to be the value of β_1^2 or λ_1^2 depending on the value of H. The expression for the slope of the least-squares line was

$$\lambda_1^2 \text{ or } \beta_1^2 = \frac{n\sum_{i=1}^{n} z_i S_i - \left(\sum_{i=1}^{n} z_i\right)\left(\sum_{i=1}^{n} S_i\right)}{n\sum_{i=1}^{n} z_i^2 - \left(\sum_{i=1}^{n} z_i\right)^2}. \tag{E.8}$$

Because the temperature data for the outer wall were taken at equal intervals and z_i therefore had a constant increment, the above equation can be simplified to yield

$$\lambda_1^2 \text{ or } \beta_1^2 = \frac{12}{(n-1)\,n(n+1)\,\Delta z}\sum_{i=1}^{n}\left(i - \frac{n+1}{2}\right) S_i, \tag{E.9}$$

where

n--numbers of data points;

Δz--increment of z_i.

The expression for the Nusselt number becomes

H < 1:

$$Nu_{1FD}^{\circ} = \frac{H}{1-H}\,\frac{12}{(n-1)(n)(n+1)\,\Delta z}\sum_{i=1}^{n}\left(i - \frac{n+1}{2}\right)\ell n\left[\xi_2(1,z) + \frac{H(1-\epsilon)}{1-H}\right]; \tag{E10.a}$$

H > 1:

$$Nu_{1FD}^{\circ} = \frac{H}{H-1}\,\frac{12}{(n-1)(n)(n+1)\,\Delta z}\sum_{i=1}^{n}\left(i - \frac{n+1}{2}\right)\ell n\left[\frac{H-\epsilon}{H-1} - \xi_2(1,z)\right], \tag{E10.b}$$

or

$H < 1$:

$$Nu_{iFD}^{\circ} = \frac{H}{1 - H} \frac{12}{(n-1)\, n(n+1)\, \Delta z} \sum_{i=1}^{n} \left(i - \frac{n+1}{2} \right) \ell n \left[\frac{\Delta T_{W_i}(1 - H) + H \Delta T_0 (1 - \epsilon)}{\Delta T_0 (1 - H)} \right]; \quad \text{(E11.a)}$$

$H > 1$:

$$Nu_{iFD}^{\circ} = \frac{H}{H - 1} \frac{12}{(n-1)\, n(n+1)\, \Delta z} \sum_{i=1}^{n} \left(i - \frac{n+1}{2} \right) \ell n \left[\frac{(H - \epsilon)\, \Delta T_0 - \Delta T_{W_i}(H - 1)}{\Delta T_0 (H - 1)} \right], \quad \text{(E11.b)}$$

where

$$\Delta T_{W_i} = \overline{T}_1(0) - T_2(r_{22}, \ell).$$

Because of the fact that

$$\sum_{i=1}^{n} i - \left(\frac{n+1}{2} \right) = 0, \quad \text{(E.12)}$$

the expression for Nu_{iFD}° may be further simplified:

$H < 1$:

$$Nu_{iFD}^{\circ} = \frac{H}{1 - H} \frac{12}{(n-1)\, n(n+1)\, \Delta z} \sum_{i=1}^{n} \left(i - \frac{n+1}{2} \right) \ell n \left[\Delta T_{W_i}(1 - H) + H \Delta T_0 (1 - \epsilon) \right]; \quad \text{(E13.a)}$$

$H > 1$:

$$Nu_{iFD}^{\circ} = \frac{H}{H - 1} \frac{12}{(n-1)\, n(n+1)\, \Delta z} \sum_{i=1}^{n} \left(i - \frac{n+1}{2} \right) \ell n \left[(H - \epsilon)\, \Delta T_0 - \Delta T_{W_i}(H - 1) \right]. \quad \text{(E13.b)}$$

The expected maximum error of the logarithmic term in the above summations was computed, these errors summed, and the error in Nu_{iFD}° computed from the following expression:

$H \lesseqgtr 1$:

$$\delta_{Nu_{iFD}^{\circ}} = \pm \frac{1}{|H - 1|} \left[0.005\, Nu_{iFD}^{\circ 2} + \frac{144 H^2}{(n-1)^2\, n^2 (n+1)^2\, \Delta z^2} \delta_{\Sigma} \right]^{1/2}, \quad \text{(E.14)}$$

where

δ_{Σ} --expected maximum error of the summation in Eqs. (E.13a-b).

The expected maximum error for Nu°_{iFD} for the experimental runs with the 47-L/D_1 test section is tabulated in Table E-2.

TABLE E-2. Expected Maximum Error for Nusselt Number

47-L/D_1 Test Section

Run	δNu°_{iFD}	$\delta Nu^{\circ}_{iFD}/Nu^{\circ}_{iFD}$ (%)	Run	δNu°_{iFD}	$\delta Nu^{\circ}_{iFD}/Nu^{\circ}_{iFD}$ (%)
43	0.814	16.8	63	1.166	28.5
44	0.706	13.9	64	0.739	16.6
45	1.463	27.2	65	0.620	13.4
46	6.840	123.4	66	2.655	52.8
47	2.208	35.7	67	2.214	41.3
48	1.309	19.6	68	1.074	19.3
49	1.090	15.4	69	0.886	15.1
50	0.994	13.6	70	0.785	12.4
51	4.654	118.1	71	0.740	11.0
52	1.137	28.5	72	0.725	10.2
53	0.726	15.8	73	0.743	9.9
54	2.413	49.2	74	1.334	31.5
55	3.081	64.0	75	1.637	29.2
56	1.444	28.4	76	0.786	15.1
57	0.720	14.0	77	0.644	12.3
58	0.708	12.7	78	0.578	9.7
59	2.262	37.3	79	0.617	8.6
60	13.223	192.8	80	0.598	9.1
61	2.727	37.7	81	0.621	8.3
62	1.678	22.9	82	0.629	8.0

ACKNOWLEDGMENTS

The author wishes to express his gratitude to the many people who aided him in the course of this investigation. Special thanks are extended to Mr. Ralph Stein, who suggested and carefully supervised the work, and to Dr. Stuart T. McComas, who maintained an active interest throughout the investigation. Thanks are also extended to Messrs. Albert M. Stogsdill, James P. O'Grady, and Joseph R. Kemp, who aided in the construction, maintenance, and operation of the experimental apparatus.

This investigation was supported by the joint fellowship program of Associated Midwest Universities and Argonne National Laboratory. The research was carried out under the auspices of the United States Atomic Energy Commission, Division of Reactor Development, Engineering Development Branch.

BIBLIOGRAPHY

1. Sleicher, C. A., and Tribus, M., *Heat Transfer in a Pipe with Turbulent Flow and Arbitrary Wall-temperature Distribution*, Trans. ASME *79*, 789-797 (1957).

2. Martinelli, R. C., *Heat Transfer to Molten Metals*, Trans. ASME *69*, 947-959 (1947).

3. Knudsen, J. G., and Katz, D. L., *Fluid Dynamics and Heat Transfer*, McGraw-Hill Book Co., Inc., New York (1958).

4. Eckert, E. R. G., and Drake, R. M., *Heat and Mass Transfer*, 2nd Ed., McGraw-Hill Book Co., Inc., New York (1959).

5. Buleev, N. I., *Theoretical Model of the Mechanism of Turbulent Exchange in Fluid Flow*, Teplopesedacha, U.S.S.R. Academy of Science *64* (1962).

6. Dwyer, O. E., and Tu, P. S., *Unilateral Heat Transfer to Liquid Metals Flowing in Annuli*, Nucl. Sci. Eng. *15*, 58-68 (1962).

7. Dwyer, O. E., *On the Transfer of Heat to Fluids Flowing through Pipes, Annuli, and Parallel Plates*, Nucl. Sci. Eng. *17*, 336-344 (1963).

8. Dwyer, O. E., *Recent Developments in Liquid Metal Heat Transfer*, BNL-9597 (1965).

9. Dwyer, O. E., *Eddy Transport in Liquid-metal Heat Transfer*, AIChE J *9*(2), 261-268 (1963).

10. Lyon, R. N., *Liquid Metal Heat Transfer Coefficients*, Chem. Eng. Prog. *47*, 75-79 (1951).

11. Werner, R. C., King, E. C., and Tidball, R. A., *Heat Transfer with Sodium-Potassium Liquid Alloys*, NP-5169 (1949).

12. Bailey, R. V., *Heat Transfer to Liquid Metals*, ORNL-521 (1950).

13. Bentwich, M., and Sideman, S., *Temperature Distribution and Heat Transfer in Annular Two-phase (Liquid-Liquid) Flow*, Can. J. Chem. Eng. *42*, 9-13 (1964).

14. Ting, A. P., *Heat Transfer in Packed Beds*, Ind. Eng. Chem. *47*, 2293-2299 (1955).

15. Lightfoot, E. N., *Countercurrent Heat or Mass Transfer between a Turbulent and a Laminar Stream*, AIChE J *8*(3), 416 (1962).

16. Stein, R. P., *Liquid Metal Heat Transfer*, Advances in Heat Transfer, Vol. III (T. F. Irvine, J. P. Hartnett, Eds.), Academic Press, New York (1966).

17. Stein, R. P., *Mathematical and Practical Aspects of Heat Transfer in Double Pipe Heat Exchangers*, Proceedings of the Third International Heat Transfer Conference, Vol. I, 139 AIChE J, New York (1966).

18. Stein, R. P., *The Graetz Problem in Cocurrent-flow, Double-pipe Heat Exchangers*, ANL-6889 (1964).

19. Nunge, R. J., and Gill, W. N., *Analysis of Heat or Mass Transfer in Some Countercurrent Flows*, Int. J. Heat Mass Transfer *8*, 873 (1965).

20. Nunge, R. J., and Gill, W. N., *An Analytical Study of Laminar Counterflow Double-pipe Heat Exchangers*, AIChE J *12*(2), 279 (1966).

21. Nunge, R. J., Gill, W. N., and Stein, R. P., *Analysis of a Counterflow Parallel-plate Heat Exchanger*, unpublished manuscript.

22. Stein, R. P., *Heat Transfer Coefficients in Liquid Metal Cocurrent Flow Double Pipe Heat Exchangers*, paper presented at Third Annual High-temperature Liquid-metal Heat-transfer Technology Conference, September 4-6, 1963, Oak Ridge National Laboratory.

23. Merriam, R. L., *An Investigation of Liquid Metal Heat Transfer in a Cocurrent-flow, Double-pipe Heat Exchanger*, ANL-7056 (1965).

24. King, C. J., UCRL-11196 (1964).

25. Stein, R. P., *Computational Procedures for Recent Analyses of Counterflow Heat Exchangers*, AIChE J *12*(6), 1217 (1966).

26. Nunge, R. J., *On the Theory of Multiphase, Indirect-contact, Forced-convection, Laminar Heat Transfer*, Ph.D. Thesis, Syracuse University (1965).

27. Blanco, J. A., Gill, W. N., and Nunge, R. J., *Computational Procedure for Recent Analyses of Counterflow Heat Exchange*, AIChE J *14*, 505 (1967).

28. Stein, R. P., *The Mathematics of Counter-flow Heat Exchangers with Equal Heat Capacity Flow Rates*, paper presented at 9th Nat. Heat Transfer Conference, ASME-AIChE J, Seattle, Washington (1956).

29. Lubarsky, B., and Kaufman, S. J., *Review of Experimental Investigations of Liquid-metal Heat Transfer*, NACA-1270 (1956).

30. Gilliland, E. R., Musser, R. J., and Page, W. R., *Heat Transfer to Mercury*, Gen. Disc. on Heat Transfer, IME and ASME, 402-404 (1951).

31. Elser, D., *Heat Transfer Measurements with Mercury*, AEC-tr-2016 (1949).

32. Lyon, R. N., *Forced-convection Heat Transfer Theory and Experiments with Liquid Metals*, ORNL-361 (1949).

33. Seban, R. A., *Heat Transfer Measurements on Lead-Bismuth Eutectic in Turbulent Pipe Flow*, NRO-35-324 (1950).

34. Trefethen, L. M., *Heat Transfer Properties of Liquid Metals*, NP-1788 (1950).

35. Doody, T. C., and Younger, A. H., *Heat Transfer Coefficients for Liquid Mercury and Dilute Solutions of Sodium in Mercury in Forced Convection*, AIChE J Preprints, 79-98 (Dec 1951).

36. Lubarsky, B., *Experimental Investigation of Forced-convection Heat-transfer Characteristics of Lead-Bismuth Eutectic*, NACA-TM-E51G02 (1951).

37. Bailey, D. L. R., Cope, W. F., and Watson, G. G., *Heat Transfer to Mercury*, HEAT-13 (1952).

38. Hall, W. B., and Jenkins, A. E., *Heat Transfer Experiments with Sodium and Sodium-Potassium Alloy*, J. Nucl. Energy *1*, 244 (1955).

39. Brown, H. E., Amstead, B. H., and Short, B. E., *Temperature and Velocity Distribution and Transfer of Heat in a Liquid Metal*, Trans. ASME *79*, 279-285 (1957).

40. Baker, R. A., and Sesonske, A., *Heat Transfer in Sodium-Potassium Alloy*, Nucl. Sci. Eng. *13*, 283-288 (1962).

41. Andreev, A. S., and Kalachev, D. M., *Heat Transfer during Heating and Cooling of Heavy Metal in a Tube*, AEC-tr-6554, 114 (1963).

42. Kokorev, L. S., and Ryaposov, V. N., *Measurements of the Temperature Distribution in the Turbulent Flow of Mercury in a Circular Tube*, AEC-tr-6554, 124 (1963).

43. Sawochka, S. G., and Schleef, D. J., *Liquid Heat-transfer Coefficients for Potassium during Vertical Upflow inside a Tube*, Trans. ASME paper 64-WA/HT-19 (1964).

44. Awad, A., *Heat Transfer and Eddy Diffusivity in NaK in a Pipe at Uniform Wall Temperature*, Ph.D. Thesis, University of Washington, Seattle, Washington (1965).

45. Stein, R. P., *A Method for the Determination of Local Heat Fluxes in Liquid Metal Heat Exchangers*, ANL-7100, 483 (1965).

46. Untermeyer, unclassified data from a classified report.

47. English, D., and Barrett, T., *Heat Transfer Properties of Mercury*, Gen. Disc. on Heat Transfer, IME and ASME, 458-460 (1951).

48. MacDonald, W. C., and Quittenton, R. C., *A Critical Analysis of Metal "Wetting" and Gas Entrainment in Heat Transfer to Molten Metals*, AIChE J Preprint No. 8 (1953).

49. Stromquist, W. K., *Effect of Wetting on Heat Transfer Characteristics of Liquid Metals*, ORO-93 (1953).

50. Chelemer, H., *Effect of Gas Entrainment on the Heat Transfer Characteristics of Mercury under Turbulent Flow Conditions*, ORO-139 (1955).

51. Bonilla, C., and Wang, S. J., *Interfacial Thermal and Electrical Resistance between Stationary Mercury and Steel*, NYO-3091 (1952).

52. Mizushina, T., Iushi, S., Sasano, T., and Tamura, H., *Thermal Contact Resistance between Mercury and a Metal Surface*, Int. J. Heat Mass Transfer *1*, 139-146 (1960).

53. Poppendiek, H. F., and Harrison, W. B., *Remarks on Thermal Entrance Region Heat Transfer in Liquid-metal Systems*, AIChE J Preprint No. 7 (1953).

54. Rickard, C. L., Dwyer, O. E., and Dropkin, D. D., *Heat Transfer Rates to Cross-flowing Mercury in a Staggered Tube Bank-II*, paper presented at Reactor Heat Transfer Conference, USAEC, New York (1956).

55. Lyon, R. N. (Ed.), *Liquid Metals Handbook*, 2nd Ed., USAEC (1952).

56. Kays, W. M., and London, A. L., *Compact Heat Exchangers*, The National Press, Palo Alto, California (1955).

57. von Karman, T., Trans. ASME *61*, 705 (1939).

58. Petrovichev, V. I., *Heat Transfer in Mercury through Annular Channels*, Atomnaya Energiya *7*, No. 4, 366-369 (1959).

59. Poppendiek, H. F., *Turbulent Liquid-metal Heat Transfer in Channels*, Nucl. Sci. Eng. *5*, 390-404 (1959).

60. Abramowitz, M. (Ed.), *Handbook of Mathematical Functions*, NBS Applied Mathematics Series 55 (1964).

61. Johnson, H. A., Hartnett, J. P., Clabaugh, W. J., and Fried, L., *Orifice-metering Coefficients and Pipe Friction Factors for the Turbulent Flow of Lead-Bismuth Eutectic*, Trans. ASME *79*, 1079-1084 (1957).

62. Bocher, M., Bull. Amer. Math. Soc., Vol. XXI, 6 (1914).

63. Ince, E. L., *Ordinary Differential Equations*, Dover, New York (Sections 10.61, 10.71, 10.72) (1956).

64. Stein, R. P., unpublished notes (March 1967).

65. Weatherford, W. D., Tyler, J. C., and Ku, P. M., *Properties of Inorganic Energy Conversion and Heat Transfer Fluids for Space Applications*, WADD TR 61-96 (1961).

66. Kays, W. M., and Leung, E. Y., *Heat Transfer in Annular Passages--Hydrodynamically Developed Turbulent Flow with Arbitrarily Prescribed Heat Flux*, Int. J. Heat Mass Transfer *6*, 537-557 (1963).

67. Khabakhpasheva, E. M., and Il'in, Yu. M., *Heat Transfer to a Melt of Sodium and Potassium in Annular Clearances*, Atomnaya Energiya *9*, No. 6, 494-496 (1960).

68. Seban, R. A., and Shimazaki, T. T., *Heat Transfer to a Fluid Flowing Turbulently in a Smooth Pipe with Walls at Constant Temperature*, Trans. ASME *73*, 803-809 (1951).

69. Tebo, F. J., *Selected Values of the Physical Properties of Various Materials*, ANL-5914 (1958).

70. Chao, B. T., Li, H. L., and Scott, E. J., *On the Solution of Ill-conditioned, Simultaneous, Linear, Algebraic Equations by Machine Computation*, University of Illinois Bulletin *58*, No. 63 (1961).

B